Coordination Chemistry Reviews 448 (2021) 214172

Contents lists available at ScienceDirect

Coordination Chemistry Reviews

journal homepage: www.elsevier.com/locate/ccr

Review

Catalytic systems mimicking the [FeFe]-hydrogenase active site for visible-light-driven hydrogen production

Juan Amaro-Gahete [a,*], Mariia V. Pavliuk [b], Haining Tian [b], Dolores Esquivel [a], Francisco J. Romero-Salguero [a], Sascha Ott [b,*]

[a] Departamento de Química Orgánica, Instituto Universitario de Nanoquímica (IUNAN), Facultad de Ciencias, Universidad de Córdoba, 14071 Córdoba, España
[b] Department of Chemistry, Ångström Laboratories, Uppsala University, Box 523, 751 20 Uppsala, Sweden

ARTICLE INFO

Article history:
Received 18 May 2021
Accepted 16 August 2021
Available online 1 September 2021

Keywords:
Photochemistry
Biomimetic chemistry
Artificial photosynthesis
Light-driven hydrogen evolution
Bioinorganic chemistry

ABSTRACT

A global hydrogen economy could ensure environmentally sustainable, safe and cost-efficient renewable energy for the 21st century. Solar hydrogen production through artificial photosynthesis is a key strategy, and the activity of natural hydrogenase metalloenzymes an inspiration for the design of synthetic catalyst systems.

[FeFe]-hydrogenase enzymes, present in anaerobic bacteria and green algae, are the most efficient class of biological catalysts for hydrogen evolution. The enzymes operate in an aqueous environment, utilizing electrons that ultimately stem from photosynthesis as the only energy source. Functional synthetic models of the [FeFe]-hydrogenase enzyme active site have garnered intense interest as potential catalysts for the reduction of protons to molecular hydrogen.

Herein, we take an extensive journey through the field of biomimetic hydrogenase chemistry for light-driven hydrogen production. We open with a brief presentation of the structure and redox mechanism of the natural enzyme. Synthetic methodologies, structural characteristics, and hydrogen generation metrics relevant to the synthetic diiron catalysts ([2Fe2S]) are discussed. We first examine multicomponent photocatalysis systems with the [2Fe2S] cluster, followed by photosensitizer-[2Fe2S] dyads and molecular triads. Finally, strategies for the incorporation of [2Fe2S] complexes into supramolecular assemblies, semiconductor supports, and hybrid heterogeneous platforms are laid out. We analyze the individual properties, scope, and limitations of the components present in the photocatalytic reactions. This review illuminates the most useful aspects to rationally design a wide variety of biomimetic catalysts inspired by the diiron subsite of [FeFe]-hydrogenases, and establishes design features shared by the most stable and efficient hydrogen producing photosystems.

Contents

* Corresponding authors.
E-mail addresses: q22amgaj@uco.es (J. Amaro-Gahete), Sascha.Ott@kemi.uu.se (S. Ott).

https://doi.org/10.1016/j.ccr.2021.214172
0010-8545/

1. Introduction

The depletion of non-renewable energy sources has prompted the scientific community to search for inexhaustible, economically viable and environmentally friendly alternative energy supplies [1,2]. The conversion and storage of energy from sunlight in fuels is a promising alternative to satisfy the future energy demand of our society on a large scale [3]. Solar energy applied to the chemical decomposition of water is a key strategy for obtaining hydrogen [4–6]. Many future sustainable energy systems are based on hydrogen as an energy carrier due to its high gravimetric energy storage density (142 MJ kg^{-1}), zero emissions, non-toxicity and potential to be sourced from water, an abundant resource [7,8]. Hydrogen can be utilized in the presence of oxygen by combustion or in fuel cells that generate electricity. Hydrogen gas is also essential to carry out many industrial processes, but it is currently obtained largely from steam reforming of fossil fuels [9].

Nature uses sunlight to generate chemical energy through photosynthesis, which consists of sequential chain reactions carried out in thylakoid membranes of algae, bacteria and higher plants. The processes of light capture by antenna pigments (mainly chlorophyll and carotenoid), water splitting, $NADP^+$ reduction, and ATP formation take place in several protein complexes of oxygenic organisms [10–13]. The process is driven by absorption of photons from sunlight by the light-harvesting complexes of photosystem (PS) I and PSII. Light-driven water oxidation in PSII generates electrons that pass along an electron-transport chain via plastoquinone (PQ), cytochrome b_6/f (cyt b_6/f), plastocyanin (PC), PSI and ferredoxin (Fd). The photoexcitation of the antenna complex in PSI activates the electron transfer from the ferredoxin-ADP^+ oxidoreductase enzyme to $NADP^+$ with the subsequent formation of NADPH. The protons released in the oxygen evolution reaction (OER) are taken up by ATP synthase to produce ATP molecules from ADP. The ATP and NADPH that are generated in the process provide the energy needed for the fixation of CO_2 in the Calvin Benson cycle to produce sugars- plant fuel- such as glucose and starch.

Under anaerobic conditions, [FeFe]-hydrogenase enzymes in the chloroplasts of unicellular green algae catalyze the hydrogen evolution reaction (HER) [14]. A simplified scheme of the natural photosynthesis carried out by these systems is presented in Fig. 1. The reaction cycle begins with the initial absorption of light by the PSI primary electron donor (P700), ultimately leading to reduced ferredoxin (Fd). The catalytically active [FeFe] hydrogenases accept electrons from reduced Fd which are then used for the HER [15–17]. [FeFe] hydrogenase metalloenzymes catalyze the reversible interconversion of protons and electrons into molecular hydrogen ($2H^+ + 2e^- \rightarrow H_2$) at the remarkable rate of up to 9000 hydrogen molecules per second per enzyme [18,19].

The structure of the [FeFe] hydrogenase active site (H-cluster) was determined by X-ray crystallography to consist of an organometallic diiron subcluster [2Fe]. The proximal iron (Fe_p) is linked to a cubane subcluster [4Fe-4S] by the sulfur of a cysteine residue (Fig. 1) [20,21]. While Fe_p has a saturated coordination

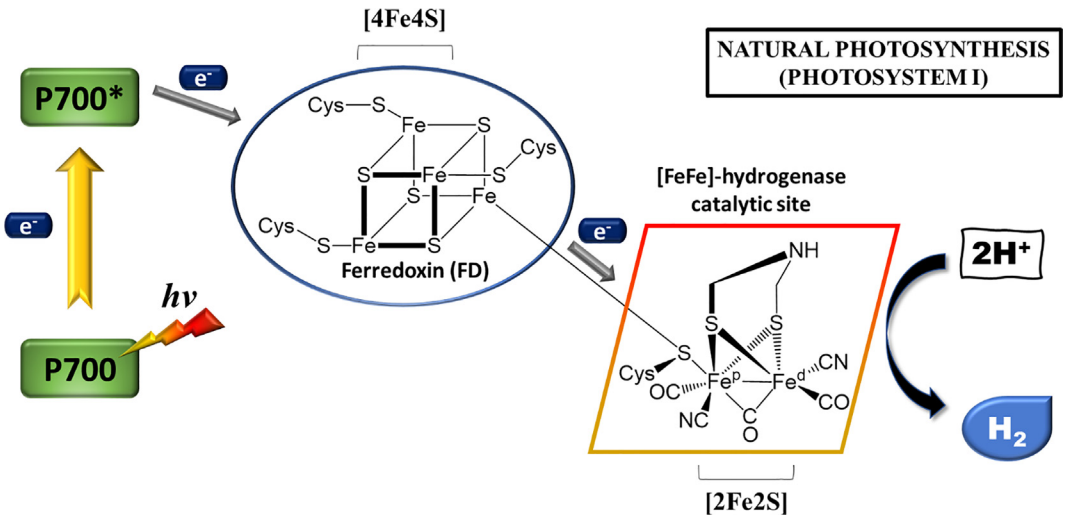

Fig. 1. Schematic representation of electron flow from Photosystem I to an [FeFe]-hydrogenase via a ferredoxin redox mediator (Photosystem I).

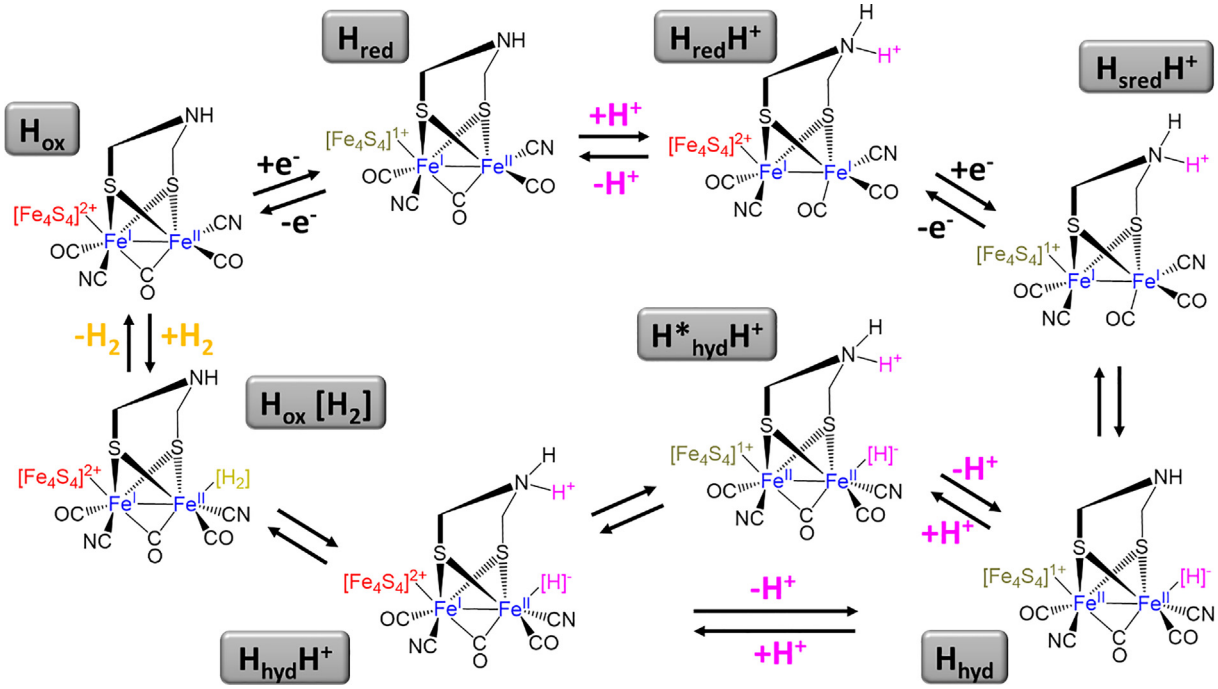

Fig. 2. Proposed mechanistic cycle for hydrogen evolution by [FeFe]-hydrogenase adapted from Lubitz et al. [25] with permission from Elsevier.

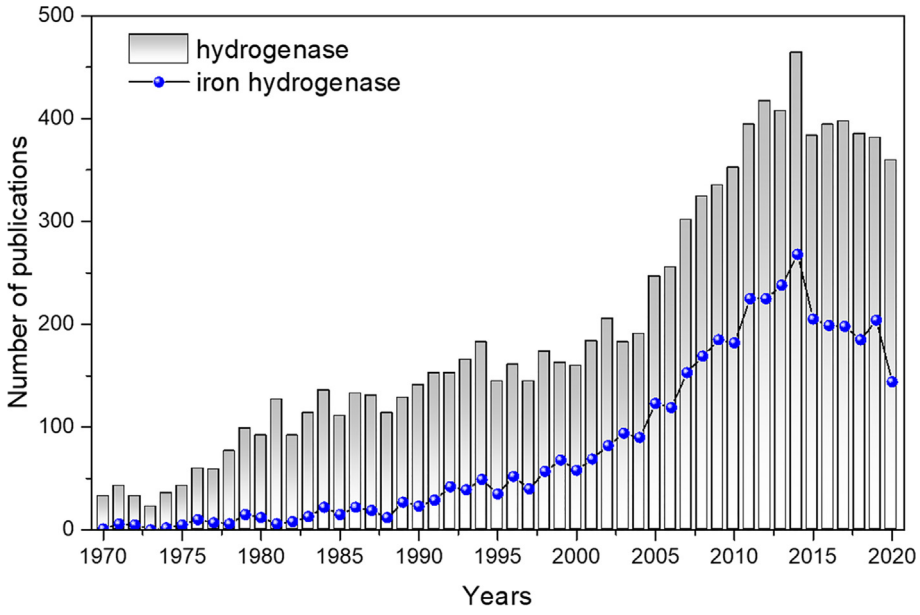

Fig. 3. Number of publications per year in the period (1970–2020) following Web of Science (WOS) database. Column and line correspond to searches with words in title, abstract or keywords as reported in the inset.

sphere, the distal iron (Fe_d) provides an available coordination site for proton or hydrogen binding [22]. The [2Fe2S] cluster contains a bridging azadithiolate ligand (aza-propane-1,3-dithiolate, adt), two terminal cyanide and carbon monoxide strong-field ligands at the low-valent iron sites, as well as a carbon monoxide ligand bridging both metal centers. The H-cluster is deeply buried within the protein scaffold in a hydrophobic pocket where catalysis takes place. This arrangement aids proton and electron transport to and from the active site and confers a certain degree of O_2 tolerance [23,24].

The enzymatic hydrogen formation mechanism as proposed by Lubitz and co-workers [25,26] is shown in Fig. 2. In the enzyme's most oxidized resting system (H_{ox}), the [4Fe4S] cubane is in a 2 + oxidation state while the catalytic subcluster [2Fe] is a mixed valence $Fe^{I}Fe^{II}$ state. The first one-electron reduction results in the formation of the H_{red} state where the [4Fe4S] subcluster is reduced to a 1 + oxidation state. Protonation of the adt-*N* triggers an intramolecular charge shift to form $H_{red}H^+$ in which the [4Fe4S] cubane is in the 2 + state and the [2Fe] subsite reduced to a homovalent $Fe^{I}Fe^{I}$ state. Subsequent one-electron reduction of the subcluster [4Fe4S] gives rise to the "super-reduced" state $H_{sred}H^+$, well-characterized by EPR and FTIR spectroscopy [27]. In the next step of the catalytic cycle, an intermediate hydride state [H_{hyd}] is formed by an intramolecular proton shift from the adt-*N*

to the distal iron F_d, a process that is coupled to an electron rearrangement in the [2Fe] subsite, leading to a formal $Fe^{II}Fe^{II}$ oxidation state. Recently, this terminal hydride intermediate has been detected directly by ^1H NMR spectroscopy at room temperature [28]. Addition of a second proton coupled to another charge shift from the reduced [4Fe4S] to the [2Fe] subsite either in one or two discrete steps gives rise to [$H_{hyd}H^+$] that is characterized by a formal Fe^IFe^{II} oxidation state. At this point, there is an equilibrium between the $H_{hyd}H^+$ and $H_{ox}[H_2]$ in which the hydride and the proton are combined to a hydrogen molecule at the distal iron of the system. The catalytic cycle is closed by H_2 release, returning to the initial H_{ox} configuration. For more details on the species involved in each step of this reaction mechanism as deduced from X-ray crystallography, spectroelectrochemical studies, EPR and DFT theoretical calculations, the reader is referred to excellent literature contributions [29–34].

Hydrogenase metalloenzymes show high turnover rates for hydrogen production at mild reduction potential in neutral aqueous solution [24,35,36], making them competitive with commonly used platinum-based metal catalysts [37]. However, they exhibit irreversible deactivation in the presence of oxygen. Detailed studies on the mechanism of enzymatic inactivation of the dinuclear subsite by oxygen have been carried out to understand and improve the resistance against irreversible oxidative degradation and/or inhibition of the catalytic cycle [38–40]. Similarly, intermediate reaction species of [FeFe]-hydrogenases have been characterized using spectroscopic techniques and theoretical calculations [24,41,42]. Progress on O_2 tolerance in the artificial maturation of [FeFe]-hydrogenases has been reported to overcome this obstacle [43,44]. Thus, understanding the chemistry of [FeFe]-hydrogenases is key to deducing principles essential for the design of artificial biomimetic systems based on these enzymes.

Due to the low availability of natural hydrogenases, numerous studies have focused on the development of biomimetic catalysts that exhibit similar activity as the enzymes, with the aim of designing an artificial photocatalytic system for light-driven proton reduction [45,46]. Fig. 3 shows a bibliometric analysis that highlights how the interest in hydrogenase enzymes in general (columns) and, [FeFe]-hydrogenases in particular (line), as a research topic has grown in recent years.

In an artificial light-driven system for solar fuel generation, light absorption is followed by the separation of electrons and holes. Electrons are used in the catalytic fuel formation reaction, and the holes are replenished by electrons from water oxidation. However, photon absorption leads to the separation of single electron-hole pairs, while both water oxidation and fuel production involve multiproton and multielectron reactions. Therefore, the accumulation of electrons and holes (accumulative charge separation) by successive absorption of photons is necessary to complete all the catalytic reactions [47]. Engineering a molecular system that combines both the fuel production and water oxidation half reactions and that is powered by light-induced charge separation is still a challenge for the scientific community. Among others, the following difficulties can be identified: i) charge recombination before catalyst turnover, ii) balancing the rates of the two half reactions and iii) undesirable secondary reactions, such as, for example, peroxide instead of oxygen formation.

To address this, the separate half-reactions - water oxidation or fuel production - have been optimized separately, in particular, by achieving long-lived high-energy charge-separated states, that can then be coupled via a redox compartmentalization [47–50]. The independent half-reactions are powered either electrochemically or by the use of sacrificial oxidants or reductants [51]. Photochemical catalysis employs a photosensitizer and a sacrificial electron acceptor or donor to supply the redox equivalents for water oxidation and hydrogen production, respectively. For the light-induced hydrogen generation catalyzed by [FeFe]-hydrogenase active site mimics, a schematic representation is shown in Fig. 4. Excitation of the photosensitizer initiates the photocatalytic process. Photoinduced charge separation from the excited photosensitizer (PS) provides electrons in a diffusional process to the [2Fe2S] catalyst that is responsible for driving proton reduction. The sacrificial electron donor (ED) must be easily oxidizable to make the overall electron transfer process (ET) thermodynamically feasible and to ensure rapid recovery of the PS before charge recombination can occur. This process has to be repeated twice to accumulate two electrons in the [2Fe2S] catalyst, which can then reduce two protons to produce a H_2 molecule [52].

The concept of artificial photosynthesis in sacrificial half-reactions was first reported in 1977 by Lehn and co-workers. In this seminal paper, light-driven proton reduction was achieved in a photochemical system consisting of $Ru(bpy)_3^{2+}$ as the visible-light-absorbing PS, $Rh(bpy)_3^{2+}$ as the electron mediator, triethanolamine (TEOA) as the sacrificial agent and colloidal platinum as the catalyst [53,54]. Similar systems were reported a year later by Grätzel's research group, using the same $Ru(bpy)_3^{2+}$ photosensitizer, methyl viologen as the electron mediator and EDTA electron donors [55–57]. These early reports have influenced the development of model complexes mimicking the structure and function of natural [FeFe]-hydrogenase enzymes and the optimization of other components that participate in the photosystem (PS and ED), as well as other influencing parameters (solvent, pH, excitation wavelength and power), with the aim of maximum efficiency for light-driven hydrogen evolution.

The electron donor is a sacrificial agent such as triethylamine (TEA), triethanolamine (TEOA), ethylenediaminetetraacetic acid (EDTA) or ascorbic acid (AscOH) that can be easily oxidized. This property ensures the thermodynamic viability of the catalytic reac-

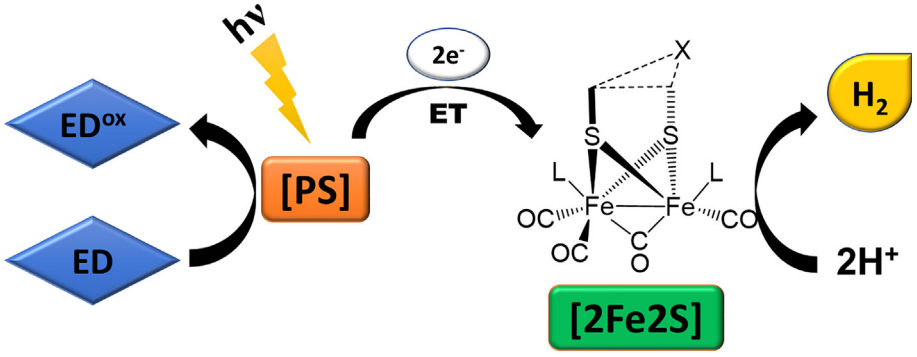

Fig. 4. Schematic representation of light-driven hydrogen production mechanism. ED: electron donor, PS: photosensitizer and [2Fe2S]: diiron active site (L: CN^-, CO or PR_3, X: CH_2, CH_2R, NH, NHR, O or OR, dashed lines: different linking possibilities in the dithiolate subcluster).

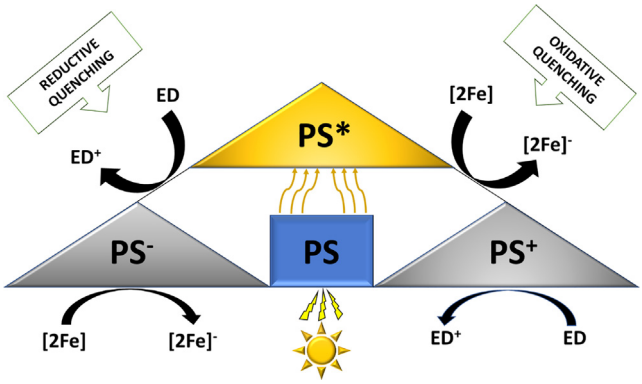

Fig. 5. Oxidative and reductive quenching pathways for reduction of [2Fe] active subsite.

tions and prevents unproductive back-electron transfer [58]. In this context, the pH of the reaction medium of the ED is very important as it determines the acid-base equilibria. In the case of ascorbic acid, for example, the anionic ascorbate ($AscO^-$) is a stronger reducing agent than its protonated form, AscOH, and therefore requires a pH above 4 (pK_{a1} = 4.17) [59,60]. EDTA contains two amino groups and four carboxylic acid groups that can act as electron donors at a more neutral pH between 5 and 7 [61]. If TEA (pK_a = 7.9) or TEOA (10.7) is used as a sacrificial agent, it is essential to work at a pH close to their pKa values to avoid the excessive protonation of the free amine that would inhibit its function as ED [61]. The selection of the most suitable ED is mainly empirical, and depends on the functional units present in the photocatalytic system. Considerations must be given to the relative redox potentials, solubility, and the pH of the reaction medium that, in turn, is set to optimize hydrogen production.

Visible light harvesting by the PS is essential for efficient electron transfer reactions and to obtain a maximum quantum yield (QY) in the photocatalytic hydrogen evolution. A wide absorption range, a redox potential suitable for electron transfer from the ED to the excited PS, long excited state lifetimes, high photostability and appropriate solubility in the reaction solution are all important aspects [62]. Organic dyes such as rose Bengal [63] and Eosin Y [64], among others [65], and metal complexes such as $[Ru(bpy)_3]^{2+}$ and $[Ir(bpy)(ppy)_2]PF_6$ have been extensively studied for several decades. Metal-free organic dyes are cheap, easily engineered, environmentally friendly and readily accessible. They feature high molar extinction coefficients compared to metal complexes but also suffer from some drawbacks such narrow absorption bands in the visible region, quenching of the photoluminescence promoted by multichromophoric interactions, photochemical instability and sometimes short excited state lifetimes [65–69]. $[Ru(bpy)_3]^{2+}$ is the most widely employed PS in photocatalysis for hydrogen production, presenting a broad absorption band in the visible light range (λ_{max} = 450 nm) and a relatively long lifetime of its excited state. A usual problem with this PS is its frequent instability under experimental photocatalytic conditions [70,71]. In contrast, PSs based on Ir (III) are considered highly effective because they exhibit good stability and excellent excited-state properties [72]. However, their large-scale application is limited by Ir scarcity and high cost. These challenges have been addressed through the investigation of alternative light harvesters, such as semiconductor nanoparticles (ZnS or TiO_2) or quantum dots (CdSe or CdTe), which exhibit long-term stability and broad absorption bands in the visible part of the spectrum.

The concentration of both the PS and ED has a crucial influence on the rate of hydrogen production. Frequently, an excess of ED is used in a photocatalytic reaction for hydrogen evolution to ensure the kinetic control and high charge separation yield, while a higher concentration of PS usually results in faster hydrogen productivity. In tethered systems, also the distance between the PS and the catalyst or ED must be controlled to avoid competing reaction pathways. More details about the use of ED and PS in photosystems for light-induced hydrogen evolution are discussed in the next sections of this review.

Concerning the diiron catalyst, the reduction of the active subsite [2Fe2S] can be carried out in two different ways, *i.e.* by following an oxidative or reductive quenching pathway of the excited PS (Fig. 5) [14]. In the first case, oxidation of the excited *PS occurs by transferring an electron to [2Fe2S]. The oxidized PS is regenerated by the ED. On the other hand, the ED can perform a reductive quenching of the excited species *PS. The thereby produced, photo-reduced PS can successively reduce the catalytic [2Fe2S] cluster by transfer of an electron, recovering the original state of the PS. The exact mechanism will depend on the excited-state oxidation and reduction potentials of the PS, the reduction potential of the catalyst for the reduction of protons and the oxidation potential of the ED to re-establish the original state of the PS. In the event that both pathways are thermodynamically feasible, the predominant mechanism will be the one with the highest quenching rate [73].

In recent decades, great efforts have been directed towards the design of diiron complexes that mimic the structure and function of natural [FeFe]-hydrogenases, and to include them in schemes for light-induced hydrogen formation. Biologically inspired functional models of hydrogenases contain first, second, and outer coordination spheres, each contributing to the photocatalytic process [74,75]. The first coordination sphere describes the ligands directly bound to the diiron core [2Fe] influencing the properties of the metal center: vacant coordination sites for substrate binding, modification of redox potentials, electron density, and steric hindrance for the accessibility of reactants. Strong-field ligands such as cyanide (CN^-) or carbon monoxide (CO) are present in the enzyme active site to ensure low-spin complexes. The second coordination sphere includes functional groups of the ligands that react with the substrate. They play a fundamental role in moving electrons through the [4Fe-4S] cubane and shuttling protons via amino acids and the amine bridgehead of the active site. The outer coordination sphere of metalloproteins has dimensions normally>4 Å from the metal and encompasses the entire remaining scaffold of [FeFe]-hydrogenase [76]. Artificial bioinspired diiron complexes can be fine-tuned by engineering each of these coordination spheres in the following ways:

a) First coordination sphere: ligand substitutions of the archetypical dithiolate-bridged hexacarbonyl diiron complexes are essential for the formation of the mixed-valence state $Fe^{II}Fe^{I}$, to reproduce the "rotated conformation" of the enzyme, and the formation of terminal hydride species [75,77–80]. In general, two strategies have been taken: i) the replacement of CO with CN^- to stabilize a specific orientation of the diiron subcluster in the active site and promote the formation of the hydride intermediates; or ii) the substitution of CO with electron-rich phosphine ligands, among others, to provide photostability, higher electron density, and proton relays.

b) Second coordination sphere: The exhaustive control in the design of the second coordination sphere is crucial for the protonation mechanism of the complex [81], the creation and stabilization of hydride species [24], assistance in the heterolytic H_2 cleavage/-formation, [82] and proton-coupled electron transfer reactions (PCET) [83]. In addition, problems intrinsic to most diiron hydrogenase mimics such as the large overpotentials required for the catalytic proton reduction process can be addressed. The following modifications can be beneficial: i) the incorporation of ligands in the dithiolate bridging group bearing novel features such as pen-

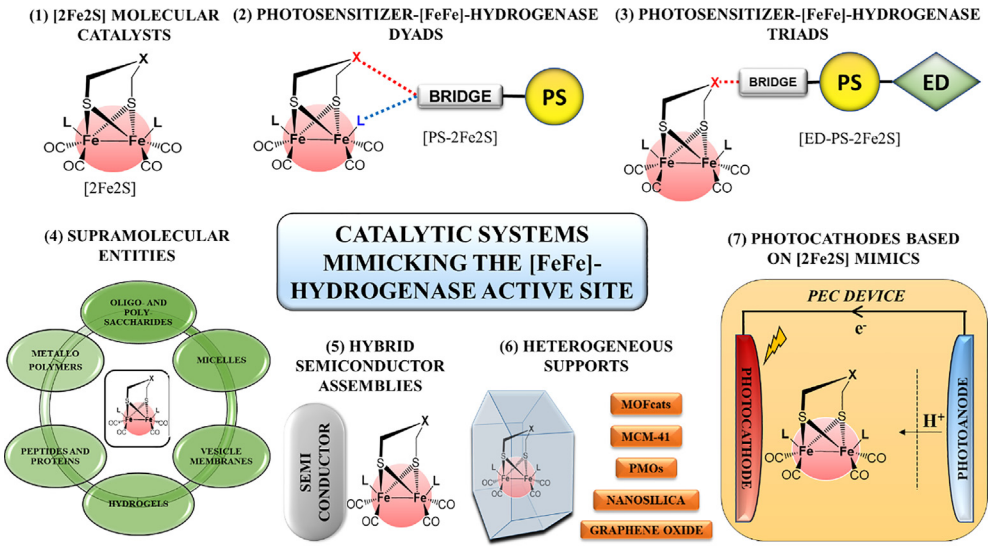

Fig. 6. Overview of catalytic systems mimicking the [FeFe]-hydrogenase active site: (1) [2Fe2S] molecular catalysts (Section 2), (2) Photosensitizer-[FeFe]-hydrogenase dyads (Section 3), (3) Electron donor-photosensitizer-[FeFe]-hydrogenase triads (Section 4), (4) Supramolecular entities (Section 5), (5) Hybrid semiconductor assemblies (Section 6), (6) Heterogeneous supports (Section 7) and (7) Photocathodes based on [2Fe2S] for PEC devices (Section 8) . The nomenclature used for catalytic systems 1, 2 and 3 is indicated while for catalytic systems 4, 5, 6, and 7, the molecular catalyst and supramolecular entity, semiconductor, support or photocathode will be included following the nomenclature reported by the authors in the corresponding articles.

dant amine groups or substituted aromatic dithiolate bridgehead; ii) the addition of functional groups or reactive structures at the ligands on the [2Fe] core in the first coordination sphere. Modification of the secondary coordination sphere can allow the integration of functionalized amino groups similar to those existing in the natural enzyme, or the addition of novel functionalities in the bridging dithiolate, for example, a photosensitizer to allow for *intra*molecular photo-induced charge separations.

c) Outer coordination sphere: most [FeFe] hydrogenase active site models are only soluble in an organic phase. Supramolecular control via outer coordination sphere interactions is of vital importance to create and modulate an analogous protein environment around diiron catalysts that enables operation in aqueous solvents [23,36]. Protein scaffolds, supramolecular cage assemblies or heterogeneous supports can be used to control the hydrophilic/hydrophobic catalytic environment of the functionalized [2Fe2S] subunit (isolated or dye-linked).

Considering the primary and extended coordination spheres in the synthesis of [2Fe2S] complexes provides opportunities to enhance the performance of light-driven hydrogen production by promoting electron and proton transfer [84,85], catalyst stability and reactivity [86], and catalyst solubility in aqueous solutions [87,88].

Herein, we present a comprehensive review of [FeFe]-hydrogenase inspired catalysts for light driven hydrogen production, highlighting the most recent trends in this topic. The different systems will be presented in groups by increasing complexity and their chronological development (Fig. 6). In **Section 2**, catalysts inspired by the [FeFe]-hydrogenase ([2Fe2S]) active site will be described in the presence of PS and ED. The incorporation of PS in the catalytic system gives rise to photosensitizer-[FeFe]-hydrogenase active site model dyads [PS-2Fe2S], which will be reviewed in **Section 3**. Further, linking ED to the dyads results in triads [ED-PS-2Fe2S], reported in **Section 4**. In **Section 5**, we explore covalent or non-covalent interaction of [2Fe2S] with different supramolecular entities. Direct assembly of the catalyst on inorganic materials will be subject of **Section 6 and 7**. In **Section 6**, the inorganic component is a semiconductor, which acts as photosensitizer, whereas in **Section 7**, the inorganic component is simply a support. In **Section 8**, photoelectrochemical (PEC) hydrogen evolution catalyzed by photocathodes bearing [2Fe2S] catalysts is addressed.

2. Bioinspired [2Fe2S] catalysts: Bimolecular reactions

In this section, we focus on catalytic systems composed of a photosensitizer and a molecular catalyst with the [2Fe2S] unit, abbreviated as PS/[2Fe2S]. Diffusional PS/[2Fe2S] reactions are considered as bimolecular reactions where electron transfer takes place between the excited or reduced state of a suitable PS (depending on the quenching mechanism, see above) and an [2Fe2S] catalytic center. These catalytic systems offer the opportunity to screen a wide variety of [2Fe2S] catalysts using conventional PSs. The [PS:2Fe2S] ratio can be tuned to modulate the generation of reducing equivalents for optimal photocatalytic hydrogen production [14]. Additionally, [2Fe2S]-containing molecular catalysts have the following advantages: i) the synthesis of the biomimetic model is often relatively simple, following well-established strategies; ii) the redox properties and stability can be adjusted by replacing ligands in the first coordination sphere or by incorporating functionalities in the second coordination sphere via the dithiolate bridging group [82,86,89]; iii) electrochemical/spectroscopic characterization and computational elucidation of reaction mechanisms can be applied to well-defined molecular catalysts [24].

Inspired by these features, herein we review bioinspired [2Fe2S] catalysts that have been used in molecular photocatalysis systems, the structures of which are shown in Fig. 7**.** Their performance in light-driven hydrogen production reactions, as measured in turnover number (TON), along with the applied PS and selected reaction conditions are detailed in Table 1.

In 2007, electron transfer between a PS and a [2Fe2S] active site was demonstrated by Sun and co-workers. They identified reduced $Ru(bpy)_3^+$ species photogenerated by reductive quenching using a diethyldithiocarbamate sacrificial agent with a strong driving force for electron transfer from $Ru(bpy)_3^+$ to the [2Fe2S] active site $\{(\mu\text{-}SCH_2)_2X)\}[Fe(CO)_3)_2]$ (X: CH_2 or $NCH_2C_6H_5$). Time-resolved optical spectroscopy showed a decrease in the lifetime of this strong reductant $Ru(bpy)_3^+$ in the presence of the [2Fe2S] complex, con-

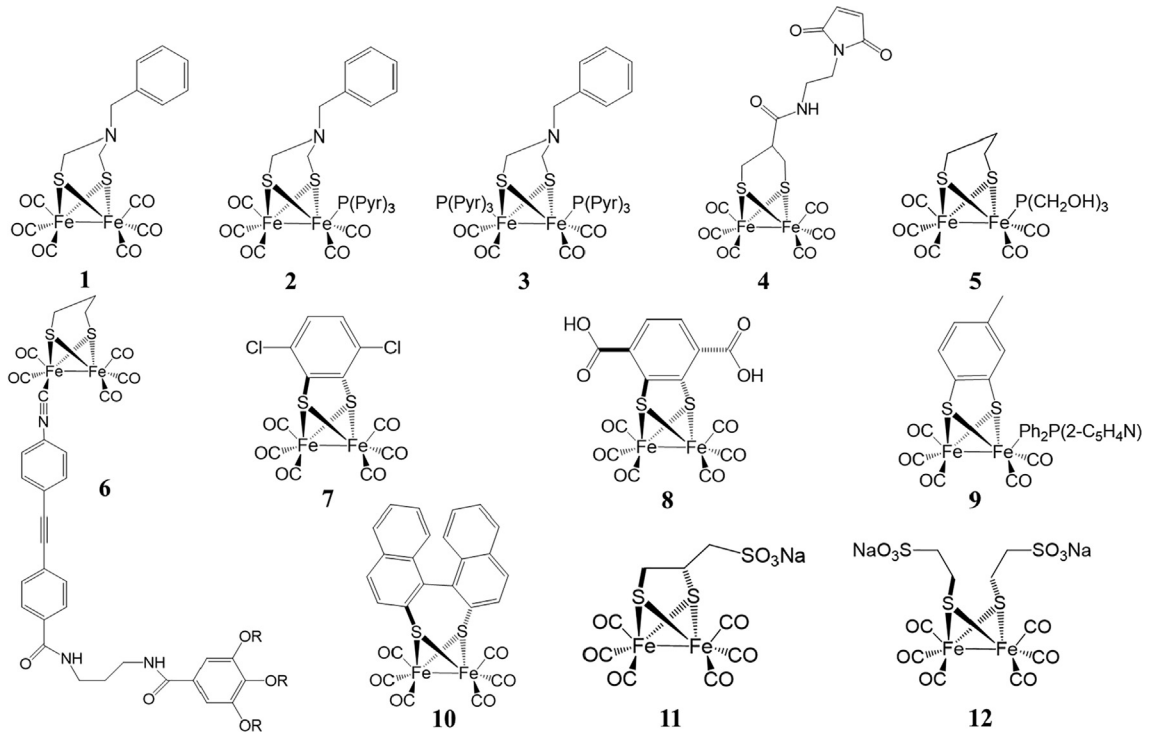

Fig. 7. Structures of biomimetic [2Fe2S]-hydrogenase catalysts that operate in conjunction with a PS reported in literature.

Table 1
Photocatalytic performance of artificial biomimetic [FeFe]-hydrogenase molecular photocatalysts [2Fe2S] in light-induced hydrogen formation and the conditions selected.

Entry	[2Fe2S] MC	PS	Selected conditions[1]	Light	Time	TON[2]	Ref.
1	**1**	$Ru(bpy)_3^{2+}$	H_2O/MeCN (1:1), 1 mM **1**, 0.1 mM PS, 100 mM AscOH, pH = 3.7	Xe lamp (500 W), λ > 400 nm	3	0.78	[91]
2	**2**	$Ru(bpy)_3^{2+}$	H_2O/MeCN (1:1), 1 mM **2**, 0.1 mM PS, 100 mM AscOH, pH = 3.7	Xe lamp(500 W), λ > 400 nm	3	4.3	[91]
3	**2**	$[Ir(ppy)_2(bpy)]^+$	Acetone/H_2O (9:1), 0.05 mM **2**, 0.05 mM PS, 140 mM TEA, pH = 11.0	Xe lamp (500 W), λ > 400 nm	8	466	[98]
4	**3**	$Ru(bpy)_3^{2+}$	H_2O/MeCN (1:1), 1 mM **3**, 0.1 mM PS, 100 mM AscOH, pH = 3.7	Xe lamp (500 W), λ > 400 nm	3	1.7	[91]
5	**4**	$Ru(bpy)_3^{2+}$	H_2O/THF (1:0.04), 2.1 μM **4**, 140 μM PS, 200 mM, $AscO^-$, pH = 4.5	Hg lamp (power not specified), λ > 400 nm	2	180	[100]
6	**5**	Eosin Y	EtOH/H_2O (1:1, v/v) solution, 0.1 mM **5**, 1.0 mM PS, 10% TEA, pH = 10	LED (3 W), λ > 450 nm	15	226	[101]
7	**6**	MPA–CdTe	Water, 156 μM **6**, 50 μM PS, 85.2 mM AscOH, pH = 4.03	Hg lamp (500 W), λ > 400 nm	10	505	[103]
8	**7**	$Ru(bpy)_3^{2+}$	DMF/H_2O (1:1), 14 μM **8**, 140 μM PS, 100 mM AscOH, pH = 5.5	Lamp not specified, λ = 455–850 nm	2.5	200	[110]
9	**8**	$Ru(bpy)_3^{2+}$	Water, 59 μM **9**, 0.5 mM PS, 100 mM AscOH, 1 M acetate buffer, pH = 5.0	LED (power not specified), λ > 470 nm	2.5	1.7	[111]
10	**9**	TPP-GO	EtOH/H_2O (1:24), 4.8 μM **10**, 44 μM PS, 1.8 mM cysteine, pH = 1.5	Hg lamp, (450 W), λ > 380 nm	5	2.82	[112]
11	**10**	Eosin Y	MeCN/H_2O (1:1), 0.2 μM **11**, 0.2 μM PS, 10 % TEA, pH = 10.0	Xe lamp, (300 W), λ > 420 nm	2	224	[114]
12	**11**	$Ru(bpy)_3^{2+}$	Water, 0.1 mM **13**, 0.4 mM PS, 100 mM AscOH, pH = 4.0	Hg lamp, (500 W), λ > 400 nm	4	88	[115]
13	**11**	CdSe QD	Water, 1 μM **13**, 5.2 μM PS, 200 mM AscOH, pH = 4.0	LED (power not specified), λ > 450 nm	12	18,800	[116]
14	**12**	$Ru(bpy)_3^{2+}$	Water, 1 μM **14**, 0.1 mM PS, 200 mM AscOH, pH = 4.0	LED (power not specified), λ > 450 nm	6	178	[116]
15	**12**	CdSe QD	Water, 1 μM **14**, 5.2 μM PS, 200 mM AscOH, pH = 4.0	LED (power not specified), λ > 450 nm	12	26,500	[116]

[1] Solvents and reagents abbreviations: MeCN: acetonitrile, THF: tetrahydrofuran, EtOH: ethanol, DMF: N,N-Dimethylformamide, H_2O: water, AscOH: ascorbic acid, $AscO^-$: ascorbate, TEA: triethylamine.
[2] TON based on [2Fe2S] catalyst.

firming the visible light-driven intermolecular electron transfer and serving as proof-of-concept for future photochemical hydrogen production experiments catalyzed by [2Fe2S] complexes [90]. Sun et al. later reported the first bimolecular system for light-induced hydrogen production using AscOH as both a proton source and reductive quencher [91].

Since most diiron hexacarbonyl complexes are gradually degraded under light irradiation, resulting in CO-release from the complexes to the reaction media [92], replacement of CO by common phosphine ligands improves the photostability and raises electron density of the [2Fe2S] core. However, functional analogues of [2Fe2S] active sites with strong electron-donating phosphines ligands are characterized by cathodically shifted reduction potentials that make electron transfer from the PS to the [2Fe2S] complex thermodynamically challenging [93–95]. Accordingly, [2Fe2S] complexes with weaker electron donor N-pyrrolyl phosphines ($P(Pyr)_3$) ligands [96,97] were evaluated for photochemical hydrogen production (Fig. 7: **1, 2** and **3**). In water/acetonitrile solution (1:1), the monosubstituted $P(Pyr)_3$ diiron complex **2** showed the highest photostability and catalytic activity achieving a TON

of 4.3 per catalyst (Table 1, entry 2). This result was justified by the increased feasibility of electron transfer from $Ru(bpy)_3^+$ to **2** due to the small cathodic shift in reduction potential (ΔE = 30 mV) compared to the all-CO diiron complex **1**, thus resulting in the highest rate of hydrogen production (6.7×10^{-7} mol/min) because of the photostability provided by the $P(Pyr)_3$ ligand [91]. However, the diiron catalyst still decomposed by CO ligand release under light irradiation, as detected by FTIR spectroscopy, limiting TONs. Nevertheless, this work established and demonstrated the fundamentals of photochemical hydrogen production using bioinspired [2Fe2S]. Under optimized conditions, catalyst **2**, a cyclometalated iridium (III) PS and triethylamine (TEA) as a sacrificial ED working at basic pH in acetone/water provided a TON of 466 after irradiation for 8 h [98]. Additionally, it was reported that the performance of this system is limited by the decomposition of the iridium PS [99], since the re-addition of cyclometalated iridium complex after 8 h of reaction re-established activity at the initial rate.

Following the structural skeletons of **1, 2, 3** but replacing the amine in the adt bridge with a methylene resulted in [2Fe2S] complexes **4**, **5** and **6** (Fig. 7) with a propyldithiolate (pdt) bridge. Inagaki et al. carried out the synthesis of the [2Fe2S] complex **4** tethered with a maleimide group and all-CO ligands and grafted it onto a heterogeneous support (see **Section 7**) [100]. Working in a homogeneous system using the photosensitizer $Ru(bpy)_3^{2+}$ and AscOH as a sacrificial agent in 4% THF aqueous solution under optimized conditions (Table 1, entry 5), a remarkable TON of 180 was obtained. However, decomposition of the catalyst was observed after 20 min under irradiation. The bioinspired diiron complex **5** (Fig. 7) reported by Sun and co-workers was designed with a simple structure containing a pdt bridge and a CO ligand replaced by a water-soluble phosphine ($P(CH_2OH)_3$) [101]. In this case, they used an inexpensive xanthene PS, Eosin Y, and TEA as ED in water–ethanol solution under alkaline conditions (Table 1, entry 6). This system displayed a great efficiency for hydrogen production with a TON of 226 after 15 h of reaction under visible light irradiation. A unique mechanism for photocatalytic hydrogen formation was proposed in this photosystem because the high reduction potential of **5** precludes the electron transfer (ET) from the xanthene dye. EPR, fluorescence transient absorption, time-resolved UV–Vis and thermodynamic studies elucidated an alternative pathway based on the formation of neutral alkyl radicals $Et_2N\dot{C}HCH_3$ [102] by reductive quenching of the triplet excited state of the PS. This directs ET from these photogenerated TEA radicals towards **5**, enabling the hydrogen formation. Using the same diiron dithiolate catalytic structure as **5**, Wu et al. reported the [2Fe2S] complex **6** (Fig. 7) by exchanging a terminal CO at the proximal iron by an isonitrile ligand that contains multiple ether groups [103]. This functionality resulted in a water-soluble molecular photocatalyst that was employed along with a CdTe quantum dot PS stabilized with 3-mercaptopropionic acid (MPA-CdTe) and AscOH as a sacrificial ED and proton source. Under optimized conditions (Table 1, entry 7), this three-component system showed high efficiency for light-induced hydrogen formation achieving a TON of up to 505 and a turnover frequency (TOF) of 50 h^{-1}, the highest photocatalytic activity reported using [2Fe2S] thus far (Fig. 7, **1-5**).

An appropriately substituted aromatic dithiolate bridgehead is a promising design strategy for a bioinspired [2Fe2S] to overcome the limitations inflicted by the relatively irreversible reductions at negative potentials that are typical for aliphatic dithiolate bridged catalysts. Some reviews on aromatic dithiolate-bridges incorporated in [2Fe2S] mimics have highlighted the interest in these compounds [104,105] due to: i) their structural robustness and rigidity that enhance the integrity of the reduced [2Fe2S] cluster, stabilize hydride intermediates and avoid dimerization or degradation by loss of CO ligands; ii) the tunability of redox properties by substituents at the conjugated bridges; iii) the exhibition of reversible reduction processes in the absence of substrate; iv) the possibility of incorporation, encapsulation or chemisorption in supramolecular scaffolds, heterogeneous supports or electrodes for subsequent application in electro- and photocatalytic processes.

Substituted benzenedithiolate (bdt) bridges incorporated in diiron complexes have been mainly investigated for their redox-tunable properties and high synthetic yields [106,107]. In 2008, Ott et al. investigated the electron-withdrawing effect in diiron arenedithiolate complexes ($[Fe_2(\mu\text{-}S_2Ar)(CO)_6]$) that featured different aromatic moieties (Ar), *i.e.* benzene, toluene, 3,6-dichlorobenzene and quinoxaline. A direct relationship was found between increased electron-withdrawing character of the bridging ligands and a lower electron density of the diiron core, resulting in a decreased applied potential that is needed for electrocatalytic proton reduction [108]. Electron-withdrawing bridging ligands however also weaken the Fe-S bonds, leading to a somewhat compromised complex stability. Later, Felton et al. [109] corroborated this study by evaluating analogous diiron bdt systems with chlorine substituents as electron-withdrawing groups.

Some representative examples of [2Fe2S] with bridgehead aromatic substituents applied in hydrogen photoproduction are shown in Fig. 7 (**7**–**10**). Building on their previous findings, Ott and co-workers reported the use of $[Fe_2(\mu\text{-}Cl_2bdt)(CO)_6]$ (Cl_2bdt = 3,6-dichlorobenzene-1,2-dithiolate) complex **7** with two electron-withdrawing chloride substituents as catalyst for light-driven hydrogen evolution [110]. The photochemical system consisted of **7**, $Ru(bpy)_3^{2+}$ as a PS and $AscO^-$ as a sacrificial ED in a DMF/H_2O mixture to ensure the complete solubility of all reaction components. Under optimal conditions, a TON of 200 and a TOF of 2.7 min^{-1} was obtained (Table 1, entry 8). DFT calculations and transient absorption spectroscopy suggested that the catalytic cycle occurred by intramolecular electron transfer. The delivery of the second electron to **7** was found to be the limiting step. The analogous complex **8**, *i.e.* [FeFe]-(dcbdt)$(CO)_6$ (dcbdt = 1,4-dicarboxylbenzene-2,3-dithiolate), contained two carboxylic groups at the aromatic ring [111], offering the possibility for incorporation in heterogeneous system (see **Section 7**). This photocatalyst was first evaluated in a completely water-soluble photosystem using $Ru(bpy)_3^{2+}$ as PS and $AscO^-$ as ED in an acetate buffer medium at pH = 5.0, but low TON values were obtained (Table 1, entry 9).

Tolyl-functionalized monophosphine substituted diiron complexes were synthesized by Jang et al. to study how distinct monophosphine ligands effect the reduction potentials for catalytic hydrogen production [112]. Using a different photocatalyic system, tetraphenylporphyrin (TPP) covalently linked to graphene oxide (GO) as a PS and cysteine were used to further simulate the protein environment in the [FeFe]-hydrogenase enzyme [113]. The analysis of the diiron complex by UV/Vis, fluorescence emission and time-resolved fluorescence techniques suggested that the high absorptivity and electrical conductivity of the GO improved electron transfer from the photosensitizer to the catalyst. The tolyl-functionalized diiron complex with a monophosphine ligand $[Fe_2(CO)_5(L)\{\mu\text{-}SC_6H_3(CH_3)S\}]$ (L = $Ph_2P(2\text{-}C_5H_4N)$ represented as **9** in Fig. 7 showed the lowest reduction potential for catalytic H_2 evolution. With a TON of 2.82, **9** exhibited superior photocatalytic results (Table 1, entry 10) compared to the other diiron complexes synthesized in this work. The experimental results demonstrated that the presence of the N heteroatom in pyridine plays a fundamental role in accelerating proton transfer to the catalytic center, thereby enhancing photocatalytic hydrogen production.

A new contribution in diiron complexes with substituted bridgehead aromatic dithiolate compounds was reported in 2016 by Hou et al. who synthesized the biomimetic complex **10** $[(\mu\text{-BNT})Fe_2(CO)_6]$ (BNT=(R)-1,1′-binaphthalene-2,2′-dithiol) with a binaphthalene-derived ligand with a high electron-withdrawing

capacity [114]. The diiron complex **10** produced hydrogen with high efficiency under visible light irradiation in a homogeneous photocatalytic system consisting of **10**, Eosin Y xanthene PS (EY^{2-}) and TEA as sacrificial ED in MeCN:H_2O (1:1) solution. Fluorescence experiments elucidated the electron transfer pathway via the reductive quenching mechanism between the $^{3*}EY^{2-}$ triplet excited state and TEA as reported previously [101]. By optimizing key photoreaction parameters, a TON of 224 per catalyst was obtained (Table 1, entry 11), the highest value for [2Fe2S] compounds with bridgehead aromatic substituents applied in light-driven hydrogen evolution.

Another subset of [2Fe2S] complexes are those with hydrophilic groups incorporated in the bridging dithiolate ligand. These compounds are more stable and soluble in aqueous solution. Wu and co-workers designed water-soluble [2Fe2S] complexes by introducing hydrophilic sulfonate groups into the dithiolate bridge (Fig. 7, **11 and 12**). In 2012, they reported complex **11** incorporating a propane sulfonate group linked to the dithiolate ligand [115]. The photosystem using a $Ru(bpy)_3^{2+}$ photosensitizer and AscOH as an ED and proton source was evaluated in aqueous solution, organic phase or in a mixture of organic solvent and water in order to observe the effect of reaction media on the efficiency of light-driven hydrogen evolution. Under optimal conditions (Table 1, entry 12), the highest photocatalytic performance was obtained using water as a homogeneous solvent system, achieving a TON of 88 based on **11**. The rationale for the higher activity in water than in organic solvents was clarified by spectroscopic analysis and electrochemical studies. The reduction potential of **11** was more positive in water and so favored the electron transfer (ET) from the PS to the photocatalytic diiron center. In addition, the extended lifetime of the reduced state of the PS generated through reductive quenching and the facile release of protons and $AscO^-$ reducing species from the sacrificial ED further contributed to the efficiency of the photocatalytic system for hydrogen production in water.

Four years later, this research group reported an attractive comparative study of light-induced hydrogen production using a water-soluble homogeneous photosystem consisting of: 1) the previous [2Fe2S] **11** or a new [FeFe]-hydrogenase active site model with two sulfonate groups incorporated in the dithiolate site (Fig. 7, **12**) as proton reduction catalyst, 2), cadmium-selenide quantum dot (CdSe QDs) or molecular $Ru(bpy)_3^{2+}$ as photosensitizers and 3) AscOH as the ED [116]. Motivated by the unparalleled record TON (505) obtained using CdTe QDs (Table 1, entry 7), Wu et al. selected this type of photosensitizers due to their wide absorption in the visible spectrum and dispersibility in water [117,118]. The photocatalytic activity of [2Fe2S] **12** using the Ru $(bpy)_3^{2+}$ photosensitizer showed an increase in TON up to 178 (Table 1, entry 14) compared to the TON of 88 obtained for [2Fe2S] **11** in the earlier work [115]. The oxidative quenching of the CdSe QDs system by the diiron complexes **11** and **12** with hydrophilic sulfonate substituents is characterized by a high driving force for electron transfer, resulting in enhanced photocatalysis compared that using $Ru(bpy)_3^{2+}$ as PS. The TON values of the CdSe QDs system were as high as 18,800 and 26,500 for **11** and **12**, respectively (Table 1, entry 13 and 15), the best catalytic performance reported in bimolecular photocatalytic reactions.

3. Photosensitizer-[2Fe2S] dyads: [PS-2Fe2S]

Biomimetic models of the [FeFe]-hydrogenase active site have been covalently linked to molecular photosensitizers for light-induced hydrogen production. Photosensitizer-[2Fe2S] dyads, [PS-2Fe2S], organize both components with high space and distance control. These multicomponent complexes promote fast intramolecular electron transfers and charge separation, and can avoid recombination between the redox states generated during the photocatalytic cycle. The initial step for photochemical hydrogen production in covalently linked dyads is often the formation of reduced $Fe^{I}Fe^{0}$ species by oxidative quenching, whereas bimolecular systems often operate through the reductive quenching of the excited PS* by an ED [89]. The molecular engineering of [PS-2Fe2S] is based on two different design strategies: (1) In the first approach, the PS and the catalytic cluster [2Fe2S] are connected through the organic dithiolate bridge, or (2) the PS is coordinated directly to one of the iron centres through a ligand in the first coordination sphere (Fig. 8).

The first example of strategy (1) was reported already in 2003, when ruthenium (II) bipyridine PS were covalently linked to [2Fe2S] systems through their organic dithiolate bridges (Fig. 9, **13 and 14**). [PS-2Fe2S] **13** [119] was synthesized via palladium-mediated cross-coupling protocols using an acetylene-functionalized ruthenium bis(terpyridine) complex with well-defined geometry [120] and an adt-bridged dinuclear iron complex. Spectroscopic and electrochemical studies of [PS-2Fe2S] **13** revealed that oxidative quenching of the photoexcited $^{*}[Ru(terpy)_2]^{2+}$ by the diiron complex was uphill by 0.59 eV [121]. [PS-2Fe2S] **14** consisting of an amino-functionalized complex of the diiron active site linked to a carboxylic acid of a ruthenium (II) tris-bipyridine PS was prepared by the same group, and laid out the concept for light-driven hydrogen evolution from dyad systems [45]. Hydrogen formation by an oxidative quenching mechanism of the Ru excited states was however not feasible due to the reduction potentials of the [2Fe2S] sites being too negative. Consequently, the free energy change for photo-driven electron transfer was positive and the reduced state of the [2Fe2S] catalytic unit thermodynamically out of reach.

Following strategy (1) and based on the synthesis of a [PS-2Fe2S] previously proposed by Song et al. [122], Sun and co-workers prepared the [PS-2Fe2S] assembly **15**, consisting of a metalloporphyrin (zinc tetraphenylporphyrin) and a pyridyl-functionalized [2Fe2S] that are tethered through an axial coordination bond (Fig. 9) [123]. Porphyrins as photosensitizers offer multiple advantages, including their ability to absorb high proportions of the solar spectrum, while also having long lifetimes of their triplet excited states [124,125]. The non-covalent interac-

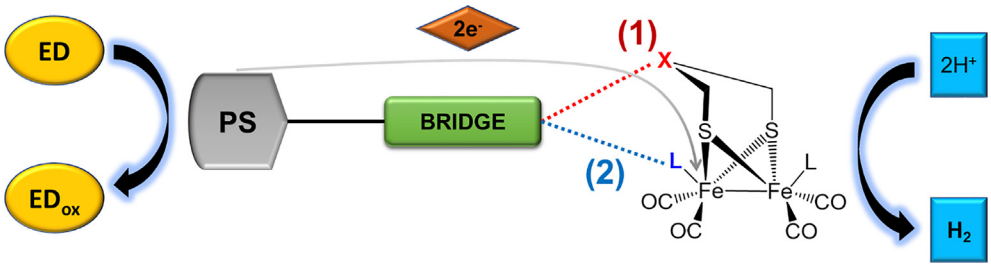

Fig. 8. Schematic representation of photosensitizer-[2Fe2S]-hydrogenase dyads [PS-2Fe2S] structures for light-driven hydrogen production.

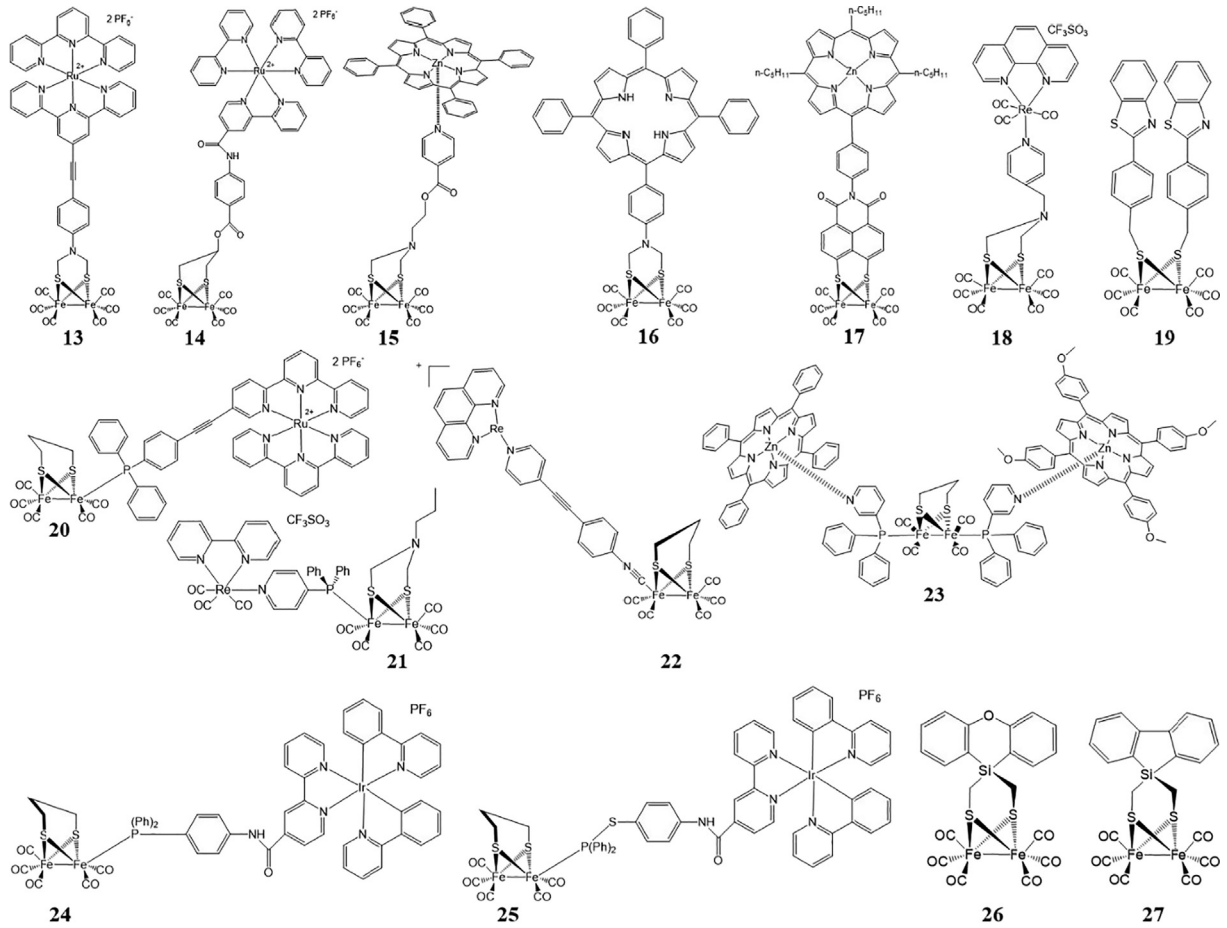

Fig. 9. Structures of photosensitizer-[2Fe2S]-hydrogenase dyads [PS-2Fe2S] reported in the literature.

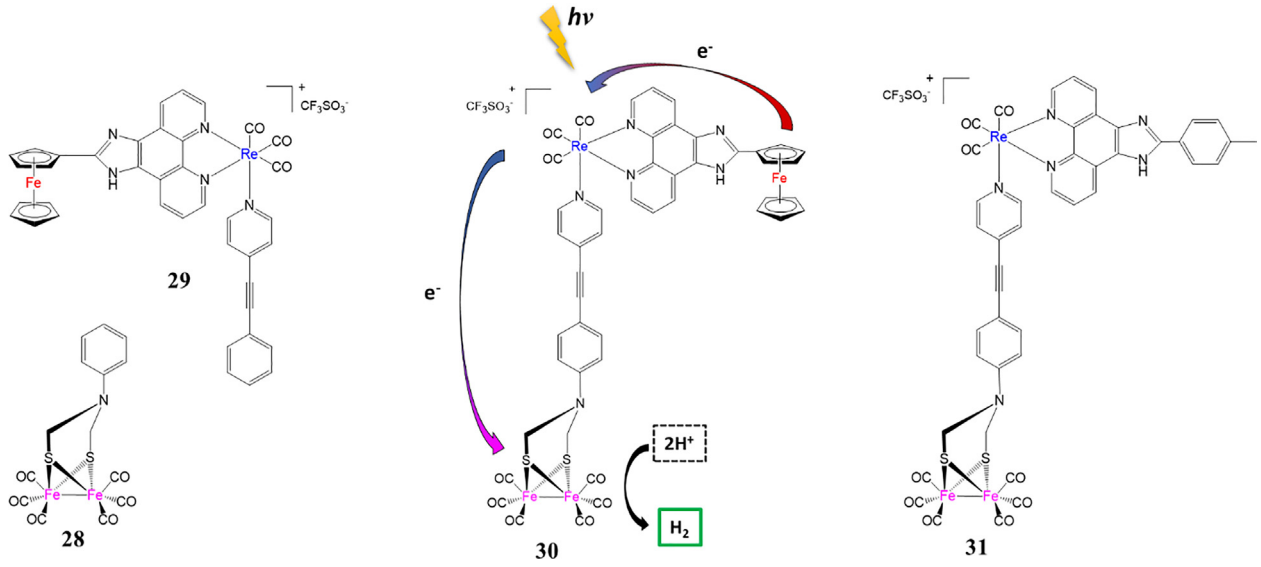

Fig. 10. Molecular structures of ferrocene-Re(I) complex-[2Fe2S] triad **30** and reference complexes **28**, **29** and **31** [145].

tions in this dyad system provide a great opportunity to obtain a long-lived charge separation, as demonstrated by lifetime fluorescence experiments. Both subunits in the dyad remain in dynamic equilibrium, which is advantageous to effectively avoid fast charge recombination after photo-induced electron transfer. Transient absorption studies by nanosecond flash photolysis were carried out, confirming the intramolecular electron transfer from the excited singlet state of the molecular metalloporphyrin to the [2Fe2S] center. Based on this, it was found that visible light drove hydrogen evolution using [PS-2Fe2S] **15**, 2-mercaptobenzoic acid (ArSH) as sacrificial ED and trifluoroacetic acid (TFA) in dichloromethane solution, albeit with low catalytic activity (Table 2, entry

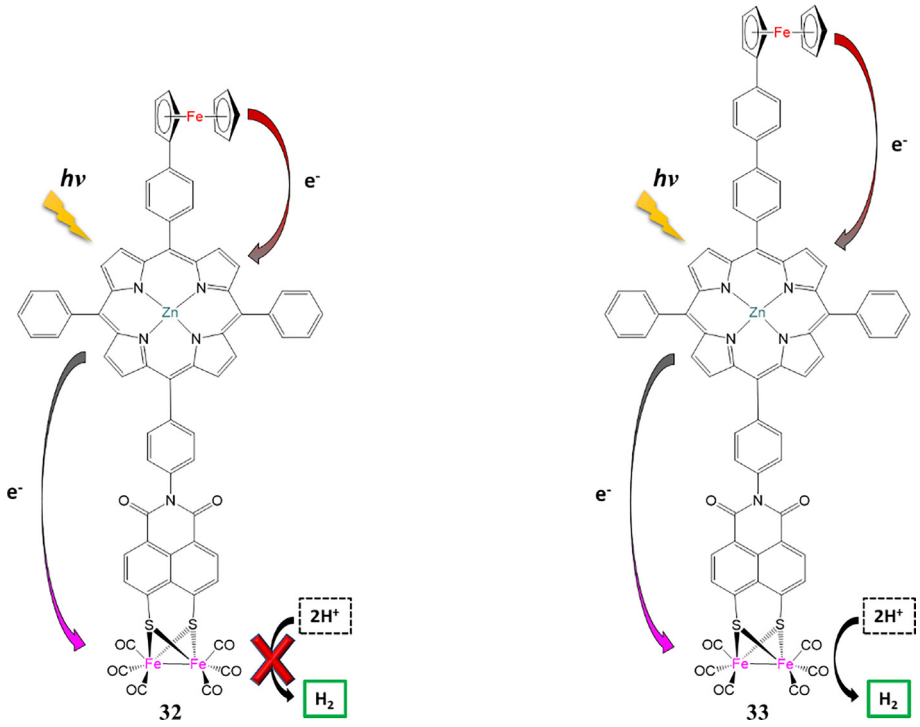

Fig. 11. Molecular structures of ferrocene-Zn metalloporphyrin-[2Fe2S] triad **32** and **33** for photocatalytic H_2 production [152].

1). Despite of a TON of 0.16, this system gained special interest by being the first photoactive dyad [PS-2Fe2S] for hydrogen formation based on the self-assembly principle.

Song and co-workers pursued an alternative design in [PS-2Fe2S] **16** where a photosensitizing tetraphenylporphyrin was covalently attached to the nitrogen heteroatom of a diiron adt complex (Fig. 9) [126,127]. This covalently assembled system was found to be photoactive for hydrogen production under suitable conditions through an intramolecular electron transfer process. However, its photocatalytic performance using ethanethiol (EtSH) as the sacrificial ED and TFA as the proton source remained low, with a TON of 0.31 (Table 2, entry 2). The [PS-2Fe2S] **17** (Fig. 9), analogues to **15** and **16**, was constructed by Wasielewski et al. through covalent linking a naphthalene monoamide dithiolate ligand of a diiron complex to a zinc porphyrin PS [128]. Incorporating the strongly electron-withdrawing naphthalene-imide stabilized the reduced diiron complex. This resulted in a less negative reduction potential, making the photoinduced electron transfer from the PS to the catalytic center thermodynamically feasible. Nevertheless, the slight increase in TON to 0.45 was still low for photocatalytic hydrogen formation reactions (Table 2, entry 3).

Hou and co-workers recently synthesized the [PS-2Fe2S] dyad **19** (Fig. 9) through covalent interaction of a [2Fe2S] complex with two organic chromophores through bridging thiolates [129]. Photo-induced intramolecular electron transfer from the photoexcited organic chromophores to [2Fe2S] was demonstrated by electrochemical and spectroscopic studies to be thermodynamically favorable. This inexpensive and easily accessible [PS-2Fe2S] **19** had the highest photocatalytic performance amongst the dyads synthesized by strategy (1) (Fig. 5), where the PS is connected to the catalytic center through the dithiolate bridge (Fig. 9, **13-19**). The construct achieved a TON of 31.8 in the presence of EtSH as sacrificial ED and TFA as proton source under visible- light irradiation (Table 2, entry 5).

Strategy (2) towards [PS-2Fe2S] dyads was first described by Ott et al. in 2006. In this study, the PS was decorated with a phosphine functionality which was used as a ligand to one of the iron atoms of $[Fe_2(pdt)(CO)_6]$ (pdt = propyldithiolate) [130] (Fig. 9, **20**). Two years later, Sun and co-workers synthesized [PS-2Fe2S] dyad **21** by coordination of an aminodiphenylphosphine-functionalized $[Re(bpy)(CO)_3py]^+$ PS to an azadithiolate (adt)-bridge diiron complex $[Fe_2adt(CO)_6]$ [131]. A drawback of the Re complex in the $[Fe_2adt(CO)_6]$-containing dyad **21** was its exclusive absorption in the UV spectral region, a part of the spectrum that was found destructive to the diiron site. The presence of the electron-donating phosphine ligand in the coordination sphere of both dyads **20** and **21** caused a cathodic shift of the oxidation and reduction potentials of around 300 mV compared to all-CO diiron complexes, rendering the oxidative quenching from the excited state of the photosensitizer (*PS) to the [2Fe2S] site thermodynamically unfavorable. In fact, there is a thermodynamic driving force for the reverse electron flow, *i.e.* the reductive quenching of the *PS by the [2Fe2S] center, giving rise to transient oxidized [2Fe2S] sites that are known to be structurally unstable. The possibility of an oxidative quenching mechanism in the rhenium-based dyad **21** was similarly difficult, considering the negative reduction potential of the [2Fe2S] site in this system. Alternatively, electron transfer in these [PS-2Fe2S] systems could proceed by reductive quenching in the presence of an easily oxidizable sacrificial external ED to produce a photogenerated reduced PS. Additionally, the incorporation of a second electron donor ligand (cyanide or phosphine) in the [2Fe2S] coordination sphere is suggested to generate protonation sites and shift the reduction potential to milder values in both dyads. In this way, structurally similar complexes may be active in photocatalytic hydrogen generation, while **20** and **21** have not yet been evaluated in light-induced reactions.

Further studies on rhenium-based dyads were reported in subsequent years. Several [PS-2Fe2S] systems were synthesized by coordination of various rhenium complexes to one of the iron centers in $[\mu\text{-}S_2(CH_2)_3]Fe_2(CO)_5CN$ [132]. The highest TON of 0.14 was obtained for [PS-2Fe2S] **22** (Fig. 9) in a mixture of solvents (MeCN/MeOH/H_2O) in which MeOH was used as sacrificial ED (Table 2, entry 6). Spectroscopic studies revealed that the ^{3}MLCT state of

the Re(I) complex in the dyad was completely quenched by intramolecular electron transfer from the diiron catalytic center. Subsequent studies by Liu et al. showed improved photocatalytic hydrogen production using rhenium-based dyads. These authors synthesized [PS-2Fe2S] **18** (Fig. 9) by covalent binding of a rhenium PS to the pyridyl-attached azadithiolate diiron complex (strategy 1, Fig. 5) obtaining a TON of 11.8 (Table 2, entry 4) [133].

Another approach by Reek et al. assembled the chromophore-associated structure [PS-2Fe2S] **23** (Fig. 9) by connecting two different types of zinc(II) porphyrin to a pyridyl-functionalized phosphine ligand coordinated to the diiron core [134]. Under certain reaction conditions (Table 2, entry 7), a TON of 1.96 was obtained using [$NiPr_2EtH$][OAc] ionic liquid as ED. This study was modular in design and enabled optimization of photocatalytic hydrogen evolution efficiency by altering the building blocks while keeping a controlled distance.

Chen et al. introduced a novel [PS-2Fe2S] dyad system, **24** and **25** (Fig. 9), by covalent anchoring of a photosensitizing iridium molecular complex to a [2Fe2S] complex via amide bonds [135]. Both molecular photocatalysts, **24** and **25,** showed a high yield for photoinduced hydrogen production under visible light (>400 nm) with TON values of 82 and 127, respectively, using TEA as ED in an acetonitrile/water mixture (Table 2, entry 8 and 9). Replacing TEA by TEOA reduced the catalytic activity in the system, demonstrating the superior electron donor ability of TEA in light-driven hydrogen evolution using iridium-based photosensitizers [98,136]. The difference in hydrogen generation performance by dyads **24** and **25** stems from the addition of an S atom in structure **25** that changes the coordination configuration and electron distribution with respect to dyad **24**. Density functional theory (DFT) studies and spectroscopic measurements showed that the presence of the sulfur atom in the second coordination sphere of [PS-2Fe2S] **25** reduces the charge density and conjugation in the diiron core. The resultant greater electron-accepting ability prevents the unwanted back electron-transfer and increases light-induced hydrogen formation.

In view of the moderate activities for hydrogen production obtained under light irradiation using dyads containing ruthenium- or rhenium-based photosensitizers or organic fluorophores, a new class of dyads that is based on silicon-containing [2Fe2S] complexes has emerged in recent years [137,138]. A compact, heavy-metal-free PS in direct proximity to diiron active sites is an advantageous property of these systems. Silicon-aromatic compounds have attracted great interest for their broad light emission and absorption range, electroluminescent properties and physicochemical characteristics [139–141]. Based on this, Weigand et al. prepared silicon-containing [2Fe2S] complexes by reacting 1,1̂-bis-(chloromethyl)-1-silafluorene and the diiron complex [(μ-$S)_2Fe_2(CO)_6$] affording [PS-2Fe2S] **27** (Fig. 9) [142]. Electrochemical measurements, electroluminescence studies and DFT calculations demonstrated that the silicon-aromatic compound promoted effective photo-induced intramolecular electron transfer to the [2Fe2S] site. The dyad generated hydrogen photochemically using TFA as a proton source and TEA as the ED. The TON of 29 after 13 h of irradiation (Table 2, entry 10) can be considered a significant improvement compared to many of the other dyads. In 2017, Weigand et al. proposed an enhanced photocatalytic system using the same [PS-2Fe2S] **27** and modified concentrations of TFA and TEA, respectively (Table 2, entry 12) [143]. After 7 h of illumination, a TON of 539 and a TOF of 77 $h^{-1}$was obtained under optimal reaction conditions. The TOF is the highest reported catalytic rate for dyad systems with a diiron complex directly coordinated to a molecular PS. The same work presented an additional dyad consisting of a [2Fe2S] complex tethered to an alternative silafluorene unit, affording the [PS-2Fe2S] **26** (Fig. 9). Light-induced hydrogen evolution was evaluated under the optimal reaction conditions, achieving a TON of 389 (Table 2, entry 11). Additionally, DFT calculations, spectroscopic measurements and electrochemical analysis assigned the photocatalytic mechanism in these systems to an EECC pathway (where "E" represents an electrochemical reduction and "C" a chemical protonation) [73].

4. Molecular triads based on [2Fe2S] complexes [ED-PS-2Fe2S]

Triad systems [ED-PS-2Fe2S] integrate the electron donor, the photosensitizer, and the [2Fe2S] cluster, and thereby constitute the closest functional mimics to the natural [FeFe]-hydrogenase enzyme. The realization of fully functional artificial triad systems however presents numerous challenges. Apart from the obvious synthetic challenges, the main objective is to develop molecular building blocks that promote rapid electron transfer between the different functional units of the triad system. Competitive photophysical phenomena such as the recombination of charges in the sequential steps of photo-induced electron transfer (PET) must be avoided to achieve long-lived charge separation for photocatalytic hydrogen evolution.

Considering the design requirements, Wu et al. synthesized a molecular triad [ED-PS-2Fe2S] **30** consisting of a [2Fe2S] complex, [144] a Re-based PS and a ferrocene donor, together with the reference [2Fe2S] complex (**28)** and the rhenium (I) complex (**29)** (Fig. 10) [145]. The three components were chosen to exhibit a strong driving force for photo-driven electron transfer, while the long distance between the terminal ferrocene and the [2Fe2S] site as well as the weak electronic coupling between them were anticipated to prevent charge recombination during the photocatalytic reaction. Triad **30** and diiron complex **28** exhibited similar UV/Vis absorption bands characteristic of [2Fe2S] complexes at 300–400 nm and 450–600 nm and typical infrared vibrations corresponding to the CO ligands coordinated to the [2Fe2S] core. In contrast, complex **29** showed only two weak absorption peaks common to rhenium-based complexes at < 350 nm and > 400 nm attributed to ligand-to-ligand charge transfer (LLCT) and the $d\pi(Re) \rightarrow \pi^*(N\text{-}N)$ ^{1}MLCT state, respectively [146]. These results indicated that the ferrocene-appended rhenium(I) complex did not have significant electronic interaction with the [2Fe2S] cluster in the ground state. Electrochemical studies [147] corroborated the thermodynamic feasibility of a photo-induced electron transfer (PET) cascade to form the fully charge separated state with a reduced diiron site and an oxidized ferrocene donor. The PET dynamics were further examined by time-resolved absorption spectroscopy and electrochemical data. For the reference system, addition of the [2Fe2S] complex **28** to a solution of **29** resulted in a new transient absorption at 400 nm very similar to that observed also for the triad **30**. This absorption band is characteristic for [Fe^I-Fe^0] species, and agrees well with reference spectra obtained by electrochemical reduction of diiron complexes [148–150]. A significantly longer lifetime of the [Fe^IFe^0] species was shown for the triad **30** (>2 ms) compared to that of the combination of **28** and **29** (708 μs), highlighting the stability of the formed species. Accordingly, a decreased rate for back electron transfer was observed (k_{CR} = <0.5 × 10^2 s^{-1}) for triad **30** compared to that of the combination of **28** and **29** (k_{CR} = 1.41 × 10^3 s^{-1}). Thus, the [ED-PS-2Fe2S] **30** was anticipated to be a powerful photosystem candidate for light-induced hydrogen evolution. Indeed, triad **30** showed a higher TON (TON = 0.35 based on [2Fe2S] catalyst concentration) than the combination of **28** and **29** (TON = 0.04) for hydrogen evolution using AscOH as a proton and electron source. Despite not being a catalytic process (TON < 1), a multistep PET chain was established by assembling a ferrocene donor, a rhenium chromophore and a diiron catalyst for light-assisted hydrogen production.

The same group reported dyad **31** (Fig. 10) by fusing [2Fe2S] **28** with a complex derived from **29** without the ferrocene group. Characteristic transient absorptions of [$Fe^{I}Fe^{0}$] species analogous to those shown in the triad **30** could be observed upon laser excitation [151]. Hydrogen evolution experiments with 1,4-dihydropyridine as sacrificial ED and proton source were carried out with improved photocatalytic performance, resulting in a TON of 34 for dyad **31** and up to 47 for triad **30**.

In parallel, Wasielewski and co-workers developed [ED-PS-2Fe2S] systems **32** and **33** (Fig. 11) composed of a naphthalene monoamide (NMI) diiron complex [NMI-$Fe_2S_2(CO)_6$], and a ferrocene electron donor that is covalently linked to a zinc metalloporphyrin (ZnTPP) via one or two phenyl groups, respectively [152]. In these triads, the lifetime of the charge separated state was envisaged to be longer as compared to that in the previously reported dyad **17** [128] (see **Section 3**, Fig. 9). Interestingly, upon laser excitation to form the PS excited state, two competing pathways are observed. While in **32**, the main deactivation pathway for ^{1*}ZnTPP was energy transfer to ferrocene, the extra phenyl spacer in **33** decreased the electronic coupling between ferrocene and ZnTPP, thereby promoting the productive electron transfer to the diiron site instead. Consequently, the quantum yield for the fully charge separated state differ dramatically, amounting to 13 and 71 % for **32** and **33**, respectively. Owing to the extra phenyl spacer in **33**, also the lifetime of the charge separated state is considerably longer with to τ_{CR} = 67 ± 2 ns as compared to that of triad **32** (to τ_{CR} = 9 ± 1 ns). The increased charge separation lifetime was the main factor for triad **33** to catalyzed photo-driven hydrogen production (100 W Xe lamp, λ = 500–800 nm light). Unfortunately, a TON (based on catalyst) of only 0.56 was obtained after 14 h in CH_2Cl_2, which was explained by the decomposition of the photosystem, as evidenced by the detection of CO using gas chromatography (GC) and ESI-MS. When 2-mercaptobenzoic acid was tested as sacrificial ED, hydrogen generation did not increase as the oxidation potential of this ED is nearly identical to that of ferrocene [153].

The research papers discussed above show that a biomimetic [FeFe]-hydrogenase active site model can be covalently linked to a molecular PS and ferrocene ED. The resultant triads form an integrated artificial photocatalytic system with a multistep PET chain that can sustain long-lived reduced states at the [2Fe2S] site, which is key for efficient light-driven hydrogen production.

5. Supramolecular assemblies of [FeFe]-hydrogenase active site mimics

The assembly of supramolecular systems relies on non-covalent interactions between substrate and receptor molecules [154–157]. Molecular recognition, supramolecular catalysis and selective transport processes as concepts in these systems opened the door for chemists to gain precise control over matter and information at the supramolecular level [158]. With appropriate subunits integrated into a supramolecular complex, efficient and selective catalytic reactions could be carried out. Analogous to an enzyme's extended coordination sphere, supramolecular assemblies could be used to precisely create substrate and product channels, redox tuning, and specially tuned microenvironments for optimized catalysis.

With this goal in mind, supramolecular strategies have been implemented in the design of biomimetic models of the [FeFe] hydrogenase active site through non-covalent intermolecular interactions. Structural and electronic considerations in the construction of a supramolecular assembly for [2Fe2S] clusters are: 1) solubility and/or functionality in water, 2) buried sites for the diiron catalyst to avoid deactivation by oxygen, 3) proton-coupled electron transfer pathways in the outer coordination sphere. The scientific community has developed numerous approaches to analyze the influence of a protein matrix or supramolecular structure on [FeFe]-hydrogenase active site mimics.

5.1. Physical entrapment of [2Fe2S] active sites in supramolecular assemblies

5.1.1. Confinement of [2Fe2S] complexes in oligosaccharides and polysaccharides.

The enzymatic conversion of starch produces cyclodextrins (CyD), cyclic oligosaccharides consisting of macrocyclic rings of 6 (α), 7 (β), and 8 (γ) subunits of D-glucose linked by α-(1,4) glycosidic bonds giving rise to toroidal and rigid molecular structures with specific volumes. The hydrophobic interior cavity allows the inclusion of smaller molecules forming host–guest complexes, in which the guest molecule is encapsulated in the host CyD. The hydrophilic exterior renders the system water soluble while protecting the trapped complex in its interior.

Darensbourg and co-workers pursued the approach to insert molecular [2Fe2S] complexes into CyD macrostructures, and demonstrated the self-assembly of a sulfonate-functionalized [2Fe2S] complex **34** (Fig. 14) and β-CyD by spectroscopic studies and X-ray diffraction analysis. The resulting complex was stable in water. However, there was a decrease in electrocatalytic performance for proton reduction compared to that of the free complexes. Hindered by the insulating layer of β-CyD, large cathodic potentials were required to drive electron transfer processes [159,160]. Further studies by Sun et al. were reported for host–guest complexes with the same sulfonate-functionalized diiron complex **34** encapsulated into β-CyD and γ-CyD (Fig. 12**a**). Halogenated organic dyes were included as photosensitizers for photocatalytic hydrogen production in aqueous solution [161]. The diffusion and interaction of the xanthene-derived dye with the macromolecular cyclodextrin was intended to increase their electronic interaction. Under light irradiation using Eosin Y as PS and TEA as sacrificial ED at pH = 10, the β-CyD supramolecular system (**34/β-CyD-EY**) showed the best photocatalytic performance obtaining a TON of 75 after 24 h (Table 3, entry 1). This system resulted in 9-fold increase in TON, 16-fold improvement in quantum efficiency and 3-fold extension in lifetime compared to the system lacking cyclodextrin for light-induced hydrogen generation in aqueous medium.

This research group further used the same [2Fe2S] complex **34** and CdSe quantum dots (QDs). Both components were embedded on a thiolato-functionalized β-cyclodextrin (β-CyD-6-SH), establishing close proximity for the diiron catalyst and the PS (Fig. 12**b**) [162]. The incorporation of the diiron catalyst into the β-CyD-6-SH cavity improved the photocatalytic process and stability of the water-soluble hybrid system. Photocatalytic H_2 evolution experiments for the **34/β-CyD-6-S-CdSe QDs** supramolecular system using AscOH as ED demonstrated a maximum TON of 2370 after 30 h (Table 3, entry 2) and a TOF of up to 150 h^{-1} in the initial 10 h of the reaction. Maintaining a close distance between the CdSe QDs and the diiron complex through β-CyD-6-SH resulted in optimal electron transfer and charge separation between both functional units.

In acidic medium, the natural chitosan polysaccharide provides a chelating capacity through its polycationic character arising from the protonation of primary amines. The [2Fe2S] complex **1** (see **Section 2**, Fig. 7) and 3-mercaptopropionic acid (MPA)-capped CdTe quantum dots (MPA-CdTe QDs) with negative surface charges were incorporated into cationic chitosan (Fig. 12**c**) [163]. The supramolecular hybrid system was evaluated for photocatalytic hydrogen production using AscOH as ED in a methanol/water mix-

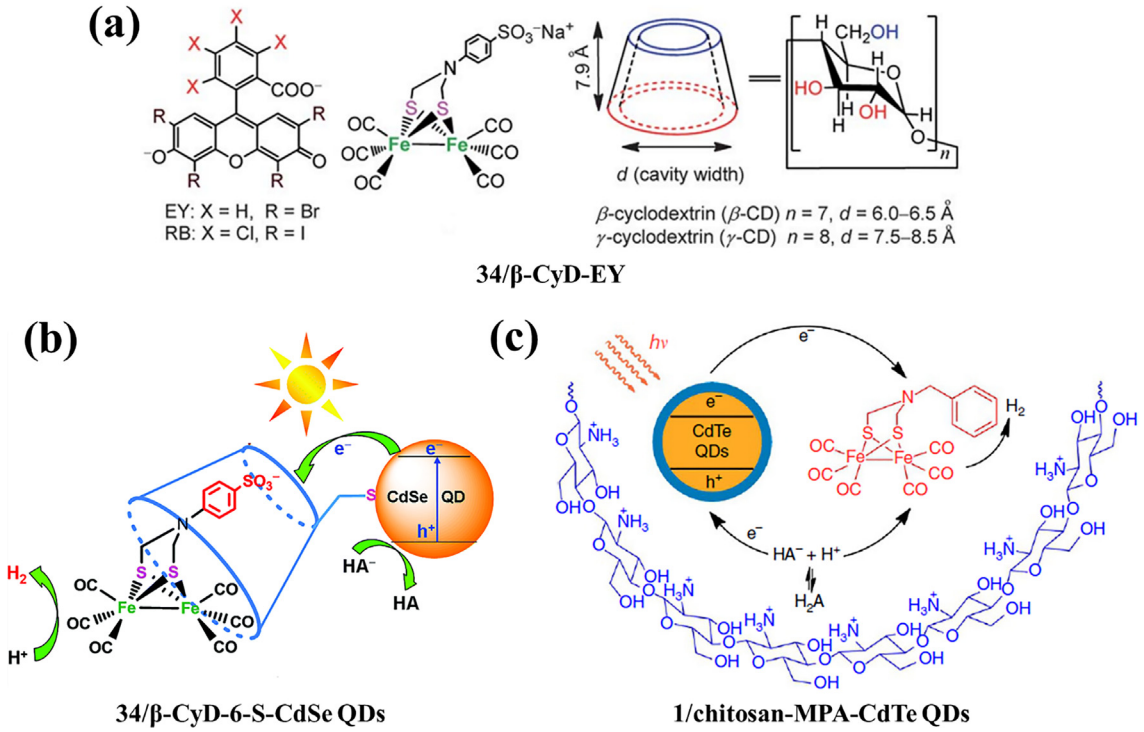

Fig. 12. (a) Cyclodextrin host–guest inclusions formed by incorporation of [2Fe2S] complex **34** and an organic halogenated xanthene dye (reproduced and modified from Ref. [161] with permission from The Royal Society of Chemistry), (b) Hybrid assembly of [2Fe2S] complex **34** and CdSe quantum dot linked through a thiolato-functionalized β-cyclodextrin for photocatalytic hydrogen evolution (reproduced and modified from Ref. [162] with permission from The Royal Society of Chemistry), and (c) chitosan-confined [2Fe2S] complex **1** and CdTe quantum dots for hydrogen photogeneration (reproduced and modified from Ref. [163] with permission of Springer Nature).

ture (1:3) at pH = 4.5. In addition, AscOH was crucial as proton source for the amine groups of chitosan and the catalytic intermediate of the diiron photoreduced complex. The self-assembled system (**1/chitosan-MPA-CdTe QDs**) showed a TON of up to 52,800 (Table 3, entry 3) and an initial TOF of 1.40 s^{-1}. Improvement in stability and catalytic performance from 8 to 60 h was especially dramatic, showing a 4160-fold increase in TON compared to the same system without chitosan.

5.1.2. Confinement of [2Fe2S] complexes in micelles.

Micelles are spherical macromolecular structures with an apolar interior that are formed from amphipathic molecules with surface polar groups. In the past decade, aqueous micelles prepared from surfactants have been used to simulate cell membranes to disperse [FeFe]-hydrogenase active site mimics in water. Some common surfactants used to form these micelles were sodium dodecyl sulfate (SDS), cetyltrimethylammonium bromide (CTAB), and dodecyltrimethylammonium bromide (DTAB), all featuring a charged surface and a hydrophobic cavity. Aqueous SDS-based micelles with negatively charged surfaces encapsulating water-insoluble diiron bdt complexes **35** (Fig. 14) were reported to be electrocatalytic for proton reduction in aqueous solutions [164,165]. Another study examined the molecular environment of complex **38** ($Fe_2(pdt)(CO)_6$, pdt = propanedithiolate) (Fig. 14) encapsulated in an aqueous DTAB-based supramolecular structure by infrared spectroscopy techniques. The results suggested that the diiron complex **38** was found in two environments: one that hydrogen bonds with water molecules penetrating the surfactant layer and the second similar to that of the complex in heptane solution. Additionally, this study revealed that water access to the interior of the hydrophobic micellar cavity was limited by the micelle size [166].

In 2010, Wu et al. carried out the first attempt at photocatalytic hydrogen evolution using an aqueous SDS-based micelle to incorporate the hydrophobic [2Fe2S] complex **1** (see **Section 2**, Fig. 7) and a rhenium-based PS [167]. Although the micelles promoted water solubility of the diiron complex, a very low TON value of 0.13 was obtained for the photosystem **1/SDS-Re(1)** in presence of AscOH as sacrificial ED (Table 3, entry 4). Diiron benzenedithiolate complexes [$(Fe_2(bdt)(CO)_4(L)_2$, L = $P(OMe)_3$] relevant to [FeFe] hydrogenases (**35**–**37**) (Fig. 14) were tested in combination with organic xanthene photosensitizers in aqueous SDS-based micelles for photochemical hydrogen production using TEA as the ED under alkaline conditions [168]. The supramolecular micellar photosystem **35/SDS-EY** achieved a TON of up to 117 and a TOF of 1.1 min^{-1} (Table 3, entry 5).

Recently, Wu and co-workers prepared a novel amphiphilic polymeric micelle (APM) from a polynorbornene random copolymer based on a hydrophobic alkyl chain (C_{12}) and three oligo(ethyleneglycol) chains with hydrophilic moieties [169]. This self-assembled macromolecular structure was used as a microreactor to confine the hydrophobic diiron propanedithiolate complex **38** [$(Fe_2(pdt)(CO)_6$]. Under optimized reaction conditions, the photosystem **38/APM-Ru(bpy)$_3^{2+}$** achieved a TON of 133 using $Ru(bpy)_3^{2+}$ as a PS and AscOH as ED in acidic aqueous solution at pH = 4.0 (Table 3, entry 6). The amphiphilic polymeric micellar system promotes interaction between the PS and the diiron catalyst in the microreactor pocket, improving the proton migration rate and thereby the efficiency of the photocatalytic process.

In another approach, [2Fe2S] complexes were tethered to a silafluorene sensitizer **27** (see **Section 3**, Fig. 9) and encapsulated in micelles formed by SDS (**27-SDS**) or CTAB (**27-CTAB**) [143]. The construct was evaluated for photochemical hydrogen generation in aqueous solution, using TEA as a sacrificial ED and TFA (2:1). The TONs of 139 and 148 achieved for **27-SDS** and **27-CTAB**, respectively, were the highest reported for micellar systems (Table 3, entries 7 and 8).

5.1.3. Adsorption of [2Fe2S] complexes into self-assembled vesicle membranes.

Functionalized vesicles with membrane-incorporated photosensitizers and [FeFe]-hydrogenase active site mimics have been developed for catalysis in aqueous solutions [170]. König et al. prepared self-assembled phospholipid vesicles with functionalized membranes by adsorption of the diiron complex **34** (Fig. 14) and $[Ru(bpy)_3]Cl_2$ photosensitizer onto the membrane (Fig. 13**a**). In a second approach, the amphiphilic ruthenium bipyridine photosensitizers ($[Ru(bpy)_2(bpy(CONHC_{12}H_{25})_2)]Cl_2$ or $[Ru(bpy)_2(bpy(CONHC_{12}H_{25})_2)]PF_6$) (Fig. 13**b**) were embedded in the membrane, while keeping **34** as the catalyst [171]. The integration of the PSs in close proximity to the diiron complex at the vesicular interface promoted strong electronic interaction, enhancing light-induced hydrogen production. Membrane functionalization with the catalytic subunit **34** and the photosensitizer $[Ru(bpy)_3]Cl_2$ was

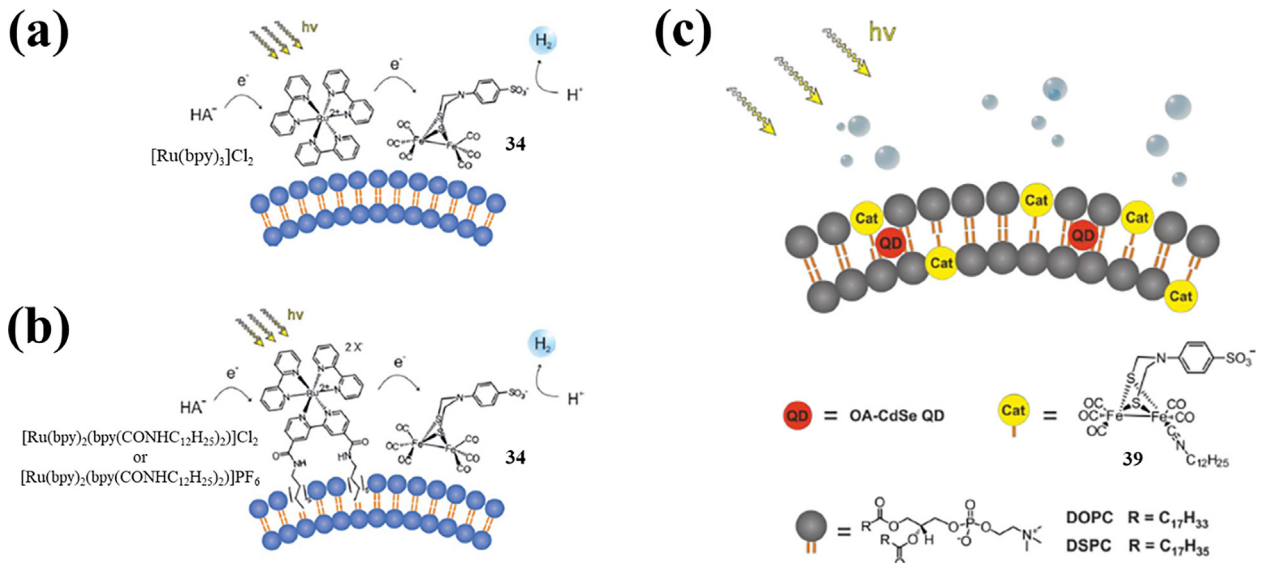

Fig. 13. Schematic representation of functionalized vesicular supramolecular systems prepared from (a) photosensitizer $[Ru(bpy)_3]Cl_2$ and diiron complex **34**, both adsorbed to the phospholipid membranes, (b) embedded ruthenium-based photosensitizers and adsorbed diiron complex **34** into phospholipid membranes, and (c) oleic acid capped CdSe quantum dots (OA-CdSe QDs) and proton reduction catalysts **39** incorporated into phospholipid membranes for light-induced hydrogen evolution. Reprinted and modified from Refs. [171,172] with permission from John Wiley and Sons.

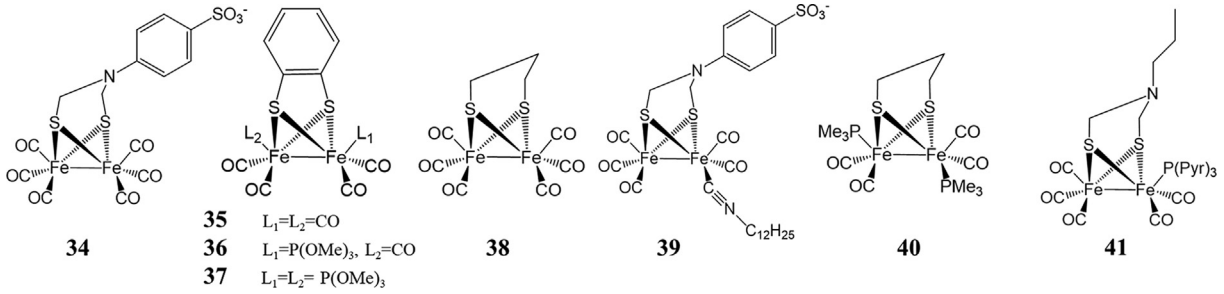

Fig. 14. Molecular structures of diiron compounds used in supramolecular systems.

Table 2
Photosensitizer-[2Fe2S]-hydrogenase dyads [PS-2Fe2S] in light-induced hydrogen formation and the selected conditions.

Entry	[PS-2Fe2S]	Selected conditions[1]	Light	Time (h)	TON[2]	Ref.
1	**15**	DCM, 25 μM **15**; 5 mM ArSH, 1 mM TFA	Xe lamp (500 W), λ > 400 nm	2	0.16	[123]
2	**16**	DCM, 0.1 mM **16**, 10 mM EtSH, 10 mM TFA	Hg lamp (500 W), λ > 400 nm	1	0.31	[127]
3	**17**	Toluene, 1 mM **17**, 1 M TFA	Xe lamp (100 W), λ = 500–800 nm	Unspecified time	0.45	[128]
4	**18**	MeCN, **18** (concentration value not available), 500 eq TEA	Xe lamp (500 W), λ > 400 nm	6.5	11.8	[133]
5	**19**	MeCN, 2.5 mM **18**, 0.01 M EtSH, 0.01 M HOAc	Xe lamp (500 W), λ = 355 nm	4	31.6	[129]
6	**22**	MeCN/MeOH/H_2O (3:2:1), 0.33 mM **21**, 0.10 mM HOAc (10 mM)	Hg lamp (500 W), λ > 400 nm	2	0.14	[132]
7	**23**	Toluene, 1 mM **22**, 10 mM ionic liquid [N^iPr_2EtH][OAc]	Xe lamp (180 W), λ > 390 nm	1.3	1.96	[134]
8	**24**	MeCN/H_2O, 0.2 mM **26**, 5 % TEA, pH = 10	Xe lamp (500 W), λ > 400 nm	4	82	[135]
9	**25**	MeCN/H_2O, 0.2 mM **26**, 5 % TEA, pH = 10	Xe lamp (500 W), λ > 400 nm	4	127	[135]
10	**27**	MeCN, 0.15 mM **27**, 0.25 mM TEA, 0.25 mM TFA	Hg lamp (15 W), λ = 254 nm	13	29	[142]
11	**26**	MeCN, 10 μM **26**, 100 mM TEA, 50 mM TFA, pH = 10	Hg lamp (15 W), λ = 254 nm	7	389	[143]
12	**27**	MeCN, 10 μM **27**, 100 mM TEA, 50 mM TFA, pH = 10	Hg lamp (15 W), λ = 254 nm	7	539	[143]

[1] Solvents and reagents abbreviations: DCM: dichloromethane, MeCN: acetonitrile, MeOH: methanol, H_2O: water, ArSH: 2-mercaptobenzoic acid, EtSH: ethanethiol, TFA: trifluoroacetic acid, HOAc: acetic acid, TEA: triethylamine.
[2] TON based on [2Fe2S] catalyst

studied for the production of hydrogen in acetonitrile/water (1:1) or pure water, with a TON of 4.2 and 3.5, respectively. In contrast, a TON of 20 was obtained using DOPC vesicles (dioleoyl-*sn*-glycero-3-phosphocholine) to encapsulate the catalyst and PS. The highest catalytic activity was achieved for the photosystem **34/DMPC-Ru(bpy)$_3^{2+}$** composed of [Ru(bpy)$_2$(bpy(CONHC$_{12}$H$_{25}$)$_2$)] PF_6) and the diiron complex **34** adsorbed on the vesicle prepared from the lipid DMPC (1,2-dimyristoyl- *sn*-glycero-3-phosphocholine). A TON of 59 was achieved using AscOH as sacrificial ED in acidic water (pH = 2.6) (Table 3, entry 9). Strongly acidic conditions favor the protonation of photoreduced [Fe^{I}Fe^{0}] species, a crucial intermediate in the catalytic cycle for hydrogen evolution, but decrease the formation of the $AscO^-$ ($pK_{a,1}$ = 4.17), which is key in regenerating the PS. The highly acidic pH of 2.6 in this study was due to the change in pKa and polarity values at the aqueous lipid interface, suggesting some influence on the electron–proton transfer features of AscOH which shifted the optimal pH to more acidic values.

In parallel, the same research group functionalized DOPC and DSPC (1,2-distearoyl-*sn*-glycero-3-phosphocholine) vesicles by co-embedding hydrophobic oleic acid-capped cadmium selenide quantum dots (OA-CdSe QDs), known for their excellent light-harvesting properties, and the sulfonate-functionalized [2Fe2S] complex **39** (Fig. 14) [172]. Under optimized conditions, the bio-inspired photosystem **39/DOPC-OA-CdSe QDs** (Fig. 13**c**) exhibited exceptional light-driven hydrogen evolution, achieving a maximum TON of 651 in purely aqueous AscOH solution (Table 3, entry 10).

5.1.4. Immobilization of [2Fe2S] complexes into hydrogels.

Hydrogels have shown promise in addressing the challenge of introducing [FeFe]-hydrogenase mimics to aqueous solutions using a non-covalent strategy. Commonly known as polymer gels, hydrogels have a wide range of applications due to their low cost, structural tunability, and high surface area. They possess a stable internal network that is compatible with the immobilization of [2Fe2S] active sites, facilitating the dispersion of these hydrophobic complexes in water [173]. Pickett et al. reported a self-supporting supramolecular gel by non-covalent encapsulation of the diiron active site complex **40** [(μ-pdt)Fe$_2$(CO)$_4$(PMe$_3$)$_2$] (Fig. 14) in an Fmoc-Leu-Leu dipeptide hydrogel. This group studied the effect of the chemical environment and the interaction of the [2Fe2S] cluster with the polymer gel peptide side chains in the hydrophobic cavity [174]. Compound **40** was chosen as the [2Fe2S] complex since the replacement of CO by two trimethylphosphine ligands $(PMe)_3$ provided an electron-rich metal center that promotes facile protonation [175,176]. This investigation showed the potential scope of this system to form a rigid H-bonding network and prevent isomerization processes caused by CO ligands in the gel.

Considering the relevant properties of hydrogels as macromolecular supports for artificial enzyme complexes, Li and co-workers used polyvinylpyrrolidone copolymer (PVP) to create a chemically inert amphipathic hydrogel by UV-induced self-crosslinking to non-covalently incorporate [2Fe2S] complex **41** (Fig. 14) [177]. This resulted in a photocatalytic hydrogen production system fabricated from the initial preparation of a composite catalyst **41/PVP** followed by the subsequent addition of the Ru $(bpy)_3^{2+}$ PS and AscOH as ED. The amphipathic PVP hydrogel provided a suitable scaffold to keep the diiron complex **41** and the ruthenium PS close, thus facilitating intermolecular electron transfer. The photosystem (**41/PVP-Ru(bpy)$_3^{2+}$**) photocatalytically produced hydrogen in aqueous solution at pH = 4 with an outstanding TON of 780 after 12 h and a TOF of 214 h^{-1} in the first hour of irradiation (Table 3, entry 11).

5.2. Covalent attachment of [2Fe2S] complexes on supramolecular assemblies

5.2.1. [2Fe2S] complexes covalently anchored on peptide and protein scaffolds

Inspired by nature, artificial metalloenzymes are hybrid catalysts constructed by incorporation of a catalytically active metal complex into a biosupramolecular scaffold [178–180]. [FeFe]-hydrogenase active site models have been successfully incorporated into peptides and protein matrices with the aim of enhancing water compatibility and catalytic performance in terms of selectivity, specificity and efficiency [181]. The synthetic procedure consists of covalently attaching the diiron complex to a peptide chain through cysteine-derived amino acids with thiolate ligands or by introducing artificial amino acids containing bridging dithiolate groups into the polypeptide backbone.

In 2007, Jones et al. were the first to report the coordination of a diiron entity $Fe_2(CO)_6$ to the surface of an α-helical peptide through the thiol group of cysteine in the CXXC motif (C = cysteine and X = any amino acid) [182]. Construct **42** (Fig. 15) was the first protein-organometallic hybrid system based on synthetic models of the [FeFe]-hydrogenase active site, inspiring further peptide engineering to fine-tune the properties of such systems.

Hayashi and co-workers developed two methodologies to synthesize artificial metalloenzymes with catalytically active diiron complexes incorporated into appropriately positioned CXXC peptide fragments that established a dithiolate bridge. The group designed a hybrid system by constructing the [2S2Fe] complex in the native CXXC motif using Cys14 and Cys17 in the cytochrome *c* protein matrix affording **43/cytochrome *c*** [Fe$_2$(μ-S(Cys))(CO)$_6$] (Fig. 15) [183]. Simulating electron transfer in the respiratory mitochondrial system, the water-soluble intermolecular photosystem (**43/Cytc-Ru(bpy)$_3^{2+}$**) was evaluated for photocatalytic hydrogen production yielding a TON of 80 over 2 h with a maximum TOF

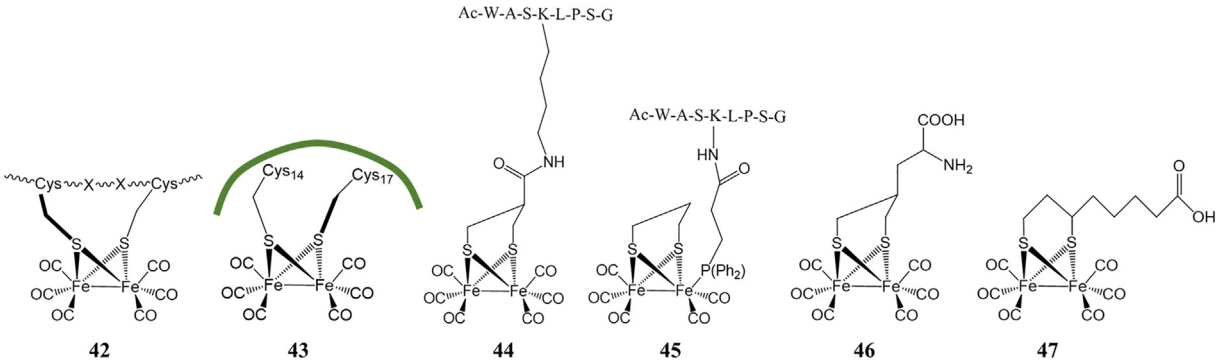

Fig. 15. Molecular structures of diiron complexes anchored within peptide and protein scaffolds.

of 2.1 min^{-1} in the presence of $Ru(bpy)_3^{2+}$ and $AscO^-$ at pH = 4.7 (Table 3, entry 13). An alternative route was reported by the same group in the construction of a peptide platform containing both a datively anchored $[Fe_2(\mu\text{-}S(Cys))(CO)_6]$ diiron complex **42** and a Ru-based PS [184]. The octadecapeptide Pep-18 (YIGKACGNCH-ENFRDKEG) contained in the sequence of cytochrome c556 (Rhodopseudomonas palustris) was selected as the matrix. The [2Fe2S] cluster was attached to the cysteine thiols and the ruthenium complex to a histidine within the CXXCH peptide fragment. Photochemical hydrogen evolution experiments demonstrated intramolecular electron transfer from the photoexcited ruthenium species to the [2Fe2S] core within photosystem **42/Cytc$_{556}$@Ru(bpy)(tpy)**, obtaining a TON of 9 and a TOF of up to 0.19 min^{-1} calculated from the initial rate of hydrogen production (Table 3, entry 12). When the photocatalytic reaction was performed using **42/Cytc$_{556}$** and externally incorporating $[Ru(tpy)(bpy)(Im)]^{2+}$ (Im = imidazole) as a PS under similar experimental conditions, H_2 evolution was not observed, verifying the crucial role of the ruthenium complex residing within the cavity of the protein matrix.

To investigate the engineering of the outer coordination sphere, Jones et al. reported a new route using an artificial amino acid for immobilization of a diiron complex on the peptide chain. The synthetic procedure involved modifying the primary amine functional group with a 1,3-dithiol moiety via on-resin coupling in solid-phase peptide synthesis to covalently anchor the [2Fe2S] **44** (Fig. 15) [185]. This synthetic strategy provided a general methodology for the covalent binding of a [2Fe2S] entity to any peptide framework with a primary amine group. However, the selectivity for the targeted amino acid during the multistep process was not ideal. In subsequent work carried out by the same group, an analogous diiron complex was incorporated into the above peptide sequence by coordination through a phosphine ligand incorporated at the distal iron atom. The synthesized structure **45** (Fig. 15) with phosphine-containing peptides was useful to increase the water solubility and served as a model strategy for the synthesis of a wide variety of biomimetic peptide-based models of [FeFe]-hydrogenases [186].

Inspired by this approach, Ghirlanda et al. prepared an artificial amino acid bearing a 1,3-dithiol moiety to covalently anchor the [2Fe2S] cluster **46** (Fig. 15) and the C terminal lysine 19 at the i and i + 3 positions of a helical peptide scaffold (**46/pepK16Dt**), simulating the H-cluster in *Clostridium pasteurianum* hydrogenase [187]. The hydrophobic protein environment promoted the stabilization of the catalytically active "rotated" structure of the [2Fe2S] cluster. In the presence of the $Ru(bpy)_3^{2+}$ and $AscO^-$, the photosystem **46/PepK16Dt-Ru(bpy)$_3^{2+}$** showed catalytic activity for photo-driven hydrogen production with a TON of 84 after 2 h reaction at pH = 4.5 (Table 3, entry 14).

In 2014, Hayashi and co-workers reported a biomimetic model of the [FeFe]-hydrogenase active site supported on a protein scaffold. The [2Fe2S] complex $Fe_2(\mu\text{-}S)_2(CO)_6$ with a maleimide moiety attached to the dithiol bridgehead **4** (see **Section 2**, Fig. 7) was covalently embedded into the cavity of a β-barrel nitrobindin (NB) protein matrix by maleimide coupling to cysteine residues [188]. Photochemical hydrogen production experiments were performed in the presence of a $Ru(bpy)_3^{2+}$ with excess $AscO^-$ in an aqueous acidic solution of Tris/HCl at pH = 4. A high photocatalytic activity was obtained using the hybrid system **4/NB-Ru(bpy)$_3^{2+}$**, yielding a TON of 130 after 6 h and an initial TOF of 2.3 min^{-1} (Table 3, entry 15). The rigid NB protein support provided an isolated specific site for the diiron complex to operate in aqueous solution and maintain the photostability of the [2Fe2S] cluster. However, the catalytic activity of the system after 2 h was slightly lower compared to that of the free diiron compound under near-identical experimental reaction conditions. Nonetheless, the protein environment maintains catalytic activity for a longer time. Another challenge to be addressed is the inaccessibility of the ruthenium PS within the rigid cavity of the NB protein where the [2Fe2S] site is located, causing a decrease in photocatalytic hydrogen production rate.

Recently, Feng and co-workers prepared a supramolecular photosystem that integrates a ruthenium-based PS Rudpqp ($[Ru(bpy)_2(dpqp)]^{2+}$), containing bipyridine and phenanthroline ligands, and the diiron catalyst **47** (Fig. 15) within the inner hydrophobic cavity of a single apoferritin (apo-HSF) via noncovalent interactions [189]. This biomimetic system presented the following advantages: stability and dispersibility in aqueous solution, tuneable **47**:PS ratio within the protein structure and close proximity of both units to promote electron transfer. The nanocomposite **47/apo-HSF@Rudpqp** synthesized with a Rudpqp:**47** concentration ratio of 2.79:1 exhibited the highest H_2 generation rate without significant leaching, providing a TON of 5 per catalyst over 4 h under visible light irradiation (Table 3, entry 16), which is tenfold that of the protein-free homogeneous photocatalytic system.

5.2.2. Polymer-supported [2Fe2S] systems

Metallopolymers have been developed in which [2Fe2S] clusters are incorporated in polymeric macrostructures either by covalent binding or intermolecular non-covalent interactions. These studies are based on knowledge from polymer chemistry that provides perspectives on suitable design and functionalization methods to tune and isolate the [2Fe2S] clusters. Appropriate macromolecular engineering of the metallopolymers by tuning the outer coordination sphere of the [2Fe2S] complex enables the construct to operate in an aqueous medium, increases the stability under experimental reaction conditions, and improves charge transport in photocatalytic processes. Various approaches have been developed using polymer-supported [2Fe2S] systems, but only a few have succeeded in designing a functional [2Fe2S]-polymer conjugate for light-driven hydrogen production.

5.2.2.1. Poly(acrylic acid) (PAA) and polyethylenimine (PEI) polymers.. Poly(acrylic acid) (PAA) is a commercial hydrophilic polymer with carboxylic acid groups along the polymeric chain that promote water solubility and offer modification sites for functionalization. Wu and co-workers reported the incorporation of the amine-modified [2Fe2S] **48** on the PAA polymer [190]. This functionalized polymer **48/PAA** (Fig. 16) was evaluated for photocatalytic hydrogen production in water using 3-mercaptopropionic acid (MPA) stabilized CdSe QDs (MPA-CdSe QDs) as PS and AscOH as source of protons and electrons (Table 3, entry 17). Under these conditions, the system achieved a splendid TON of 27,135 for 8 h and a TOF of up to 3.6 s^{-1}. Besides promoting water solubility for the diiron complex **48**, the carboxyl groups of the grafted-polymer **48/PAA** coordinated the cadmium ions of CdSe QDs, preventing the formation of QD aggregates and maintaining the catalyst close to the PS. This proximity boosted photoinduced electron transfer ($k_{ET} = 6.15 \times 10^{12}$ M^{-1} s^{-1}) from photoexcited *MPA-CdSe QDs to **48**.

In subsequent work, Wu's group designed the metallopolymer **49/PEI** (Fig. 16) by grafting a carboxylate-functionalized diiron complex **49** onto the side chains of a branched polyethylenimine polymer (PEI, MW = 600 g mol^{-1}) [191]. The branched PEI is a water-soluble polymer capable of simulating the environment of biological systems. It contains a large number of amino groups that can be protonated over a wide pH range and covalently coordinate [2Fe2S] model complexes. The **49/PEI** system was stable in aqueous solution even in neutral conditions, showing high photocatalytic H_2 production with a TON of up to 10,600 after 44 h of reaction time in the presence of a MPA-CdSe QD PS and AscOH as the sacrificial ED and proton source (Table 3, entry 18). Although

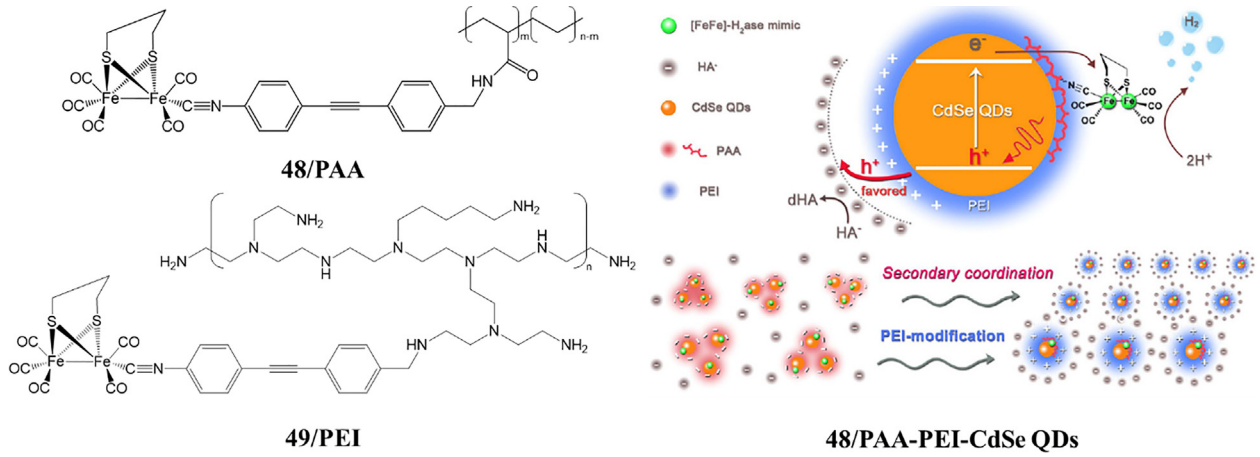

Fig. 16. Structures of water-soluble [2Fe2S]-metallopolymers for the light-induced hydrogen generation. Adapted from Refs. [192] with permission from Springe Nature.

a higher rate was obtained under acidic conditions at pH = 4 in the first 4 h, the system showed durable hydrogen production for prolongated times at neutral conditions, as is the case of the enzymatic active site that is buried within the [FeFe] hydrogenase. The high degree of protonation of the amine groups increases the self-buffering capacity and stabilizing ability of PEI that protects CdSe QDs from aggregation over a broad pH range to enhance photocatalytic activity.

Wu and colleagues have delved into the investigation of these [2Fe2S] catalysts and CdSe QDs based multi-component systems. In their previous study [190], they found that the grafted **48** on the PAA chain suffered from poor stability since the hole transfer rate was slower than the electron transfer rate. The hole electron transfer rate from CdSe QDs to AscOH was threefold slower than the electron transfer rate from CdSe QDs to **48**, slowing down hydrogen evolution as holes accumulated in the valence band of CdSe QDs. To overcome this, this research group combined the branched PEI and the previous **48/PAA** system, creating a secondary coordination sphere and taking advantage of the supramolecular interaction of both polymers. This resulted in a 30-fold acceleration of the hole transfer without affecting the electron transfer rate, improving the stability and catalytic activity [192]. The photocatalytic hydrogen evolution system (**48/PAA-PEI-CdSe QDs)** (Fig. 16) exhibited an excellent TON of 83600, which is so far the highest performance obtained from the use of [2Fe2S] complexes as catalysts for photocatalytic hydrogen production (Table 3, entry 19).

5.2.2.2. Dendritic macropolymers. Dendrimers, three-dimensional hierarchically branched macromolecules of tree-like structure, can be used for a wide variety of applications. Their high water solubility and ability to form host–guest systems, among other relevant properties, have made them attractive candidates for applications in catalysis, artificial enzymes and biomedicine

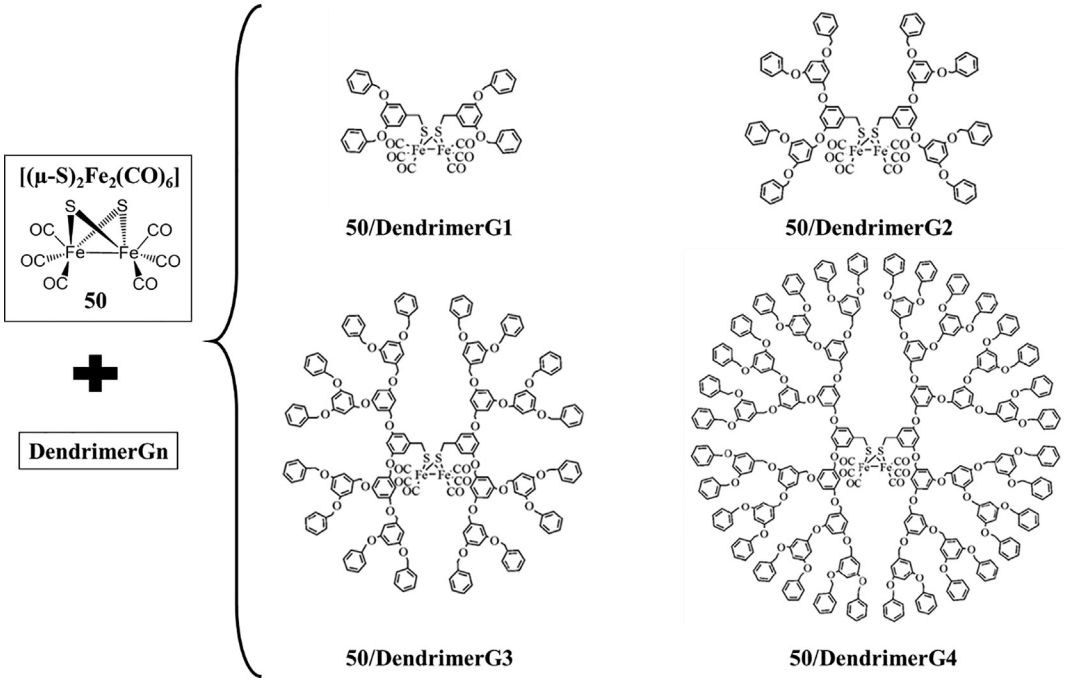

Fig. 17. Structures of dendritic hydrogenase mimics (**50/DendrimerGn**, Gn = Generation Number; n = 1–4) with the diiron active site **50** [$(\mu\text{-S})_2Fe_2(CO)_6$]. Reproduced and modified from Refs. [199] with permission from John Wiley and Sons.

[193–195]. Several investigations have also demonstrated the light-harvesting ability of dendrimers for photoenergy conversions [196–198].

Li and co-workers reported an elegant strategy to stabilize a simple [2Fe2S] complex in a hydrophobic pocket within a macromolecular dendritic architecture [199]. Four generations of benzyl ether-based Fréchet-type dendrons (Gn; generation number; n = 1–4) were attached to the $[(\mu\text{-S})_2Fe_2(CO)_6]$ diiron core **50** by covalent interaction of the sulfide ligands with the ether groups in the dendrite (Fig. 17). Dendrimer catalysts functionalized with [2Fe2S] were then evaluated in a photocatalytic system containing a molecular complex of Ir(III) $[Ir(ppy)_2(bpy)]PF_6$ as a PS and TEA as a sacrificial ED in an acetone/water mixture (9:1, v/v) to solubilize all components. **50/dendrimerGn-Ir(III)** showed excellent hydrogen productivity under visible-light irradiation with TONs of up to 18100, 19000, 21,500 and 22,200 after 8 h, initial TOFs of up to 6190, 6360, 7000, and 7240 h^{-1}, and quantum efficiencies of 0.18%, 0.21%, 0.24% and 0.28% for the dendritic diiron complexes of generations 1–4, respectively (Table 3, entry 20). Hydrogen generation increased with the size/generation of the dendritic metallopolymer architecture. The highest value of TOF and total TON was found for the system with the largest dendritic structure (**50/DendrimerG4-Ir(III)**), which also exhibited the longest lifetime of the $[2Fe2S]^-$ intermediate (86.3 μs estimated from transient absorption spectroscopy). Thus, the dendritic framework encapsulating the [2Fe2S] complex protects the active sites similarly to enzyme microenvironments that regulate electron transfer and provide effective charge separation. Although this experimental procedure is a promising approach in the design of enzyme-based artificial photocatalysts towards the conversion of solar energy into hydrogen, future advances should aim to incorporate modifications in the dendritic periphery to improve water solubility.

6. Direct assembly of [2Fe2S] compounds on inorganic hybrid semiconductor nanoparticles

Artificial photosynthetic systems using semiconductors as light-harvesters in combination with a fuel-forming catalyst such as biomimetic models of the [FeFe]-hydrogenase active site (Fig. 18) are promising candidates for solar fuel conversion.

The assembly of an appropriate catalyst onto a semiconductor can promote highly efficient charge separation, a fast electron transfer rate and decreased activation energy or overpotential, all key aspects to enhancing performance in light-driven hydrogen production. Functional groups on the catalyst are often essential for increased loading and reliable assembly on the semiconductor.

The interaction of *Clostridium acetobutylicum* [FeFe]-hydrogenase (CaI) with quantum dots of CdTe or CdS [200,201], or *Clostridium perfringens SM09* [FeFe]-hydrogenase (CpHydA) with TiO_2 semiconductors [202] has been investigated for photocatalytic hydrogen formation. Even [NiFeSe]-hydrogenases from *Desulfomicrobium baculatum* (Db-[NiFeSe]) attached to TiO_2 nanoparticles [203] or organic polymeric carbon nitride (CN_x) [204] have been used as photosystems showing excellent performance in the light-assisted hydrogen generation. However, only a few studies have demonstrated the combination of [2Fe2S] complexes on semiconductor or semiconductor nanoparticles and their subsequent application in photocatalytic hydrogen production.

Wu and co-workers used CdSe QD semiconductors to build a water-soluble system by interface-directed assembly of the [2Fe2S] complex **50** onto MPA-CdSe nanocrystals [205]. The ideal characteristics of CdSe QDs such as light-harvesting, charge separation, effective quantum confinement, rich chemistry for surface functionalization and large surface-to-volume ratio [206,207] make them potential candidates in combination with [2Fe2S] complexes for hydrogen evolution in aqueous solution. Under optimized reaction conditions, the **50/MPA-CdSe** photosystem in combination with AscOH (pH = 4) exhibited a TON of 8781 after 82 h of visible-light irradiation in water, with a TOF of up to 596 h^{-1} in the first 4 h (Table 4, entry 1). This study demonstrated that the interface-directed assembly facilitated electron transfer from the excited *CdSe to the [2Fe2S] cluster **50** and allowed the catalytic center to operate in water. Both benefits, together with the strong interaction and direct contact between the functional units, were crucial to obtain high photocatalytic hydrogen performance.

Zinc sulfide (ZnS) nanoparticles are wide-band-gap II-VI semiconductors (3.6–3.8 V) commonly used as light-harvesters in photocatalysis. However, their photocatalytic applicability has several restrictions such as fast recombination of electron/hole pairs and light absorption only in the ultraviolet region [208]. Several strategies have been used to improve catalytic activity using these nanomaterials, such as increasing the surface area, changing the morphology to mediate closer contact with reagents, promoting the absorption of visible light through doping processes, and forming heterojunctions with a cocatalyst (semiconductors or metals) to reduce the electron-hole recombination rate [209,210]. Li and colleagues reported a noble-metal-free hybrid photocatalytic system made by physical adsorption of the amino groups of the organometallic diiron hydrogenase catalyst **51** [(μ-SPh-4-

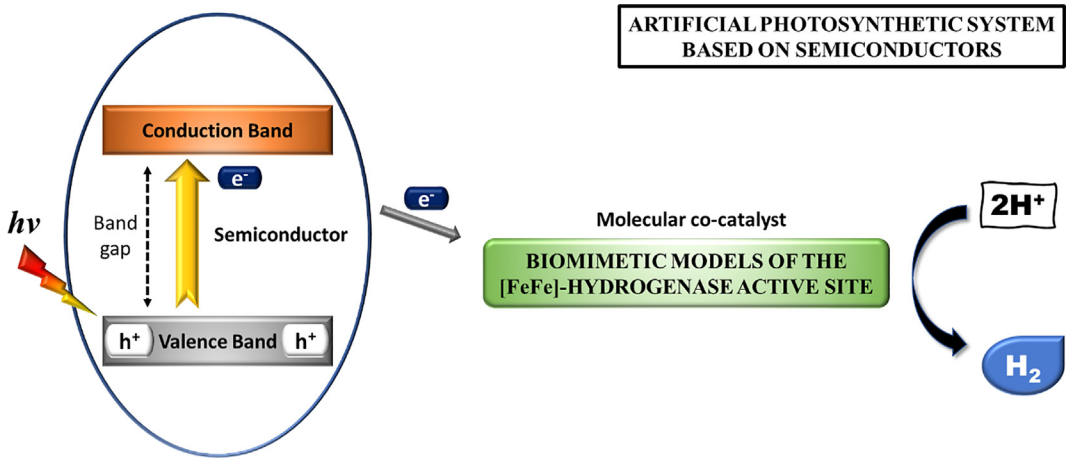

Fig. 18. Schematic representation of light-driven hydrogen production in artificial photosynthetic system using semiconductors.

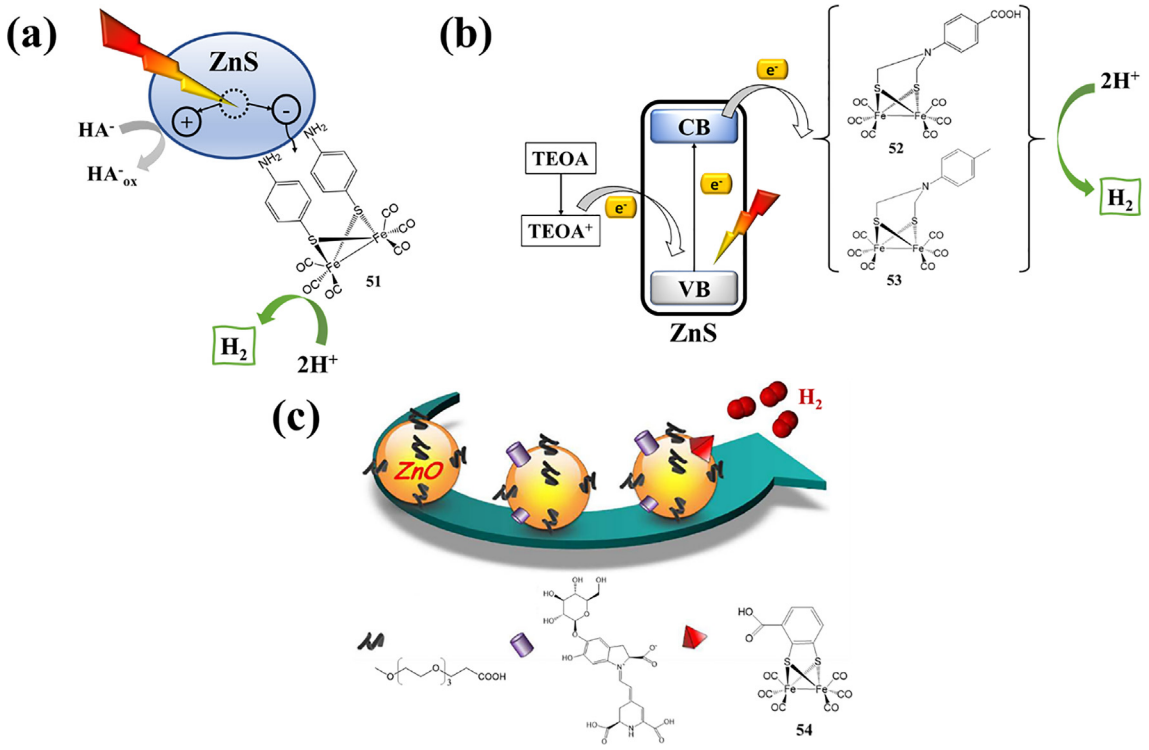

Fig. 19. Schematic representation of hybrid photocatalytic systems engineered by (a) integrating ZnS semiconductor nanoparticles and the [2Fe2S] complex **51** (reproduced and modified from Ref. [211] with permission from John Wiley and Sons), (b) assembling biomimetic diiron complexes **52** and **53** on the surface of ZnS (reproduced and modified from Ref. [212] with permission from John Wiley and Sons), and (c) anchoring betanin (B) and the synthetic diiron catalyst **54** to ZnO-OEG, for photocatalytic hydrogen evolution (reproduced and modified from Ref. [213] with permission from The Royal Society of Chemistry).

$NH_2)_2Fe_2(CO)_6$] onto ZnS semiconductor nanoparticles for photocatalytic hydrogen evolution using AscOH as ED (Fig. 19**a**) [211]. Efficient transfer of the photogenerated electrons from ZnS to the [2Fe2S] cluster was achieved in the **51/ZnS** photosystem resulting in a TON of 2607 for 38 h and an initial TOF of 100 h^{-1} (Table 4, entry 2). These results demonstrate the remarkable performance and stability of this catalytic system, which showed an even higher catalytic rate than a platinum ZnS (Pt/ZnS) reference system. In 2014, Chen et al. assembled the two structural analogues **52** and **53** to the surface of a ZnS nanomaterial [212]. While **52** is directly coordinated to the unsaturated Zn ions on the surface of ZnS through a carboxy linkage, complex **53** is physically adsorbed through the dangling S atoms at the ZnS interface (Fig. 19**b**). Photocatalytic experiments were carried out using TEOA as ED in organic alkaline solution (DMF/H_2O, 9:1), with a 3- and 5-fold improved catalytic activity upon addition of **52** and **53**, respectively, compared to pristine ZnS. Under irradiation for 38 h, a TON of 3400 was obtained by the carboxy-functionalized mimic **52** in combination with ZnS (**52/ZnS**). A TON of 4950 was achieved for the diiron complex **53** without carboxyl group incorporated in the same ZnS nanomaterial (**53/ZnS**) (Table 4, entry 3 and 4). The TOFs shown in the first 4 h were 151 and 282 h^{-1} for **52/ZnS** and **53/ZnS**, respectively. The disparity in the hydrogen production rate by the hybrid photosystems was attributed to the different absorption modes of each [2Fe2S] catalyst on the ZnS nanoparticles.

Another type of zinc-based nanoparticulate semiconductors incorporating an [2Fe2S] complex has recently been reported by Sá and co-workers [213]. Ultra-stable ZnO nanocrystals, modified with an oligoethylene carboxylate glycol shell (ZnO-OEG), provided extended electron lifetime and stabilization of the photogenerated hole, thereby slowing down charge recombination in aqueous solution [214]. The nano-hybrid photocatalytic system **ZnO-OEG@B-54** was created by anchoring the natural light-harvesting pigment betanin (B), capable of injecting two electrons per adsorbed photon into the conduction band of ZnO in a few picoseconds, and **54** [FeFe(mcbdt)$(CO)_6$] (mcbdt = 3-carboxybenzene-1,2-dithiolate) (Fig. 19**b**) [213]. Hydrogen evolution experiments under visible-light irradiation using TFA as a proton source demonstrated a TON of 11 in 4 h (Table 4, entry 5). FTIR spectroscopy revealed the construct is remarkably stable, with>95% of the initial [FeFe(mcbdt)$(CO)_6$] catalyst remaining intact after one day of photocatalysis. A second reaction cycle resulted in approximately 70% of the initial hydrogen production under the same experimental conditions for 4 h. Therefore, the ZnO-OEG nanohybrid semiconductor was an effective scaffold for achieving accumulative charge separation and prolonging the stability of the PS and [2Fe2S] **54**.

7. [FeFe]-hydrogenase active site models anchored onto heterogeneous supports

The use of a heterogeneous matrix for the immobilization of [2Fe2S] clusters via their outer coordination sphere is an appealing approach to increase structural stability of all reaction partners. These supports can provide well-ordered tailorable pores or channels, very high internal surface areas, well-defined structures, electrostatic microenvironments and hydrophobic cavities. Water-insoluble [2Fe2S] catalysts can be isolated in specially designed sites that are accessible throughout the matrix and capable of operating efficiently in aqueous media. The precise design of these platforms allows the creation of solid heterogeneous photocatalytic systems with enhanced stability, simple separation after reaction and efficient recycling for light-induced hydrogen production processes.

Metal-organic frameworks (MOFs), mesoporous molecular sieves (MCM-41), periodic mesoporous organosilicas (PMOs), silica

nanoparticles and graphene-based supports have been used as matrices for the incorporation of diiron catalysts, PSs and/or EDs to be applied in hydrogen evolution schemes.

7.1. Metal-organic frameworks platforms for [2Fe2S] complexes

MOFs are 3D porous coordination polymers formed from metal clusters and organic linker molecules. Almost limitless combinations of metal nodes and available organic linkers have sparked the use of MOFs in a wide variety of fields such as gas storage, separation, heterogeneous catalysis, drug delivery, and chemical sensing [215–218]. The use of MOFs as a support in photocatalytic applications is particularly interesting because they have well-defined structures, exceptionally high internal surface areas, remarkable chemical stability, structural flexibility and tunability [219–221]. MOFs as enzymatic platforms for hydrogen production must: i) be water stable under catalytic conditions in a wide pH range, and ii) have functional sites where the molecular catalyst can be incorporated during the framework synthesis, or through postsynthetic modification (PSM) or postsynthetic linker exchange (PSE) [222,223]. In addition, iii) the MOF must either possess pore diameters that are sufficiently large to allow transport of the PS and the ED to the active sites, or be capable of electron transport to wire catalytic sites in the interior of the crystals [224]. In the latter scenario, electrons may be generated in a light-driven process in solution, and then transferred into the MOF through the crystal surface [225].

Catalyst-containing MOFs offer improved stability, especially if organic co-linkers in the MOF backbone contain functional groups that can interact with the catalyst to enhance its selectivity and/or activity [226,227]. Photocatalytic MOFs can be built using several approaches: a) immobilization of the catalyst and external incorporation of the PS in solution, b) incorporation of a photoactive MOF with light-harvesting organic ligands or metallic clusters and external incorporation of the catalyst in solution, c) combination of both functional units in the MOF or d) creation of active hetero-junctions in MOF composite materials [226]. Only a few examples of [2Fe2S] complexes immobilized in heterogeneous MOF platforms have been reported, mainly designed following approaches a) and c).

In 2013, Cohen and Ott et al. incorporated the [2Fe2S] catalyst **8** ([FeFe]-(dcbdt)$(CO)_6$) into a thermally robust Zr(IV)-based UiO-66 MOF by PSE of 1,4-benzenedicarboxylate (bdc) ligands [111]. UiO-66 is a highly crystalline framework with a large surface area (S_{BET} = 1475 m^2 g^{-1}) and tetrahedral and octahedral cages with pore widths of ~8 and ~11 Å, respectively. Proton nuclear magnetic resonance spectroscopy (^{1}H NMR) and energy-dispersed X-ray spectroscopy (EDX) confirmed a degree of bdc linker exchange of 14%. The resulting **8@UiO-66** demonstrated enhanced photocatalytic hydrogen production when combined with the [Ru$(bpy)_3]^{2+}$ PS and $AscO^-$ as ED in aqueous acetate buffer at pH = 5 (Fig. 20**a**). A TON of 5.9 (Table 5, entry 1) was obtained, higher than that of the molecular catalyst **8** in homogeneous phase (TON = 1.7, see **Section 2**). The homogeneous reference decomposed by releasing the coordinated CO ligands from the diiron core under photoirradiation conditions. The UiO-66 matrix served to increase the stability of the catalytic diiron unit **8** within the MOF crystals, thus achieving higher TONs than the homogeneous photosystem.

The reactivity of the confined molecular catalyst **8** in a UiO-66 MOF was modified by replacement of CO ligands by phosphines of different sizes (Fig. 20**b**) [228]. Small phosphines (PX_3, X = Me, Et) can be introduced to the diiron complex within the MOF structure in yields of 50–80%. These [FeFe-(dcbdt)$(CO)_4(PX_3)_2$] complexes in the UiO-66 platform were reduced at more cathodic potentials than the analogous [FeFe-(dcbdt)$(CO)_6$] and formed hydride species under acidic conditions. Recently, Hammarström et al. proposed intra-crystal linker scrambling in the photochemical hydrogen evolution with **8@UiO-66** [229]. Under the reaction conditions shown in Table 5 (entry 1), hydrogen production ceased after a period of 3 h under visible-light irradiation. However, the molecular catalyst **8** in the MOF maintained its structural integrity after the reaction and the photocatalytic activity could be restored after a resting period of 60 min. Interestingly, recovered **8@UiO66** showed similar catalytic activity as the original photocatalysis experiment during 9 reaction cycles with 45 min of light irradiation (Fig. 20**c**).

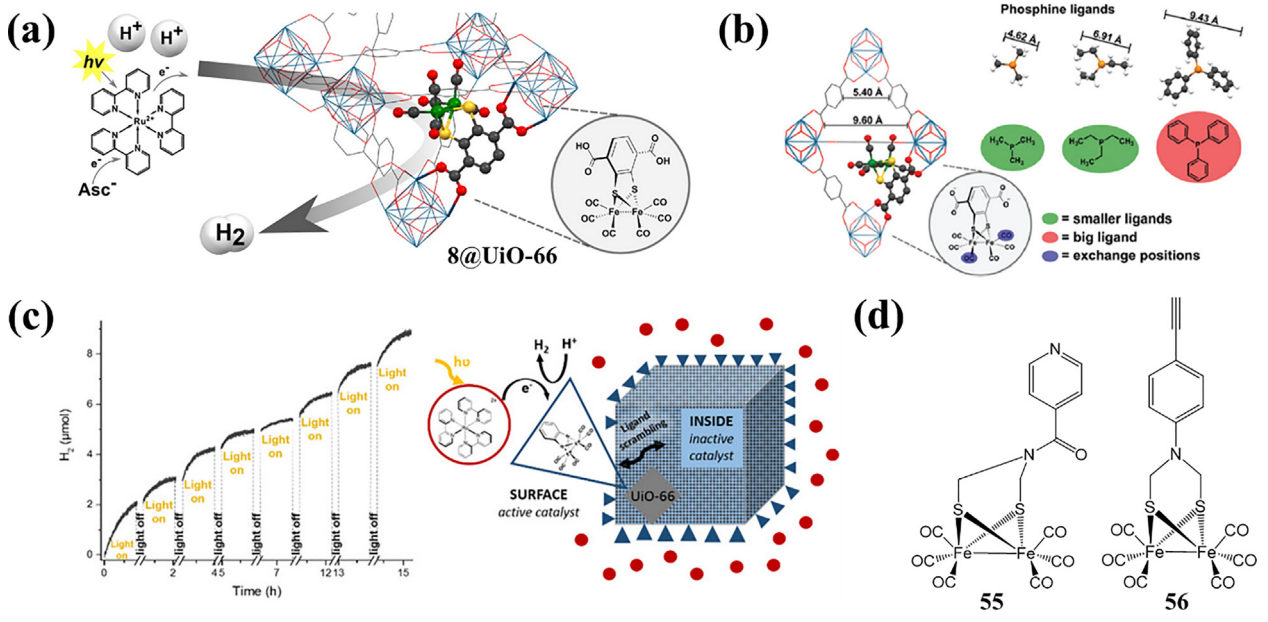

Fig. 20. (a) Reaction scheme of photochemical hydrogen evolution using **8@UiO-66** catalyst (adapted from Ref. [111]. Copyright (2013) American Chemical Society), (b) schematic representation of CO ligand exchange with different phosphine ligands in **8@UiO-66** (reprinted from Ref. [228] with permission from The Royal Chemical Society), (c) self-recovery of photocatalytic hydrogen production with **8@UiO-66** by intra-crystal linker scrambling (reprinted from Ref. [229] with permission from John Wiley and Sons), and d) structures of diiron mimetic compounds **55** and **56** incorporated into ZrPF and UiO-MOF, respectively.

Table 3
Supramolecular assemblies for [FeFe]-hydrogenase active-site mimics evaluated in light-driven hydrogen production.

Entry	SA[1]	Supramolecular photocatalytic system	Selected conditions[2]	Light	Time (h)	TON[2]	Ref.
1	**Oligo- and polysaccharides**	**34/β-CyD-EY**	Water, 0.5 mM **34**; 0.5 mM EY, 10 equiv. β-CyD, 10% TEA, pH = 10	Xe lamp(500 W), λ > 450 nm	24	75	[161]
2		**34/β-CyD-6-S-CdSe QDs**	Water, 1 μM **34**, 100 μM β-CyD-6-S-CdSe QDs, 0.28 M AscOH, pH = 4.5	Xe lamp (300 W), λ > 400 nm	30	2370	[162]
3		**1/chitosan-MPA-CdTe QDs**	MeOH/Water (1:3), 1 μM **1**, 1.71 μM MPA-CdTe QDs, 1 g/L chitosan, 0.2 M AscOH, pH = 4.5	LED, λ = 410 nm	60	52,800	[163]
4	**Micelles**	**1/SDS-Re(1)**	Water, 0.18 mM **1**, 0.18 mM Re(I) complex, 0.1 M AscOH, 0.166 M SDS	Hg lamp (300 W), λ > 400 nm	2	0.13	[167]
5		**35/SDS-EY**	Water, 0.1 mM **35**, 0.2 mM EY, 10% TEA, 10 mM SDS, pH = 10.5	LED (0.3 W), λ = 455 nm	4.5	117	[168]
6		**38/APM-Ru(bpy)$_3^{2+}$**	Water/APM, 0.03 mM **36**, 0.3 mM Ru(bpy)$_3^{2+}$, 45 mM AscOH, pH = 4.0–4.1	LED, λ = 450 nm	2	133	[169]
7		**27-SDS**	Water/SDS, 10 μM **27**, 100 mM TEA, 50 mM TFA, pH = 10	Hg lamp (15 W), λ = 254 nm	4	139	[143]
8		**27-CTAB**	Water/CTAB, 10 μM **27**, 100 mM TEA, 50 mM TFA, pH = 10	Hg lamp (15 W), λ = 254 nm	4	148	[143]
9	**Vesicle membranes**	**34/DMPC-Ru(bpy)$_3^{2+}$**	Water, 0.1 mM **34**, 0.1 mM Ru(bpy)$_3^{2+}$, 100 mM AscOH, 0.9 mM DMPC, pH = 2.6, 19 °C	LED (91 mW/cm^2), λ = 455 nm	1.5	59	[171]
10		**39/DOPC-OA-CdSe QDs**	Water, 50 μM **39**, 0.2 μM OA-CdSe QDs, 200 mM AscOH, 0.9 mM DOPC, pH = 4, 19 °C	LED (91 mW/cm^2), λ = 455 nm	72	651	[172]
11	**Hydrogels**	**41/PVP-Ru(bpy)$_3^{2+}$**	Water, 1 μM **41**, 0.5 mM Ru(bpy)$_3^{2+}$, 0.2 M AscOH, 10 mg PVP, pH = 4	Xe lamp (300 W), λ = 400–780 nm	12	780	[177]
12	**Peptides and proteins**	**42/Cytc$_{556}$@Ru(bpy)(tpy)**	Water, 140 μM **42/Cytc$_{556}$@Ru(bpy)(tpy)**, 100 mM AscO$^-$, 50 mM Tris/HCl, pH = 8.5, 25 °C	Xe lamp (500 W), λ = 410–770 nm	2	9	[184]
13		**43/Cytc-Ru(bpy)$_3^{2+}$**	Water, 14 μM **43/Cytc**, 140 μM Ru(bpy)$_3^{2+}$, 100 mM AscO$^-$, 50 mM Tris/HCl, pH = 4.7, 25 °C	Xe lamp (500 W), λ = 410–770 nm	2	80	[183]
14		**46/PepK16Dt-Ru(bpy)$_3^{2+}$**	Water, 9.33 μM **46/PepK16DT**, 150 μM Ru(bpy)$_3^{2+}$, 50 mM AscO$^-$, 50 mM citrate buffer, pH = 4.5	Xe lamp (450 W), λ = 410–770 nm	2.3	84	[187]
15		**4/NB-Ru(bpy)$_3^{2+}$**	Water, 7.8 μM **4/NB**, 140 μM Ru(bpy)$_3^{2+}$, 100 mM AscO$^-$, 50 mM Tris/HCl, pH = 4.0, 25 °C	Xe lamp (500 W), λ = 410–770 nm	6	130	[188]
16		**47/apo-HSF@Rudpqp**	Water, 11.3 μM **47,** 31.6 μM Ru(bpy)$_3^{2+}$, 100 mM AscOH, pH = 5.3.	Xe lamp (300 W), λ > 420 nm	4	5	[189]
17	**Metallopolymers**	**48/PAA-MPA-CdSe QDs**	Water, 0.25 mg/mL **47/PAA**, 0.08 mg/mL MPA-CdSe QDs, 0.1 M AscOH, pH = 4.0	LED, λ = 450 nm	8	27,135	[190]
18		**49/PEI-MPA-CdSe QDs**	Water, 1.46 μM **48/PEI**, 0.08 mg/mL MPA-CdSe QDs, 0.125 M AscOH, pH = 6.5	LED (3 W), λ = 410 nm	44	10,600	[191]
19		**48/PAA-PEI-CdSe QDs**	Water, 0.25 g/L **47/PAA**, 5.8 μM CdSe QDs, 0.46 g/L PEI, 0.1 M AscOH, pH = 4.1	LED (3 W), λ = 450 nm	28	83,600	[192]
20		**50/DendrimerG4-Ir(III)**	Acetone/Water (9:1), 1 μM **49/DendrimerG4**, 0.5 mM Ir(III) complex, 0.6 M TEA	Xe lamp(300 W), λ = 400–800 nm	8	22,200	[199]

[1] Supramolecular assembly; [2]Solvents and reagents abbreviations: MeOH: methanol, AscOH: ascorbic acid, AscO$^-$: ascorbate, TFA: trifluoracetic acid, TEA: triethylamine.
[2] TON based on [2Fe2S] catalyst.

The same group reported a functionalized MIL-101 (Cr) MOF with a larger pore diameter (29–34 Å) compared to that in UiO-66 (8–11 Å) for the covalent attachment of the diiron compound **54** [FeFe(mcbdt)(CO)$_6$] affording **54@MIL-101** [228]. The easy accessibility to these pores with windows of 12–14.5 Å, compared to the 6 Å in UiO-66, enabled increased catalyst loading throughout the entire MOF matrix. The pore size of MIL-101 allows chemical reduction of the catalyst by stabilizing the reduced catalyst intermediate in the MOF structure for hours. However, ion pairing phenomena were observed between the reduced species [FeFe]$^{2-}$ and oxidized cobaltocene reducing agent [Cp$_2$Co]$^+$ that clogged MOF channels and limited fast and efficient accessibility to the catalyst. This effect was less pronounced in MIL-101 with a lower loading of **54**. The performance of three **54@MIL-101** materials with different catalyst loadings was evaluated in photochemical hydrogen evolution experiments, demonstrating better catalytic activity than the homogeneous reference system with the diiron compound **8** ([FeFe]-(dcbdt)(CO)$_6$). The hydrogen productivity was linearly dependent on the loading of **54** within the MOF and showed a similar TON for the three systems, although the highest value was obtained for the medium loading **54@MIL-101** catalyst, reaching a TON of 18.5 after 2.3 h (Table 5, entry 2).

Feng and co-workers took the alternative strategy c) consisting of simultaneous incorporation of the PS and the diiron catalyst into the MOF support [230]. The group used a light-harvesting zinc porphyrin complex (ZnTPP) that was linked to Zr (IV)-based metal cluster nodes. The [2Fe2S] complex **55** with a pendant pyridyl group (Fig. 20**d**) was anchored to the zinc center in the porphyrin. The direct coordination of both functional units provided intimate contact between the PS and the diiron catalyst, facilitating the visible-light-driven intramolecular electron transfer from singlet excited state ^{1*}ZnTPP to **55** without the need for an electron mediator. The heterogeneous **55@ZrPF** system showed high efficiency for photochemical hydrogen production, yielding 3.5 μmol of H_2 after 2 h in an aqueous acetate buffer solution (pH = 5) with AscO$^-$ as a sacrificial ED (Table 5, entry 3). The MOF matrix provided improved stability for the anchored [2Fe2S] cluster, as the homogeneous system was stable for only 40 min under the same photoreaction conditions.

In another effort to simultaneously immobilize the PS and [2Fe2S] complex in a MOF platform, Yuan and colleagues designed the **56@UiO-MOF** consisting of a mixture of [Ru(bpy)$_3$]$^{2+}$-derived dicarboxylate linkers as light harvesters and azide-modified dicarboxylate ligands that provided covalent anchor sites for the diiron catalyst **56** (Fig. 20**d**) by a facile click reaction [231]. The closeness of both functional units in the MOF support led to an enhancement of the electron transfer efficiency and a decent photocatalytic hydrogen evolution performance. The incorporation of **56** in the

Table 4
Inorganic hybrid semiconductor systems with attached [2Fe2S] complexes for light-driven hydrogen production.

Entry	Semiconductor photocatalytic hybrid system	Selected conditions[1]	Light	Time (h)	TON[2]	Ref.
1	**50/MPA-CdSe**	Water, 2.3 μM **49**, 6.3 μM MPA-CdSe, 85 mM AscOH, pH = 4.0	LED (160 mW/cm^2), λ > 405 nm	8	8781	[205]
2	**51/ZnS**	DMF/H_2O (9:1), 3.9 μM **50**, 0.2 g ZnS, 85.2 mM AscOH	Xe lamp (300 W), λ = not avaliable	38	2607	[211]
3	**52/ZnS**	DMF/H_2O (9:1), 4 μM **51**, 10 mg ZnS, 2.5% (v/v) TEOA, pH = 11	Xe lamp (300 W), λ = not avaliable	30	3400	[212]
4	**53/ZnS**	DMF/H_2O (9:1), 4 μM **52**, 10 mg ZnS, 2.5% (v/v) TEOA, pH = 11	Xe lamp (300 W), λ not specified	30	4950	[212]
5	**ZnO-OEG@B-54**	**ZnO-OEG@B-53**, TFA. Concentration data not available	Continuous wave (CW) laser, λ = 532 nm	4	11	[213]

[1] Solvents and reagents abbreviations: DMF: N,N-dimethylformamide, AscOH: ascorbic acid, TFA: trifluoracetic acid, TEOA: triethanolamine.
[2] TON based on [2Fe2S] catalyst

UiO framework promoted the stability of the [2Fe2S] catalyst in water. Using AscOH as the sacrificial ED, the **56@UiO-MOF** photosystem exhibited decent catalytic activity, reaching a TON of up to 16 for 50 h of reaction time in an acetate buffer (pH = 5) (Table 5, entry 4).

7.2. Silica-based heterogeneous supports for [FeFe]-hydrogenase active site mimics

Silica-based mesoporous molecular sieves offer tunability of the pore size (2–50 nm), high surface area, simple synthesis, an electrostatic microenvironment, water stability, and the ability to stabilize charge-separated states in catalytic processes [232,233]. An ordered mesoporous K^+-exchanged molecular sieve MCM-41 has been used to immobilize hydrophobic [2Fe2S] complexes, improving the stability of the diiron catalyst in photochemical hydrogen evolution experiments in aqueous solution. This work by Li and Yu et al. incorporated the diiron complex **57** [{(μ-SCH_2)$_2$N(CH_2-C_6H_5)}$Fe_2(CO)_5P(Pyr)_3$] into K^+-exchanged molecular sieve MCM-41 via electrostatic interactions [234]. The resulting **57@MCM-41** system catalyzed light-induced proton reduction in water by using an iridium-based photosensitizer ([Ir(ppy)$_2$bpy]Cl) and TEA as a sacrificial ED (Fig. 21**a**). Under optimized reaction conditions, a TON of 18.3 was achieved during 1 h of irradiation under visible light (Table 5, entry 5), demonstrating that this strategy can stabilize and disperse a hydrophobic diiron catalyst in aqueous solution. The photochemical hydrogen evolution was limited by the degradation of the PS, since re-addition of more iridium PS led to recovery of the catalytic activity. In an advanced approach, the same group reported the electrostatic immobilization of a PS-[2Fe2S] dyad (**58**-Ir) into the ordered mesoporous K^+-exchanged molecular sieve MCM-41 (Fig. 21**b**) [235]. The heterogeneous system **58-Ir@MCM-41** exhibited an enhanced photocatalytic activity, 3-fold higher than that of the dyad **57**-Ir without the MCM-41 matrix, obtaining a TON of 5 in MeCN/H_2O (9:1) under visible-light irradiation (Table 5, entry 6). This enhanced catalytic performance was attributed to the stabilization of the diiron catalyst in the molecular sieve, which was further confirmed by transient absorption studies.

Periodic mesoporous organosilicas (PMOs) are a class of silica-based hybrid materials prepared by the combination of a surfactant as template and a silsesquioxane as the organosilica precursor. PMOs exhibit the typical ordering of mesoporous silicas, and the diversity of synthetic procedures provides a range of functionalities which suggest these systems for applications as catalysts, adsorbents (metal ions, toxic organic compounds and even gasses), chromatography phases, and biological/biomedical supports, among others [236]. In 2018, Inagaki and co-workers designed a heterogeneous photochemical system by covalently anchoring a [2Fe2S] complex tethered with a maleimide group (**4**) on the pore

Table 5
Biomimetic models of the [FeFe]-hydrogenase active site anchored on heterogeneous supports for light-driven hydrogen production.

Entry	Heterogeneous photocatalytic system	Selected conditions[1]	Light	Time (h)	TON[2]	Ref.
1	**8**@UiO-66	Water, 5 mg **8**@UiO-66 (0.59 μmol **8**), 0.5 mM $[Ru(bpy)_3]^{2+}$, 100 mM $AscO^-$, 1 M acetate buffer, pH = 5.0	LED (850 μE), λ > 470 nm	2.5	5.9	[111]
2	**54**@MIL-101	Water, 1.5 mg **53**@MIL-101 (0.15 μmol **53**), 0.5 mM $[Ru(bpy)_3]^{2+}$, 100 mM $AscO^-$, 1 M acetate buffer, pH = 4.9	LED, λ > 470 nm	2.3	18.5	[228]
3	**55**@MOF-ZrPF	Water, **54**@MOF-ZrPF (2 μM **54**), 20 mM AscOH, 1 M acetate buffer, pH = 5.0	Xe lamp (300 W), λ > 420 nm	2	Insufficient data for calculation	[230]
4	**56**@UiO-MOF	Water, 15 mg **55**-Ru@UiO-MOF (2 μmol **55**), 100 mM AscOH, 1 M acetate buffer, pH = 5.0	Solid-state white light source, λ > 420 nm	50	16	[231]
5	**57**@MCM-41	Water, 4.5 mg **56**@MCM-41 (43 μmol/g **56**), 0.25 mM [Ir(ppy)$_2$bpy], 0.28 M TEA	Xe lamp (300 W), λ = 400–800 nm	1	18.3	[234]
6	**58**-Ir@MCM-41	MeCN/H_2O (9:1), 5.5 mg **57**-Ir@MCM-41 (19.1 μmol/g **57**), 0.8 M TEA, pH = 10	Xe lamp (300 W), λ = 400–800 nm	8	5	[235]
7	**4**@SH-PMO	Water, 0.3 mg **4**@SH-PMO (21 nmol **4**), 140 μM $[Ru(bpy)_3]^{2+}$, 200 mM $AscO^-$, pH = 4.5	Hg lamp, (λ > 400 nm)	2	310	[100]
8	**4**-Ru@SH-PMO	Water, 0.5 mg **4**-Ru@SH-PMO (250 μmol/g **4**, 115 μmol/g Ru), 200 mM $AscO^-$, pH = 4.5	Hg lamp, (λ > 400 nm)	2	1.3	[100]
9	**38**@nanosilica	MeCN/H_2O/TEA (7:1:2), 30 mg **38**@NanoSilica (1.86 μmol **38**), 0.9978 mM [Ir(ppy)$_2$(bpy)]PF_6	Xe lamp (300 W), λ > 400 nm	5	324	[238]
10	**38**-Fc-TPP@GO	Water, 0.1 mg **38**-TPP@GO (12 μM 3Fe2S, 5.8 μM TPP), 1.8 mM cysteine, pH = 1.0	Hg lamp (450 W), λ > 380 nm	5	3.9	[239]

[1] Solvents and reagents abbreviations: MeCN: Acetonitrile, TEA: triethylamine.
[2] TON based on [2Fe2S] catalyst.

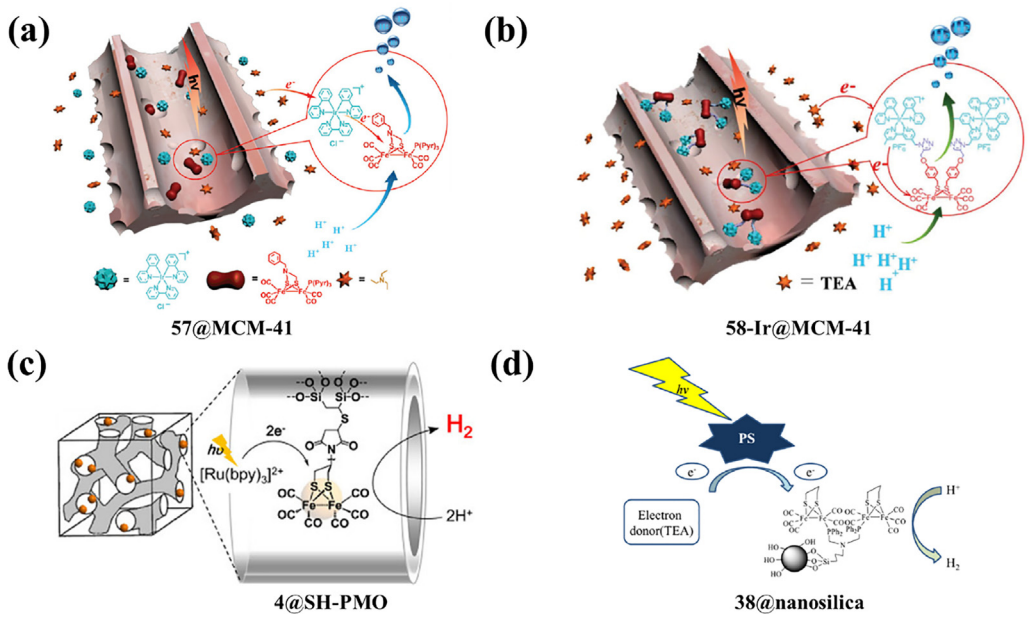

Fig. 21. Schematic illustration of the light-driven hydrogen production by (a) **57@MCM-41** (reproduced and modified from Ref. [234] with permission from John Wiley and Sons), (b) **58-Ir@MCM-41** (reproduced and modified from Ref. [235] with permission from The Royal Society of Chemistry), (c) **4@SH-PMO** (reproduced and modified from Ref. [100] with permission from John Wiley and Sons), and (d) **38@nanosilica** (reproduced and modified from Ref. [238] with permission from Elsevier).

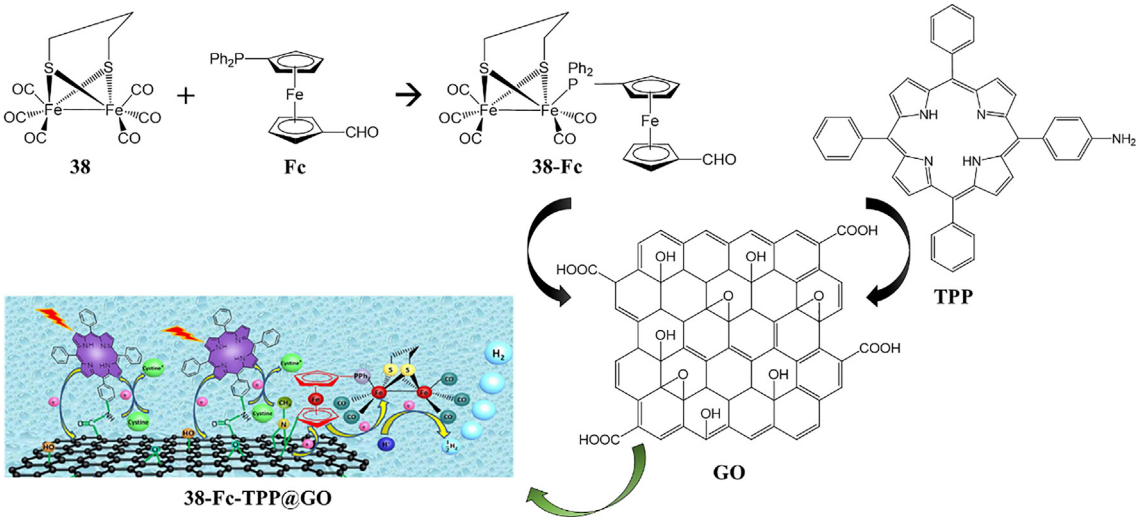

Fig. 22. Synthetic route towards a graphene-based [2Fe2S] system for photocatalytic hydrogen evolution in aqueous solution. Schematic representation adapted from Ref. [239] with permission from Elsevier.

surface of a thiol-functionalized PMO (SH-PMO) [100,237]. The **4@SH-PMO** showed photocatalytic hydrogen production (Fig. 21**c**) without the decomposition of the diiron center, achieving a high TON of 310 over 2 h in an aqueous solution containing the photosensitizer $[Ru(bpy)_3]^{2+}$ and the $AscO^-$ ED (Table 5, entry 7). This heterogeneous system had higher photocatalytic activity than the corresponding homogeneous reference complex **4** (TON = 180, see **Section 2**) under analogous experimental conditions. It also out-performed the [2Fe2S] systems immobilized on MOFs and mesoporous silica MCM-41 (TON = 6–19), described earlier in this section. The enhanced hydrogen generation rate was attributed to the periodic mesostructure of the PMO that provided a robust and rigid solid matrix to stabilize the immobilized **4**, overcoming water solubility and photostability issues associated with the [2Fe2S] catalyst. This work was extended by co-immobilizing diiron catalyst **4** and a $[Ru(bpy)_3]^{2+}$ photosensitizer functionalized with a maleimide on PMO via covalent coupling by thiol groups affording **4-Ru@SH-PMO**. This all-solid-state photocatalyst with a loading of 250 and 115 μmol/g of **4** and Ru, respectively, showed photoinduced hydrogen production with a TON of 1.3 (Table 5, entry 8,). This was higher than the **4@SH-PMO** reference system (TON = 0.6) with the homogeneous $[Ru(bpy)_3]^{2+}$ photosensitizer in solution, even with a Ru/**4** ratio analogous to that of **4-Ru@SH-PMO**. Indeed, the difference in TON obtained for the heterogeneous **4@SH-PMO** and **4-Ru@SH-PMO** systems was attributed to vastly different Ru/**4** ratios in the two systems of 67 and 0.46, respectively.

Recently, the use of nanosilica as a solid support for anchoring diiron catalysts has been reported by Wang et al [238]. The heterogeneous system **38@nanosilica** consisting of complex **38**, [Fe_2(-

pdt)$(CO)_6$], immobilized on modified nanosilica was used in a photocatalytic system in conjunction with [Ir$(ppy)_2$(bpy)]PF_6 as a PS, TEA as a sacrificial ED, H_2O as a proton source and MeCN as the solvent (Fig. 21**d**). After irradiation for 5 h with visible light, a TON of 324 per catalyst was achieved (Table 5, entry 9). The degradation of the catalyst after the reaction was demonstrated by IT spectroscopy. Furthermore, a decreased iron content (1.18%) with respect to the original loading (1.39%) on the nanosilica was observed by atomic absorption spectroscopy (AAS), thus corroborating the decomposition and associated leaching of the diiron complex.

7.3. Graphene-based [FeFe]-hydrogenase active site model nanohybrids

In recent years, a novel approach for the preparation of a heterogeneous photosystem containing a [2Fe2S] catalyst and a molecular PS immobilized on graphene oxide (GO) was reported [239]. GO has extraordinary physicochemical and structural properties used in wide-ranging applications such as photocatalysis, energy conversion or biosensing [240]. Surface oxygen-containing groups (carboxylic, hydroxy and epoxy) provide high water solubility and reactive sites for chemical modification. Jang and colleagues developed a graphene-based nanohybrid (**38-Fc-TPP@GO**) composed of the [2Fe2S] complex (**38**) bound to a ferrocene group (**Fc**) forming (**38-Fc**) and a porphyrin light harvester (**TPP**). Both functional units were anchored on the GO nanosheets to assemble a photocatalytic system in aqueous solution (Fig. 22) [239]. The **38-Fc** unit operates at mild redox potentials and mimics the [4Fe4S] cubane cluster present in the [FeFe]-hydrogenase enzyme [241]. Photochemical hydrogen production experiments were carried out with **38-Fc-TPP@GO**, and a light-induced electron transfer was demonstrated by emission fluorescence data. A variety of common sacrificial EDs were evaluated (AscOH, TEOA, glucose or $Na_2S_2O_3$) but the best efficiency for hydrogen generation was found in cysteine, an amino acid present in the natural metalloenzyme. Under visible light irradiation, the **38-Fc-TPP@GO** nanohybrid system exhibited a TON of 3.9 over 5 h in the presence of cysteine in an aqueous solution at pH = 1 (Table 5, entry 10). This catalytic activity surpassed that of the intramolecular (**38**-Fc-TPP) or intermolecular (**38**-Fc + TPP and **38**-Fc + TPP@GO) photocatalytic reference systems. These results corroborated the crucial role of GO for enhancing electron transfer to increase the photoinduced hydrogen productivity in water. The stability of **38-Fc-TPP@GO** was studied by reusing the material in repeated photoreaction experiments. Hydrogen evolution was maintained at 86.5% of the initial value after the third reaction cycle with a remaining [2Fe2S] content of 81.7% calculated by ICP-AES, confirming the reusability of this nanohybrid system.

8. Photocathodes based on [FeFe]-hydrogenase active site mimics

Water-splitting photoelectrochemical (PEC) cells are comprised of two electrode compartments in which the oxidation and reduction half-reactions occur. The energy for the thermodynamically uphill half-reactions comes from the absorption of photons from visible light, potentially complemented by an external applied bias. Light absorption is ensured by semiconductor materials that either absorb visible photons directly through band gap excitation, or that are decorated with PS molecules for light absorption. In the latter case, electron or hole injection from the PS excited state into the conduction and valence band of the semiconductor, respectively, will produce oxidized or reduced PS that drive the half-reactions. While, in principle, only one of the two electrodes need to be light-driven to qualify as a PEC device, tandem PEC devices in which both electrodes are photo-active offer higher theoretic efficiencies (Fig. 23) [242]. In analogy to the examples in the previous sections, photoanode and photocathode are often investigated separately in the laboratory. An electrochemical potential can be applied to complement the available energy from the photoelectrodes, and such systems thus omit the need for sacrificial reagents.

For optimal function, precise engineering of the catalyst/semiconductor interface is crucial to achieve decent performance of molecular PEC devices. Factors to consider in particular include interfacial stability, suitable light-absorptivity of the semiconductor electrode, efficient charge separation and electron transfer enhanced at the interface [243–245].

In this section, we focus on photocathodes for H_2 evolution based on catalysts that mimic the [FeFe] hydrogenase active site. Photocathodes for CO_2 reduction and photoanodes for water oxidation are reviewed elsewhere [246–250]. [2Fe2S] complexes have been used as catalysts at photocathodes in which the photoactive component is either a light-absorbing p-type inorganic semiconductor (**Section 8.1**) or a molecular PS deposited on a p-type semiconductor (**Section 8.2**).

8.1. [2Fe2S] catalysts immobilized on light-absorbing p-type inorganic semiconductors

Molecular catalysts based on the [2Fe2S] motif anchored directly on the surface of a light-harvesting p-type solid-state inorganic semiconductor constitutes a first group of photoelectro-

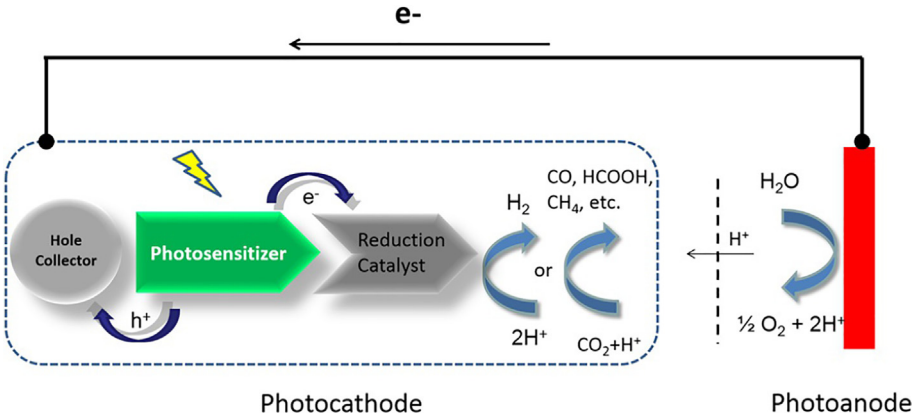

Fig. 23. Schematic representation of a tandem PEC device. Reprinted from Ref. [242] with permission from John Wiley and Sons.

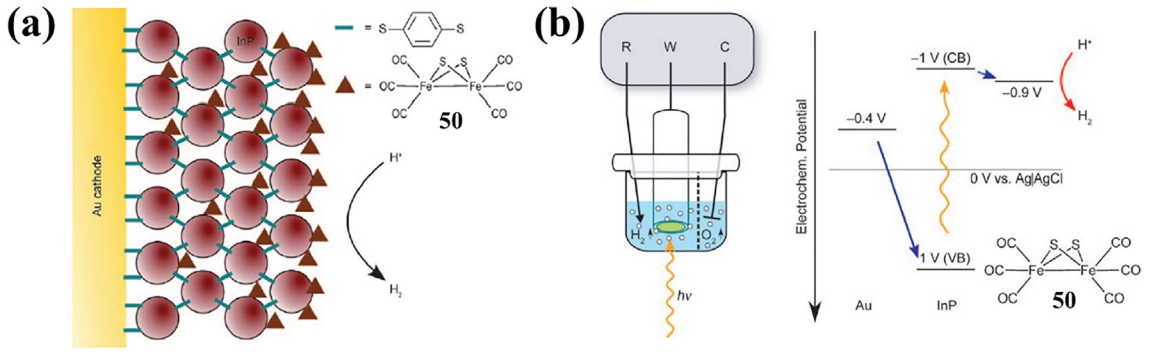

Fig. 24. (a) InP nanocrystal-modified gold photocathode with diiron complex **50** integrated. (b) Electrochemical cell used and energy levels (R: reference electrode, W: working electrode, C: counter electrode, CB: conduction band, VB: valence band). Reproduced and modified from Ref. [253] with permission of John Wiley and Sons.

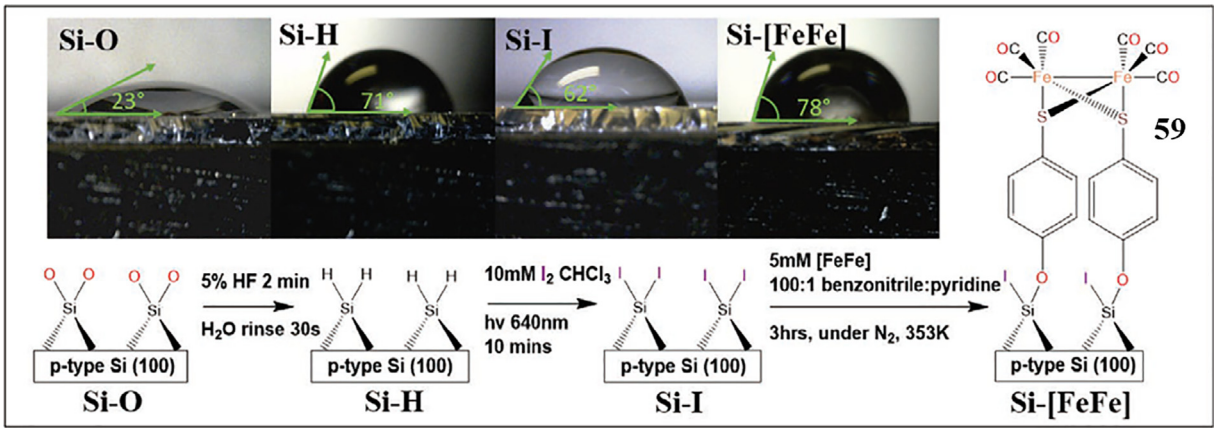

Fig. 25. Schematic modification strategy for preparation of photocathode with [2Fe2S] **59** covalently bonded and contact angle measurements in the different synthesis steps. Reproduced and modified from Ref. [256] with permission from John Wiley and Sons.

chemical architectures for hydrogen evolution [251]. Typically, these photoelectrodes use low bandgap p-type semiconductors that absorb visible-light (InP, Si, GaP or Cu_2O, among others) and have a conduction band potential below the equilibrium thermodynamic potential of the H^+/H_2 couple to provide effective transfer of the excited electrons in the conduction band to the [2Fe2S] catalyst [242,252].

The first example of this design by Nann, Pickett and co-workers in 2010 reported a photocathode that was composed of a gold substrate with indium phosphide (InP) nanocrystals that were cross-linked by 1,4-benzenedithiolates and decorated with the [2Fe2S] catalyst **50** through interactions with the sulfide groups (Fig. 24**a**) [253]. The driving force for electron transfer between the conduction band of the InP semiconductor and catalyst **50** was found exergonic by 0.1 V. Photoelectrochemical hydrogen production was performed in a three-electrode system (Fig. 24**b**) under irradiation at 395 nm using a LED array with a bias potential of −0.4 V versus Ag/AgCl, reaching photocurrents of 250nA/cm^2 in 0.1 M $NaBF_4$ electrolyte solution. After 1 h of light-driven electrolysis, a Faradaic efficiency of 60 % was obtained.

Subsequently, Ott, Kubiak and co-workers prepared a photoelectrochemical system for homogeneous catalytic proton reduction based on p-type silicon (p-Si) photocathode with a narrow band gap of 1.8–2.2 eV, diiron benzenedithiolate catalyst **35** [$(bdt)Fe_2(CO)_6$], and $HClO_4$ as a proton source [254]. Reduction of the [2Fe2S] complex was achieved at an illuminated p-type Si at a reduction potential 0.5 V less negative than that at a glassy carbon electrode. Homogeneous photocatalytic reduction of protons to molecular H_2 was achieved with 100 % Faradaic efficiency, a high current density of 38 mA cm^{-2}, and a light conversion efficiency of 8 % under illumination at λ = 661 nm for five hours at −900 mV versus Fc^+/Fc^0.

Further work based on p-Si in combination with [FeFe] hydrogenase active site mimics by Nann, Voelcker and co-workers reported hierarchically nanostructured photocathodes in which a porous p-Si electrode was sensitized with InP quantum dots and [2Fe2S] complex **50** [255]. The obtained photocurrent density was −1.2 mA/cm^2 at low bias potentials of 0.5 V. The applied bias photo-to-current efficiency (ABPE) was calculated to 0.63%. Unfortunately, the photocurrent density was lower compared to the results previously obtained by Ott et al. [254] although hydrogen generation and the protection of the electrode surface against possible oxidation processes were demonstrated.

Recently, Gu et al. investigated the activity and electrochemical decomposition pathways of catalyst **59** covalently attached to a p-Si photocathode [256]. Contact angle measurement and GATR-FTIR were used to monitor the modifications on the semiconductor-catalyst interface in the different synthesis steps in order to confirm the effectiveness of the grafting procedure and to analyse the distribution of [2Fe2S] **59** along the surface of the p-Si (Fig. 25). The integration of this molecular catalyst passivates the silicon interface for>300 h, preventing the growth of undesirable SiO_2, and thus improves the stability of the device. Photoelectrochemical hydrogen production of the electrode under illumination was as high as 2.31x10^{-5} mol h^{-1} cm^{-2} at −0.78 V versus RHE. Compared to the unmodified hydrogen-terminated Si photoelectrode, the presence of the [2Fe2S] catalyst gives rise to a reduced overpotential of 100 mV to reach a current density of 10 mA cm^{-2}

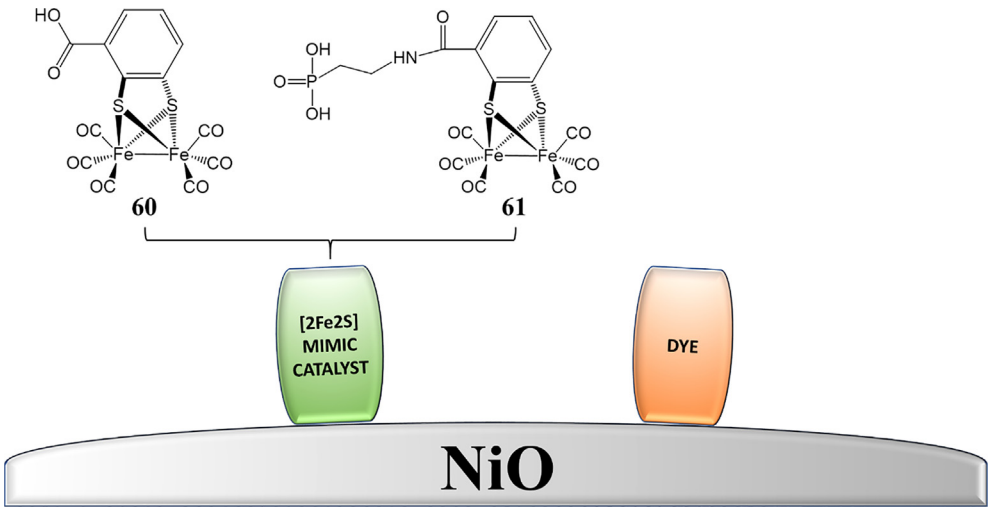

Fig. 26. Schematic drawing of dye-sensitized NiO photocathodes integrating [2Fe2S] mimics.

under illumination. Spectroscopic surface analysis techniques (XPS and GATR-FTIR) were useful tools to reveal structural rearrangements on the photocathode due to degradation of the catalyst by dissociation of the Fe-S bond after 1 h of electrolysis. This study enables the detailed elucidation of the decomposition pathways for the photoelectrode-catalyst interface which will allow the preparation of more active and efficient photocathodes in the future.

8.2. [2Fe2S] catalysts anchored on dye-sensitized NiO photocathodes

p-Type dye-sensitized solar cells (p-DSSCs) have served as inspiration for the design of dye-sensitized p-type semiconductor HER photocathodes [242,252,257]. In analogy to the working principle of p-DSSCs, excitation of the PS on the photocathode results in hole injection into the valence band of the metal oxide. The thereby generated reduced PS transfers an electron to the hydrogen generation catalyst. An alternative mechanism includes charge separation between excited photosensitizer and the catalyst prior to hole injection into the VB of the semiconductor. In the last decade, p-type NiO semiconductor has been commonly used as electrode substrate to anchor both photosensitizer and [2Fe2S] catalysts.

In 2012, Hammarström, Ott and co-workers made the first attempt in this field with the development of a dye-sensitized photocathode by co-adsorption of the Coumarin-343 (C343) photosensitizer and a mononuclear iron dithiolate complex on the surface of mesoporous NiO films [258]. Light-driven electron transfer from the reduced PS to the proton reduction catalyst was spectroscopically demonstrated. The reversible reduction of the catalyst after dye excitation occurred within 50 ns, while the interfacial charge recombination between the reduced HER catalyst and the valence band holes in NiO occurred on a 100 μs time scale following non-exponential kinetics. This research represented an essential proof-of-concept for the preparation of dye-sensitized NiO photocathodes by a co-grafting strategy and its application for photoelectrochemical hydrogen evolution in the absence of sacrificial donor reagents.

Subsequently, an advanced study reported by the same group showed ultrafast electron transfer from the reduced C343 dye to the [2Fe2S] catalyst **60** (Fig. 26) on the co-sensitized surface of p-type NiO films [259]. Transient optical spectroscopy revealed that hole injection occurred on a femtosecond time scale (200 fs) from NiO to the excited dye followed by rapid surface electron transfer from reduced dye to the [2Fe2S] catalyst ($t_{1/2} \approx 10$ ps). Charge recombination between the reduced catalyst **60** and the NiO holes was considerably slower (several tens of μs) compared to previous research. The obtained long-lived charge separation state and the resulting ultrafast electron transfer between dye and catalyst, both co-immobilized on NiO, were crucial for the subsequent design of efficient photocathodes incorporated into p-DSSCs for the electrochemical reduction of protons to H_2.

Based on these works, Hammarström's group reported the first dye-sensitized solar fuel device (DSSFD) based on a [2Fe2S] complex. The employed [2Fe2S] complex **61** (Fig. 26) has a molecular structure analogous to that of complex **60** but with a pendant phosphonate group binding on the C343-sensitized NiO photocathode [260]. Subpicosecond hole injection from the excited dye to NiO mesoporous films ($t_{50\%} \sim 6$ ps) followed by ultrafast surface electron transfer led to catalyst reduction with an approximate yield of 70% as verified by femtosecond transient absorption spectroscopy. The slow charge recombination of the reduced catalyst (2 μs – 20 ms) made protonation and second reduction step of the catalyst feasible. The device containing the C343:**61**/ NiO photocathode showed a photoelectrochemical hydrogen production activity with a Faradaic efficiency of ~50%. Unfortunately, catalyst degradation and desorption from the NiO surface were observed by infrared spectroscopy and gas chromatography techniques.

More recently, the same group analysed the viability of the charge transfer reactions between dye/catalyst **61** co-adsorbed on NiO photocathode by femtosecond mid-infrared transient absorption spectroscopy [261]. An organic push–pull dye (E2) and C343 dye were used as molecular photosensitizers independently. Spectroscopic signatures of the reduced **61** were monitored upon photo-excitation of the dye at a few picosecond time scales although kinetic differences were observed in the first reduction step of the catalyst depending on the dye co-adsorbed into NiO films. In the C343-sensitized NiO films, hole injection into NiO occurred prior to the catalyst **61** reduction with a lifetime $\tau > 5$ ns. In contrast, direct electron transfer occurred between the excited E2 * and the catalyst in E2-sensitized NiO films with a decreased lifetime ($\tau = 50$ ps) of the singly reduced catalyst. These mechanistic changes were attributed to the different arrangement of the dye and diiron catalyst **61** on the surface of the NiO films, highlighting the importance of the dye/catalyst packing on the efficiency of co-sensitized NiO photocathodes.

An alternative approach that includes utilization of a QD-sensitized NiO photocathode was proposed by Wu, Li and co-

workers. CdSe QDs and [2Fe2S] complex **50** loaded onto a NiO substrate resulted in efficient proton reduction to H_2 at a bias ~ 0.3 V vs. NHE in neutral water [262]. A high photocurrent density of −56 μA cm^{-2} at −0.1 V (vs. NHE) under visible-light illumination was obtained, making this photoelectrode a promising candidate to enhance the performance of PEC cells.

9. Summary and outlook

Photocatalytic systems based on biomimetic models of the [FeFe]-hydrogenase active site have evolved substantially during the last two decades. Chemical engineering to reproduce architectures analogous to those found in the natural hydrogenase enzyme, mechanistic elucidation of the role of the hydride, and electrochemical investigation of the [2Fe2S] complexes had a decisive impact on their application as catalysts in visible-light-driven hydrogen production. The basic molecular [2Fe2S] catalysts have the general formula $Fe_2S_2RL_6$, where the two sulphur atoms are part of a bridging unit that tethers together the Fe cations, each of which is further coordinated by three ligands L, often carbon monoxide. These metallic clusters can be precisely modified by replacing the L ligands or the dithiolate bridge, allowing the tuning of electronic and photophysical properties of the complex for optimal employment in photocatalysis.

The wide range of reaction conditions for photocatalysis using hydrogenase active site mimics precludes a direct comparison between the catalytic performances of different [2Fe2S] complexes. Nevertheless, some conclusions can be drawn from this literature review. First, the performance of [FeFe]-hydrogenase active site mimics can clearly be modulated through the first and second coordination sphere. The replacement of CO ligands in the [2Fe2S] cluster by phosphines renders the reduction potential of the diiron species more negative, and increases the stability of the catalyst under photoreaction conditions. Aromatic bridges stabilize the complex and anodically shift the reduction potential for proton reduction, while sulfonates in the bridgehead promote water solubility. These strategies have resulted in [2Fe2S] complexes with improved catalytic performance.

The intermolecular electron transfer between [2Fe2S] and appropriate photosensitizers can produce hydrogen using light in the presence of electron donors by a reductive quenching mechanism. *Intra*molecular electron transfer processes can be carried out using molecular dyads bearing photosensitizers directly linked to [2Fe2S] compounds. Furthermore, triads with an electron donor appended to PS-[2Fe2S] complexes have demonstrated a strong driving force for photoinduced electron transfer from the photosensitizer to the diiron center via oxidative quenching. The enhanced charge separation combats undesirable recombination processes, providing a longer lifetime of the reduced $Fe^{I}Fe^{0}$ species essential for hydrogen evolution. Future efforts in the design of dyads and triads should offer production of strong reducing equivalents, optimized redox properties, enhanced electron transfer efficiency, and photostability.

Supramolecular assemblies incorporating synthetic [2Fe2S] clusters have been used to tune the outer coordination sphere and promote strong interactions and efficient electron transfer between the PS and the diiron compound in an environment mimicking that of the native metalloenzyme. Supramolecular platforms provide hydrophobic hydrogenase-like isolation sites that stabilize the charge-separated state and/or reactive intermediates, and improve water solubility. Particularly, the elegantly designed artificial hydrogenases immobilized on polysaccharides and metallopolymers in combination with quantum dot light harvesters exhibit significant stability and high photocatalytic activity for hydrogen production in aqueous solution under visible light irradiation.

Hybrid photocatalytic systems consisting of the biomimetic diiron catalyst assembled on semiconductor nanoparticles have been successfully applied in light-induced hydrogen generation reactions. In addition, the anchoring of [2Fe2S] catalysts on the surface of QD constitutes an alternative strategy for the design of a water-soluble artificial photosynthetic [2Fe2S] system. Outstanding hydrogen productivity rates have been achieved due to the broad and tunable spectral absorption range of these materials, as well as the structural stability of the molecular catalyst and the effective electron transfer and charge separation from the photoexcited semiconductor to the diiron cluster [2Fe2S].

Novel pathways have been pursued using ordered heterogeneous structures for embedding or immobilizing [2Fe2S] complexes, raising the possibility to increase the stability of the diiron molecular catalyst for large-scale applications. Metal-organic frameworks (MOFs), silica mesoporous platforms and graphene-based supports are easily separable and recyclable hybrid materials. Regarding MOFs, their well-ordered structures can provide the appropriate hydrophobic environment for anchoring [2Fe2S] sites, while promoting accessibility to the catalyst through facile diffusion of reactants and products through the framework pores. The development of future catalytic MOFs requires further catalyst design and precise engineering of transport channels. The appropriate distance between the catalytically active unit and the photosensitizer within the framework is essential for efficient charge transfer in the photocatalytic process. It is not always clear where catalysis occurrs in a MOF since the substrate, reducing equivalents and protons may not always be accessible to all catalytic units, in particular those that are deeply buried in the MOF crystals, thereby decreasing overall efficacy. Silica-based heterogeneous supports with immobilized [2Fe2S] complexes provide catalyst photostability and long-lived charge-separated states, crucial factors to increase photocatalytic hydrogen generation activity. The use of graphene-based materials to immobilize both photosensitizer and diiron catalyst is a promising alternative strategy to design a suitable electronic and stable configuration that improves intramolecular electron transfer between anchored functional units and thus enhances photoinduced hydrogen production.

The synergistic hybridization of catalysts based on [2Fe2S] complexes and solid supports in the correct environment is a promising research avenue to develop enhanced photocatalytic systems for hydrogen production by harnessing inspiration from nature.

The challenge in the future of biomimetic catalysis is coupling reductive and oxidative half-reactions to build complete artificial photosynthetic water-splitting systems for the conversion of solar energy to chemical fuels. The rational combination of a synthetic hydrogenase photosystem capable of carrying out proton reduction together with a system capable of catalyzing the water oxidation half-reaction is being evaluated in whole cell conditions and in photoelectrochemical devices [263–266]. In this field, PEC cells containing photocathodes based on p-type semiconductors with immobilized H_2-evolving [2Fe2S] catalysts have emerged in recent years as potentially inexpensive, robust and non-toxic devices for photoelectrochemical proton reduction. These efforts will put forward new inspiration and technologies based on the fascinating world of photocatalysis and biomimicry.

Declaration of Competing Interest

The authors declare that they have no known competing financial interests or personal relationships that could have appeared to influence the work reported in this paper.

Acknowledgments

J. A.-G., D. E. and F. J. R.-S. wish to acknowledge financial support from Ramon Areces Foundation, Spanish Ministry of Science, Innovation and Universities for an FPU teaching and research fellowship (FPU17/03981) and Project RTI2018-101611-B-100, Andalusian Regional Government (FQM-346 group), and Feder Funds. H.T. wants to acknowledge the Olle Engkvist Foundation (200-0523), and S. O. the Swedish Research Council (2015-04640) for financial support.

References

[1] M.S. Dresselhaus, I.L. Thomas, Alternative energy technologies, Nature 414 (6861) (2001) 332–337, https://doi.org/10.1038/35104599.
[2] I. Dincer, C. Acar, Review and evaluation of hydrogen production methods for better sustainability, Int. J. Hydrogen Energy 40 (34) (2015) 11094–11111, https://doi.org/10.1016/j.ijhydene.2014.12.035.
[3] E. Kabir, P. Kumar, S. Kumar, A.A. Adelodun, K.-H. Kim, Solar energy: Potential and future prospects, Renew. Sustain. Energy Rev. 82 (2018) 894–900, https://doi.org/10.1016/j.rser.2017.09.094.
[4] S. Chen, T. Takata, K. Domen, Particulate photocatalysts for overall water splitting, Nat. Rev. Mater. 2 (2017) 17050, https://doi.org/10.1038/natrevmats.2017.50.
[5] K. Maeda, K. Domen, Photocatalytic water splitting: recent progress and future challenges, J. Phys. Chem. Lett. 1 (18) (2010) 2655–2661, https://doi.org/10.1021/jz1007966.
[6] J.N. Armor, Catalysis and the hydrogen economy, Catal. Lett. 101 (3-4) (2005) 131–135, https://doi.org/10.1007/s10562-005-4877-3.
[7] S. Ott, Ironing out hydrogen storage, Science 333 (6050) (2011) 1714–1715, https://doi.org/10.1126/science:1211021.
[8] J.O. Abe, A.P.I. Popoola, E. Ajenifuja, O.M. Popoola, Hydrogen energy, economy and storage: Review and recommendation, Int. J. Hydrogen Energy 44 (29) (2019) 15072–15086, https://doi.org/10.1016/j.ijhydene.2019.04.068.
[9] S.E. Hosseini, M.A. Wahid, Hydrogen production from renewable and sustainable energy resources: Promising green energy carrier for clean development, Renew. Sustain. Energy Rev. 57 (2016) 850–866, https://doi.org/10.1016/j.rser.2015.12.112.
[10] P.F. Weaver, S. Lien, M. Seibert, Photobiological production of hydrogen, Sol. Energy 24 (1) (1980) 3–45, https://doi.org/10.1016/0038-092X(80)90018-3.
[11] Y. Asada, J. Miyake, Photobiological hydrogen production, J. Biosci. Bioeng. 88 (1) (1999) 1–6, https://doi.org/10.1016/S1389-1723(99)80166-2.
[12] D. Das, Hydrogen production by biological processes: a survey of literature, Int. J. Hydrogen Energy 26 (1) (2001) 13–28, https://doi.org/10.1016/S0360-3199(00)00058-6.
[13] S.I. Allakhverdiev, V. Thavasi, V.D. Kreslavski, S.K. Zharmukhamedov, V.V. Klimov, S. Ramakrishna, D.A. Los, M. Mimuro, H. Nishihara, R. Carpentier, Photosynthetic hydrogen production, J. Photochem. Photobiol. C Photochem. Rev. 11 (2-3) (2010) 101–113, https://doi.org/10.1016/j.jphotochemrev.2010.07.002.
[14] R. Lomoth, S. Ott, Introducing a dark reaction to photochemistry: photocatalytic hydrogen from [FeFe] hydrogenase active site model complexes, Dalton Trans. (45) (2009) 9952, https://doi.org/10.1039/b911129h.
[15] A. Hemschemeier, A. Melis, T. Happe, Analytical approaches to photobiological hydrogen production in unicellular green algae, Photosynth. Res. 102 (2-3) (2009) 523–540, https://doi.org/10.1007/s11120-009-9415-5.
[16] S.J. Burgess, B. Tamburic, F. Zemichael, K. Hellgardt, P.J. Nixon, Solar-driven hydrogen production in green algae, Adv. Appl. Microbiol. (2011), https://doi.org/10.1016/B978-0-12-387046-9.00004-9.
[17] W. Khetkorn, R.P. Rastogi, A. Incharoensakdi, P. Lindblad, D. Madamwar, A. Pandey, C. Larroche, Microalgal hydrogen production – A review, Bioresour. Technol. 243 (2017) 1194–1206, https://doi.org/10.1016/j.biortech.2017.07.085.
[18] M. Frey, Hydrogenases: Hydrogen-Activating Enzymes, ChemBioChem 3 (2002) 153–160, https://doi.org/10.1002/1439-7633(20020301)3:2/3<153::AID-CBIC153>3.0.CO;2-B.
[19] P.M. Vignais, B. Billoud, Occurrence, Classification, and Biological Function of Hydrogenases: An Overview, Chem. Rev. 107 (2007) 4206–4272, https://doi.org/10.1021/cr050196r.
[20] J.W. Peters, X-ray crystal structure of the fe-only hydrogenase (CpI) from Clostridium pasteurianum to 1.8 angstrom resolution, Science. 282 (1998) 1853–1858, https://doi.org/10.1126/science.282.5395.1853.
[21] Y. Nicolet, C. Piras, P. Legrand, C.E. Hatchikian, J.C. Fontecilla-Camps, Desulfovibrio desulfuricans iron hydrogenase: the structure shows unusual coordination to an active site Fe binuclear center, Structure. 7 (1) (1999) 13–23, https://doi.org/10.1016/S0969-2126(99)80005-7.
[22] D. Mulder, E. Shepard, J. Meuser, N. Joshi, P. King, M. Posewitz, J. Broderick, J. Peters, Insights into [FeFe]-hydrogenase structure, mechanism, and maturation, Structure 19 (8) (2011) 1038–1052, https://doi.org/10.1016/j.str.2011.06.008.
[23] P. Knörzer, A. Silakov, C.E. Foster, F.A. Armstrong, W. Lubitz, T. Happe, Importance of the protein framework for catalytic activity of [FeFe]-hydrogenases, J. Biol. Chem. 287 (2) (2012) 1489–1499, https://doi.org/10.1074/jbc.M111.305797.
[24] W. Lubitz, H. Ogata, O. Rüdiger, E. Reijerse, Hydrogenases, Chem. Rev. 114 (8) (2014) 4081–4148, https://doi.org/10.1021/cr4005814.
[25] J.A. Birrell, O. Rüdiger, E.J. Reijerse, W. Lubitz, Semisynthetic hydrogenases propel biological energy research into a new era, Joule 1 (1) (2017) 61–76, https://doi.org/10.1016/j.joule.2017.07.009.
[26] P. Rodríguez-Maciá, K. Pawlak, O. Rüdiger, E.J. Reijerse, W. Lubitz, J.A. Birrell, Intercluster redox coupling influences protonation at the H-cluster in [FeFe] hydrogenases, J. Am. Chem. Soc. 139 (42) (2017) 15122–15134, https://doi.org/10.1021/jacs.7b0819310.1021/jacs.7b08193.s001.
[27] A. Adamska, A. Silakov, C. Lambertz, O. Rüdiger, T. Happe, E. Reijerse, W. Lubitz, Identification and characterization of the "Super-Reduced" state of the H-cluster in [FeFe] Hydrogenase: A new building block for the catalytic cycle?, Angew Chem. Int. Ed. 51 (46) (2012) 11458–11462, https://doi.org/10.1002/anie.201204800.
[28] S. Rumpel, C. Sommer, E. Reijerse, C. Farès, W. Lubitz, Direct detection of the terminal hydride intermediate in [FeFe] hydrogenase by NMR spectroscopy, J. Am. Chem. Soc. 140 (11) (2018) 3863–3866, https://doi.org/10.1021/jacs.8b0045910.1021/jacs.8b00459.s001.
[29] C. Tard, C.J. Pickett, Structural and functional analogues of the active sites of the [Fe]-, [NiFe]-, and [FeFe]-hydrogenases †, Chem. Rev. 109 (6) (2009) 2245–2274, https://doi.org/10.1021/cr800542q.
[30] J.A. Wright, C.J. Pickett, Protonation of a subsite analogue of [FeFe]-hydrogenase: mechanism of a deceptively simple reaction revealed by time-resolved IR spectroscopy, Chem. Commun. (38) (2009) 5719, https://doi.org/10.1039/b912499c.
[31] S. Tschierlei, S. Ott, R. Lomoth, Spectroscopically characterized intermediates of catalytic H2 formation by [FeFe] hydrogenase models, Energy Environ. Sci. 4 (7) (2011) 2340, https://doi.org/10.1039/c0ee00708k.
[32] N. Wang, M. Wang, L. Chen, L. Sun, Reactions of [FeFe]-hydrogenase models involving the formation of hydrides related to proton reduction and hydrogen oxidation, Dalton Trans. 42 (34) (2013) 12059, https://doi.org/10.1039/c3dt51371h.
[33] H. Long, P.W. King, C.H. Chang, Proton transport in Clostridium pasteurianum [FeFe] Hydrogenase I: A computational study, J. Phys. Chem. B 118 (4) (2014) 890–900, https://doi.org/10.1021/jp408621r.
[34] E.J. Reijerse, V. Pelmenschikov, J.A. Birrell, C.P. Richers, M. Kaupp, T.B. Rauchfuss, S.P. Cramer, W. Lubitz, Asymmetry in the ligand coordination sphere of the [FeFe] hydrogenase active site is reflected in the magnetic spin interactions of the aza-propanedithiolate ligand, J. Phys. Chem. Lett. 10 (21) (2019) 6794–6799, https://doi.org/10.1021/acs.jpclett.9b02354.
[35] C. Madden, M.D. Vaughn, I. Díez-Pérez, K.A. Brown, P.W. King, D. Gust, A.L. Moore, T.A. Moore, Catalytic turnover of [FeFe]-hydrogenase based on single-molecule imaging, J. Am. Chem. Soc. 134 (3) (2012) 1577–1582, https://doi.org/10.1021/ja207461t.
[36] C.A. Tooley, S. Pazicni, E.B. Berda, Toward a tunable synthetic [FeFe] hydrogenase mimic: single-chain nanoparticles functionalized with a single diiron cluster, Polym. Chem. 6 (44) (2015) 7646–7651, https://doi.org/10.1039/C5PY01196E.
[37] A. Bachmeier, F. Armstrong, Solar-driven proton and carbon dioxide reduction to fuels — lessons from metalloenzymes, Curr. Opin. Chem. Biol. 25 (2015) 141–151, https://doi.org/10.1016/j.cbpa.2015.01.001.
[38] S.T. Stripp, G. Goldet, C. Brandmayr, O. Sanganas, K.A. Vincent, M. Haumann, F. A. Armstrong, T. Happe, How oxygen attacks [FeFe] hydrogenases from photosynthetic organisms, Proc. Natl. Acad. Sci. (U.S.A.). 106 (41) (2009) 17331–17336, https://doi.org/10.1073/pnas.0905343106.
[39] C. Lambertz, N. Leidel, K.G.V. Havelius, J. Noth, P. Chernev, M. Winkler, T. Happe, M. Haumann, O 2 reactions at the six-iron active site (H-cluster) in [FeFe]-hydrogenase, J. Biol. Chem. 286 (47) (2011) 40614–40623, https://doi.org/10.1074/jbc.M111.283648.
[40] K.D. Swanson, M.W. Ratzloff, D.W. Mulder, J.H. Artz, S. Ghose, A. Hoffman, S. White, O.A. Zadvornyy, J.B. Broderick, B. Bothner, P.W. King, J.W. Peters, [FeFe]-hydrogenase oxygen inactivation is initiated at the H cluster 2Fe subcluster, J. Am. Chem. Soc. 137 (5) (2015) 1809–1816, https://doi.org/10.1021/ja510169s.
[41] J.-F. Capon, F. Gloaguen, F.Y. Pétillon, P. Schollhammer, J. Talarmin, Electron and proton transfers at diiron dithiolate sites relevant to the catalysis of proton reduction by the [FeFe]-hydrogenases, Coord. Chem. Rev. 253 (9-10) (2009) 1476–1494, https://doi.org/10.1016/j.ccr.2008.10.020.
[42] D.W. Mulder, M.W. Ratzloff, E.M. Shepard, A.S. Byer, S.M. Noone, J.W. Peters, J. B. Broderick, P.W. King, EPR and FTIR Analysis of the Mechanism of H 2 Activation by [FeFe]-Hydrogenase HydA1 from Chlamydomonas reinhardtii, J. Am. Chem. Soc. 135 (18) (2013) 6921–6929, https://doi.org/10.1021/ja4000257.
[43] J. Esselborn, C. Lambertz, A. Adamska-Venkatesh, T. Simmons, G. Berggren, J. Noth, J. Siebel, A. Hemschemeier, V. Artero, E. Reijerse, M. Fontecave, W. Lubitz, T. Happe, Spontaneous activation of [FeFe]-hydrogenases by an inorganic [2Fe] active site mimic, Nat. Chem. Biol. 9 (10) (2013) 607–609, https://doi.org/10.1038/nchembio.1311.
[44] G. Berggren, A. Adamska, C. Lambertz, T.R. Simmons, J. Esselborn, M. Atta, S. Gambarelli, J.-M. Mouesca, E. Reijerse, W. Lubitz, T. Happe, V. Artero, M.

Fontecave, Biomimetic assembly and activation of [FeFe]-hydrogenases, Nature 499 (7456) (2013) 66–69, https://doi.org/10.1038/nature12239.
[45] L. Sun, B. Akermark, S. Ott, Iron hydrogenase active site mimics in supramolecular systems aiming for light-driven hydrogen production, Coord. Chem. Rev. 249 (15-16) (2005) 1653–1663, https://doi.org/10.1016/j.ccr.2005.01.013.
[46] Y. Li, T.B. Rauchfuss, Synthesis of diiron(I) dithiolato carbonyl complexes, Chem. Rev. 116 (12) (2016) 7043–7077, https://doi.org/10.1021/acs.chemrev.5b00669.
[47] L. Hammarström, accumulative charge separation for solar fuels production: coupling light-induced single electron transfer to multielectron catalysis, Acc. Chem. Res. 48 (3) (2015) 840–850, https://doi.org/10.1021/ar500386x.
[48] D. Gust, T.A. Moore, A.L. Moore, Molecular mimicry of photosynthetic energy and electron transfer, Acc. Chem. Res. 26 (4) (1993) 198–205, https://doi.org/10.1021/ar00028a010.
[49] J.H. Alstrum-Acevedo, M.K. Brennaman, T.J. Meyer, Chemical approaches to artificial photosynthesis. 2, Inorg. Chem. 44 (20) (2005) 6802–6827, https://doi.org/10.1021/ic050904r.
[50] W.T. Eckenhoff, R. Eisenberg, Molecular systems for light driven hydrogen production, Dalton Trans. 41 (42) (2012) 13004, https://doi.org/10.1039/c2dt30823a.
[51] V. Artero, M. Fontecave, Solar fuels generation and molecular systems: is it homogeneous or heterogeneous catalysis?, Chem Soc. Rev. 42 (6) (2013) 2338–2356, https://doi.org/10.1039/C2CS35334B.
[52] A. Juris, V. Balzani, F. Barigelletti, S. Campagna, P. Belser, A. von Zelewsky, Ru (II) polypyridine complexes: photophysics, photochemistry, eletrochemistry, and chemiluminescence, Coord. Chem. Rev. 84 (1988) 85–277, https://doi.org/10.1016/0010-8545(88)80032-8.
[53] J. Lehn, J. Sauvage, Chemical storage of light energy. catalytic generation of hydrogen by visible light or sunlight. Irradiation of neutral aqueous solutions, Nouv. J. Chim. (1977) 449–451.
[54] M. Kirch, J.-M. Lehn, J.-P. Sauvage, Hydrogen generation by visible light irradiation of aqueous solutions of metal complexes. An approach to the photochemical conversion and storage of solar energy, Helv. Chim. Acta 62 (4) (1979) 1345–1384, https://doi.org/10.1002/hlca.19790620449.
[55] K. Kalyanasundaram, J. Kiwi, M. Grätzel, Hydrogen evolution from water by visible light, a homogeneous three component test system for redox catalysis, Helv. Chim. Acta 61 (7) (1978) 2720–2730, https://doi.org/10.1002/hlca.19780610740.
[56] J. Kiwi, M. Graetzel, Projection, size factors, and reaction dynamics of colloidal redox catalysts mediating light induced hydrogen evolution from water, J. Am. Chem. Soc. 101 (24) (1979) 7214–7217, https://doi.org/10.1021/ja00518a015.
[57] J. Kiwi, M. Grätzel, Hydrogen evolution from water induced by visible light mediated by redox catalysis, Nature 281 (5733) (1979) 657–658, https://doi.org/10.1038/281657a0.
[58] A.J. Esswein, D.G. Nocera, Hydrogen production by molecular photocatalysis, Chem. Rev. 107 (10) (2007) 4022–4047, https://doi.org/10.1021/cr050193e.
[59] G.M. Brown, B.S. Brunschwig, C. Creutz, J.F. Endicott, N. Sutin, Homogeneous catalysis of the photoreduction of water by visible light. Mediation by a Tris (2,2'-bipyridine)Ru(II)-Co(II) macrocycle system, J. Am. Chem. Soc. 101 (1979) 1298–1300.
[60] A. Reynal, E. Pastor, M.A. Gross, S. Selim, E. Reisner, J.R. Durrant, Unravelling the pH-dependence of a molecular photocatalytic system for hydrogen production, Chem. Sci. 6 (8) (2015) 4855–4859, https://doi.org/10.1039/C5SC01349F.
[61] Y. Pellegrin, F. Odobel, Sacrificial electron donor reagents for solar fuel production, Comptes Rendus Chim. 20 (3) (2017) 283–295, https://doi.org/10.1016/j.crci.2015.11.026.
[62] J.-H. Shon, T.S. Teets, Molecular photosensitizers in energy research and catalysis: design principles and recent developments, ACS Energy Lett. 4 (2) (2019) 558–566, https://doi.org/10.1021/acsenergylett.8b02388.
[63] D.C. Neckers, Rose bengal, J. Photochem. Photobiol. A Chem. 47 (1) (1989) 1–29, https://doi.org/10.1016/1010-6030(89)85002-6.
[64] D.A. Nicewicz, T.M. Nguyen, Recent applications of organic dyes as photoredox catalysts in organic synthesis, ACS Catal. 4 (1) (2014) 355–360, https://doi.org/10.1021/cs400956a.
[65] D. Ravelli, M. Fagnoni, Dyes as visible light photoredox organocatalysts, ChemCatChem 4 (2) (2012) 169–171, https://doi.org/10.1002/cctc.201100363.
[66] E. Arunkumar, C.C. Forbes, B.D. Smith, Improving the properties of organic dyes by molecular encapsulation, Eur. J. Org. Chem. 2005 (19) (2005) 4051–4059, https://doi.org/10.1002/ejoc.v2005:1910.1002/ejoc.200500372.
[67] M. Neumann, S. Füldner, B. König, K. Zeitler, Metal-free, cooperative asymmetric organophotoredox catalysis with visible light, Angew. Chem. Int. Ed. 50 (4) (2011) 951–954, https://doi.org/10.1002/anie.201002992.
[68] Y. Ooyama, Y. Harima, Photophysical and electrochemical properties, and molecular structures of organic dyes for dye-sensitized solar cells, ChemPhysChem 13 (18) (2012) 4032–4080, https://doi.org/10.1002/cphc.v13.1810.1002/cphc.201200218.
[69] W.H. Nguyen, C.D. Bailie, J. Burschka, T. Moehl, M. Grätzel, M.D. McGehee, A. Sellinger, Molecular engineering of organic dyes for improved recombination lifetime in solid-state dye-sensitized solar cells, Chem. Mater. 25 (9) (2013) 1519–1525, https://doi.org/10.1021/cm3036357.
[70] S. Aghazada, M. Nazeeruddin, Ruthenium complexes as sensitizers in dye-sensitized solar cells, Inorganics. 6 (2018) 52, https://doi.org/10.3390/inorganics6020052.
[71] F. Teplý, Visible-light photoredox catalysis with [Ru(bpy)3]2+: General principles and the twentieth-century roots, Phys. Sci. Rev. 5 (2020), https://doi.org/10.1515/psr-2017-0171.
[72] Y.-J. Yuan, Z.-T. Yu, D.-Q. Chen, Z.-G. Zou, Metal-complex chromophores for solar hydrogen generation, Chem. Soc. Rev. 46 (3) (2017) 603–631, https://doi.org/10.1039/C6CS00436A.
[73] W.T. Eckenhoff, Molecular catalysts of Co, Ni, Fe, and Mo for hydrogen generation in artificial photosynthetic systems, Coord. Chem. Rev. 373 (2018) 295–316, https://doi.org/10.1016/j.ccr.2017.11.002.
[74] W.J. Shaw, M.L. Helm, D.L. DuBois, A modular, energy-based approach to the development of nickel containing molecular electrocatalysts for hydrogen production and oxidation, Biochim. Biophys. Acta, Gene Struct. Expression 1827 (8-9) (2013) 1123–1139, https://doi.org/10.1016/j.bbabio.2013.01.003.
[75] S. Pullen, S. Maji, M. Stein, S. Ott, Restricted rotation of an Fe(CO) 2 (PL 3)-subunit in [FeFe]-hydrogenase active site mimics by intramolecular ligation, Dalton Trans. 48 (18) (2019) 5933–5939, https://doi.org/10.1039/C8DT05148H.
[76] S. Karlin, Z.-Y. Zhu, K.D. Karlin, The extended environment of mononuclear metal centers in protein structures, Proc. Natl. Acad. Sci. (U.S.A.). 94 (26) (1997) 14225–14230, https://doi.org/10.1073/pnas.94.26.14225.
[77] T. Liu, M.Y. Darensbourg, Fe(II)Fe(I), diiron complex reproduces the unique rotated state of the [FeFe]Hydrogenase active site, J. Am. Chem. Soc. 129 (22) (2007) 7008–7009, https://doi.org/10.1021/ja071851a.
[78] A.K. Justice, L. De Gioia, M.J. Nilges, T.B. Rauchfuss, S.R. Wilson, G. Zampella, Redox and structural properties of mixed-valence models for the active site of the [FeFe]-Hydrogenase: Progress and Challenges, Inorg. Chem. 47 (16) (2008) 7405–7414, https://doi.org/10.1021/ic8007552.
[79] R. Zaffaroni, T.B. Rauchfuss, D.L. Gray, L. De Gioia, G. Zampella, Terminal vs bridging hydrides of diiron dithiolates: protonation of Fe 2 (dithiolate)(CO) 2 (PMe 3) 4, J. Am. Chem. Soc. 134 (46) (2012) 19260–19269, https://doi.org/10.1021/ja3094394.
[80] M.E. Carroll, B.E. Barton, T.B. Rauchfuss, P.J. Carroll, Synthetic models for the active site of the [FeFe]-hydrogenase: catalytic proton reduction and the structure of the doubly protonated intermediate, J. Am. Chem. Soc. 134 (45) (2012) 18843–18852, https://doi.org/10.1021/ja309216v.
[81] S. Ezzaher, A. Gogoll, C. Bruhn, S. Ott, Directing protonation in [FeFe] hydrogenase active site models by modifications in their second coordination sphere, Chem. Commun. 46 (31) (2010) 5775, https://doi.org/10.1039/c0cc00724b.
[82] M. Rakowski DuBois, D.L. DuBois, The roles of the first and second coordination spheres in the design of molecular catalysts for H 2 production and oxidation, Chem. Soc. Rev. 38 (1) (2009) 62–72, https://doi.org/10.1039/B801197B.
[83] D.W. Mulder, M.W. Ratzloff, M. Bruschi, C. Greco, E. Koonce, J.W. Peters, P.W. King, Investigations on the role of proton-coupled electron transfer in hydrogen activation by [FeFe]-hydrogenase, J. Am. Chem. Soc. 136 (43) (2014) 15394–15402, https://doi.org/10.1021/ja508629m.
[84] C. Tard, X. Liu, S.K. Ibrahim, M. Bruschi, L.D. Gioia, S.C. Davies, X. Yang, L.-S. Wang, G. Sawers, C.J. Pickett, Synthesis of the H-cluster framework of iron-only hydrogenase, Nature 433 (7026) (2005) 610–613, https://doi.org/10.1038/nature03298.
[85] O. In-noi, K.J. Haller, G.B. Hall, W.P. Brezinski, J.M. Marx, T. Sakamoto, D.H. Evans, R.S. Glass, D.L. Lichtenberger, Electrochemical, spectroscopic, and computational study of bis(μ-methylthiolato)diironhexacarbonyl: Homoassociative stabilization of the dianion and a chemically reversible reduction/reoxidation cycle, Organometallics 33 (18) (2014) 5009–5019, https://doi.org/10.1021/om5004122.
[86] G.A.N. Felton, C.A. Mebi, B.J. Petro, A.K. Vannucci, D.H. Evans, R.S. Glass, D.L. Lichtenberger, Review of electrochemical studies of complexes containing the Fe2S2 core characteristic of [FeFe]-hydrogenases including catalysis by these complexes of the reduction of acids to form dihydrogen, J. Organomet. Chem. 694 (17) (2009) 2681–2699, https://doi.org/10.1016/j.jorganchem.2009.03.017.
[87] F. Zipoli, R. Car, M.H. Cohen, A. Selloni, Hydrogen production by the naked active site of the Di-iron hydrogenases in water, J. Phys. Chem. B 113 (39) (2009) 13096–13106, https://doi.org/10.1021/jp9059328.
[88] F. Zipoli, R. Car, M.H. Cohen, A. Selloni, Theoretical design by first principles molecular dynamics of a bioinspired electrode−catalyst system for electrocatalytic hydrogen production from acidified water, J. Chem. Theory Comput. 6 (11) (2010) 3490–3502, https://doi.org/10.1021/ct100319b.
[89] M. Wang, L. Chen, X. Li, L. Sun, Approaches to efficient molecular catalyst systems for photochemical H2 production using [FeFe]-hydrogenase active site mimics, Dalton Trans. 40 (48) (2011) 12793, https://doi.org/10.1039/c1dt11166c.
[90] Y. Na, J. Pan, M. Wang, L. Sun, Intermolecular electron transfer from photogenerated Ru(bpy) 3 + to [2Fe2S] model complexes of the iron-only hydrogenase active site, Inorg. Chem. 46 (10) (2007) 3813–3815, https://doi.org/10.1021/ic070234k.
[91] Y. Na, M. Wang, J. Pan, P. Zhang, B. Åkermark, L. Sun, Visible light-driven electron transfer and hydrogen generation catalyzed by bioinspired [2Fe2S] complexes, Inorg. Chem. 47 (7) (2008) 2805–2810, https://doi.org/10.1021/ic702010w.

[92] L.i. Long, X. Jiang, X. Wang, Z. Xiao, X. Liu, Water-soluble diiron hexacarbonyl complex as a CO-RM: controllable CO-releasing, releasing mechanism and biocompatibility, Dalton Trans. 42 (44) (2013) 15663, https://doi.org/10.1039/c3dt51281a.
[93] P. Li, M. Wang, C. He, G. Li, X. Liu, C. Chen, B. Åkermark, L. Sun, Influence of tertiary phosphanes on the coordination configurations and electrochemical properties of iron hydrogenase model complexes: crystal structures of [(μ-S2C3H6)Fe2(CO)6-nLn] (L = PMe2Ph, n = 1, 2; PPh3, P(OEt)3, n = 1), Eur. J. Inorg. Chem. 2005 (12) (2005) 2506–2513, https://doi.org/10.1002/ejic.200400947.
[94] Y. Na, M. Wang, K. Jin, R. Zhang, L. Sun, An approach to water-soluble hydrogenase active site models: Synthesis and electrochemistry of diiron dithiolate complexes with 3,7-diacetyl-1,3,7-triaza-5-phosphabicyclo[3.3.1] nonane ligand(s), J. Organomet. Chem. 691 (23) (2006) 5045–5051, https://doi.org/10.1016/j.jorganchem.2006.08.082.
[95] F. Wang, M. Wang, X. Liu, K. Jin, W. Dong, L. Sun, Protonation, electrochemical properties and molecular structures of halogen-functionalized diiron azadithiolate complexes related to the active site of iron-only hydrogenases, Dalton Trans. (34) (2007) 3812, https://doi.org/10.1039/b706178a.
[96] S.A. Serron, S.P. Nolan, Solution thermochemical study of ligand substitution reaction of novel pyrrolyl-substituted tertiary phosphine ligands in the L2Fe (CO)3 system, Inorg. Chim. Acta. 252 (1-2) (1996) 107–113, https://doi.org/10.1016/S0020-1693(96)05303-0.
[97] K.G. Moloy, J.L. Petersen, N-pyrrolyl phosphines: an unexploited class of phosphine ligands with exceptional.pi.-acceptor character, J. Am. Chem. Soc. 117 (29) (1995) 7696–7710, https://doi.org/10.1021/ja00134a014.
[98] P. Zhang, M. Wang, Y. Na, X. Li, Y.i. Jiang, L. Sun, Homogeneous photocatalytic production of hydrogen from water by a bioinspired [Fe 2 S 2] catalyst with high turnover numbers, Dalton Trans. 39 (5) (2010) 1204–1206, https://doi.org/10.1039/B923159P.
[99] L. Tinker, N. McDaniel, P. Curtin, C. Smith, M. Ireland, S. Bernhard, Visible light induced catalytic water reduction without an electron relay, Chem. Eur. J. 13 (31) (2007) 8726–8732, https://doi.org/10.1002/(ISSN)1521-3765.
[100] T. Himiyama, M. Waki, D. Esquivel, A. Onoda, T. Hayashi, P. Van Der Voort, S. Inagaki, A heterogeneous hydrogen-evolution catalyst based on a mesoporous organosilica with a diiron catalytic center modelling [FeFe]-Hydrogenase, ChemCatChem 10 (21) (2018) 4894–4899, https://doi.org/10.1002/cctc.v10.2110.1002/cctc.201801257.
[101] X. Li, M. Wang, L. Chen, X. Wang, J. Dong, L. Sun, Photocatalytic water reduction and study of the formation of FeIFe0 species in diiron catalyst sytems, ChemSusChem 5 (5) (2012) 913–919, https://doi.org/10.1002/cssc.201100490.
[102] P.J. DeLaive, T.K. Foreman, C. Giannotti, D.G. Whitten, Photoinduced electron transfer reactions of transition-metal complexes with amines. Mechanistic studies of alternate pathways to back electron transfer, J. Am. Chem. Soc. 102 (17) (1980) 5627–5631, https://doi.org/10.1021/ja00537a037.
[103] F. Wang, W.-G. Wang, X.-J. Wang, H.-Y. Wang, C.-H. Tung, L.-Z. Wu, A highly efficient photocatalytic system for hydrogen production by a robust hydrogenase mimic in an aqueous solution, Angew. Chem. Int. Ed. 50 (14) (2011) 3193–3197, https://doi.org/10.1002/anie.201006352.
[104] I.K. Pandey, M. Natarajan, S. Kaur-Ghumaan, Hydrogen generation: Aromatic dithiolate-bridged metal carbonyl complexes as hydrogenase catalytic site models, J. Inorg. Biochem. 143 (2015) 88–110, https://doi.org/10.1016/j.jinorgbio.2014.11.006.
[105] S. Gao, Y. Liu, Y. Shao, D. Jiang, Q. Duan, Iron carbonyl compounds with aromatic dithiolate bridges as organometallic mimics of [FeFe] hydrogenases, Coord. Chem. Rev. 402 (2020) 213081, https://doi.org/10.1016/j.ccr.2019.213081.
[106] F. Gloaguen, D. Morvan, J.-F. Capon, P. Schollhammer, J. Talarmin, Electrochemical proton reduction at mild potentials by monosubstituted diiron organometallic complexes bearing a benzenedithiolate bridge, J. Electroanal. Chem. 603 (1) (2007) 15–20, https://doi.org/10.1016/j.jelechem.2007.02.003.
[107] I.K. Pandey, S.M. Mobin, N. Deibel, B. Sarkar, S. Kaur-Ghumaan, Diiron benzenedithiolate complexes relevant to the [FeFe] hydrogenase active site, Eur. J. Inorg. Chem. 2015 (17) (2015) 2875–2882, https://doi.org/10.1002/ejic.201500345.
[108] L. Schwartz, P.S. Singh, L. Eriksson, R. Lomoth, S. Ott, Tuning the electronic properties of Fe2(μ-arenedithiolate)(CO)6−n(PMe3)n (n=0, 2) complexes related to the [Fe–Fe]-hydrogenase active site, Comptes Rendus Chim. 11 (8) (2008) 875–889, https://doi.org/10.1016/j.crci.2008.04.001.
[109] E.S. Donovan, J.J. McCormick, G.S. Nichol, G.A.N. Felton, Cyclic voltammetric studies of chlorine-substituted diiron benzenedithiolato hexacarbonyl electrocatalysts inspired by the [FeFe]-hydrogenase active site, Organometallics 31 (23) (2012) 8067–8070, https://doi.org/10.1021/om300938e.
[110] D. Streich, Y. Astuti, M. Orlandi, L. Schwartz, R. Lomoth, L. Hammarström, S. Ott, High-turnover photochemical hydrogen production catalyzed by a model complex of the [FeFe]-hydrogenase active site, Chem. Eur. J. 16 (1) (2010) 60–63, https://doi.org/10.1002/chem.v16:110.1002/chem.200902489.
[111] S. Pullen, H. Fei, A. Orthaber, S.M. Cohen, S. Ott, Enhanced photochemical hydrogen production by a molecular diiron catalyst incorporated into a metal-organic framework, J. Am. Chem. Soc. 135 (45) (2013) 16997–17003, https://doi.org/10.1021/ja407176p.
[112] R.-X. Li, X.-F. Liu, T. Liu, Y.-B. Yin, Y. Zhou, S.-K. Mei, J. Yan, Electrocatalytic properties of [FeFe]-hydrogenases models and visible-light-driven hydrogen evolution efficiency promotion with porphyrin functionalized graphene nanocomposite, Electrochim. Acta 237 (2017) 207–216, https://doi.org/10.1016/j.electacta.2017.03.216.
[113] R. Cammack, Hydrogenase sophistication, Nature 397 (6716) (1999) 214–215, https://doi.org/10.1038/16601.
[114] X.-B. Wang, H.-Q. Zheng, H. Rao, H.-C. Yao, Y.-T. Fan, H.-W. Hou, Synthesis of a new iron-sulfur cluster compound and its photocatalytic H 2 evolution activity through visible light irradiation, Appl. Organomet. Chem. 30 (8) (2016) 638–644, https://doi.org/10.1002/aoc.3481.
[115] W.-N. Cao, F. Wang, H.-Y. Wang, B. Chen, K.e. Feng, C.-H. Tung, L.-Z. Wu, Photocatalytic hydrogen production from a simple water-soluble [FeFe]-hydrogenase model system, Chem. Commun. 48 (65) (2012) 8081, https://doi.org/10.1039/c2cc33097k.
[116] J.-X. Jian, C. Ye, X.-Z. Wang, M. Wen, Z.-J. Li, X.-B. Li, B. Chen, C.-H. Tung, L.-Z. Wu, Comparison of H 2 photogeneration by [FeFe]-hydrogenase mimics with CdSe QDs and Ru(bpy) 3 Cl 2 in aqueous solution, Energy Environ. Sci. 9 (6) (2016) 2083–2089, https://doi.org/10.1039/C6EE00629A.
[117] Z.-J. Li, J.-J. Wang, X.-B. Li, X.-B. Fan, Q.-Y. Meng, K.e. Feng, B. Chen, C.-H. Tung, L.-Z. Wu, An exceptional artificial photocatalyst, Ni h -CdSe/cds core/shell hybrid, made in situ from CdSe quantum dots and nickel salts for efficient hydrogen evolution, Adv. Mater. 25 (45) (2013) 6613–6618, https://doi.org/10.1002/adma.201302908.
[118] Z.-J. Li, X.-B. Fan, X.-B. Li, J.-X. Li, C. Ye, J.-J. Wang, S. Yu, C.-B. Li, Y.-J. Gao, Q.-Y. Meng, C.-H. Tung, L.-Z. Wu, Visible light catalysis-assisted assembly of Ni h -QD hollow nanospheres in situ via hydrogen bubbles, J. Am. Chem. Soc. 136 (23) (2014) 8261–8268, https://doi.org/10.1021/ja5047236.
[119] S. Ott, M. Kritikos, B. Åkermark, L. Sun, Synthesis and structure of a biomimetic model of the iron hydrogenase active site covalently linked to a ruthenium photosensitizer, Angew. Chem. Int. Ed. 42 (2003) 3285–3288, https://doi.org/10.1002/anie.200351192.
[120] L. Hammarström, F. Barigelletti, L. Flamigni, M.T. Indelli, N. Armaroli, G. Calogero, M. Guardigli, A. Sour, J.-P. Collin, J.-P. Sauvage, A study on delocalization of MLCT excited states by rigid bridging ligands in homometallic dinuclear complexes of ruthenium(II), J. Phys. Chem. A 101 (48) (1997) 9061–9069, https://doi.org/10.1021/jp971875b.
[121] S. Ott, M. Borgström, M. Kritikos, R. Lomoth, J. Bergquist, B. Åkermark, L. Hammarström, L. Sun, Model of the iron hydrogenase active site covalently linked to a ruthenium photosensitizer: synthesis and photophysical properties, Inorg. Chem. 43 (2004) 4683–4692, https://doi.org/10.1021/ic0303385.
[122] L.-C. Song, M.-Y. Tang, S.-Z. Mei, J.-H. Huang, Q.-M. Hu, The active site model for iron-only hydrogenases coordinatively bonded to a metalloporphyrin photosensitizer, Organometallics 26 (7) (2007) 1575–1577, https://doi.org/10.1021/om070133u.
[123] X. Li, M. Wang, S. Zhang, J. Pan, Y. Na, J. Liu, B. Åkermark, L. Sun, Noncovalent assembly of a metalloporphyrin and an iron hydrogenase active-site model: photo-induced electron transfer and hydrogen generation, J. Phys. Chem. B 112 (27) (2008) 8198–8202, https://doi.org/10.1021/jp710498v.
[124] J.R. Darwent, P. Douglas, A. Harriman, G. Porter, M.-C. Richoux, Metal phthalocyanines and porphyrins as photosensitizers for reduction of water to hydrogen, Coord. Chem. Rev. 44 (1) (1982) 83–126, https://doi.org/10.1016/S0010-8545(00)80518-4.
[125] I. Okura, Hydrogenase and its application for photoinduced hydrogen evolution, Coord. Chem. Rev. 68 (1985) 53–99, https://doi.org/10.1016/0010-8545(85)80030-8.
[126] L.-C. Song, M.-Y. Tang, F.-H. Su, Q.-M. Hu, A Biomimetic model for the active site of iron-only hydrogenases covalently bonded to a porphyrin photosensitizer, Angew. Chem. Int. Ed. 45 (7) (2006) 1130–1133, https://doi.org/10.1002/(ISSN)1521-377310.1002/anie.v45:710.1002/anie.200503602.
[127] L.-C. Song, L.-X. Wang, M.-Y. Tang, C.-G. Li, H.-B. Song, Q.-M. Hu, Synthesis, structure, and photoinduced catalysis of [FeFe]-hydrogenase active site models covalently linked to a porphyrin or metalloporphyrin moiety †, Organometallics 28 (13) (2009) 3834–3841, https://doi.org/10.1021/om900141x.
[128] A.P.S. Samuel, D.T. Co, C.L. Stern, M.R. Wasielewski, Ultrafast photodriven intramolecular electron transfer from a zinc porphyrin to a readily reduced diiron hydrogenase model complex, J. Am. Chem. Soc. 132 (26) (2010) 8813–8815, https://doi.org/10.1021/ja100016v.
[129] S. Gao, W.-Y. Zhang, Q. Duan, Q.-C. Liang, D.-Y. Jiang, J.-X. Zhao, J.-H. Hou, An artificial [FeFe]-hydrogenase mimic with organic chromophore-linked thiolate bridges for the photochemical production of hydrogen, Chem. Pap. 71 (3) (2017) 617–625, https://doi.org/10.1007/s11696-016-0049-8.
[130] J. Ekström, M. Abrahamsson, C. Olson, J. Bergquist, F.B. Kaynak, L. Eriksson, L. Sun, H.-C. Becker, B. Åkermark, L. Hammarström, S. Ott, Bio-inspired, side-on attachment of a ruthenium photosensitizer to an iron hydrogenase active site model, Dalton Trans. (38) (2006) 4599–4606, https://doi.org/10.1039/B606659C.
[131] W. Gao, J. Liu, W. Jiang, M. Wang, L. Weng, B. Åkermark, L. Sun, An azadithiolate bridged Fe2S2 complex as active site model of FeFe-hydrogenase covalently linked to a Re(CO)3(bpy)(py) photosensitizer aiming for light-driven hydrogen production, Comptes Rendus Chim. 11 (8) (2008) 915–921, https://doi.org/10.1016/j.crci.2008.03.004.
[132] W.-G. Wang, F. Wang, H.-Y. Wang, G. Si, C.-H. Tung, L.-Z. Wu, Photocatalytic hydrogen evolution by [FeFe] Hydrogenase mimics in homogeneous solution,

Chem. Asian J. 5 (8) (2010) 1796–1803, https://doi.org/10.1002/asia.201000087.
[133] J. Liu, W. Jiang, Photoinduced hydrogen evolution in supramolecular devices with a rhenium photosensitizer linked to FeFe-hydrogenase model complexes, Dalton Trans. 41 (32) (2012) 9700, https://doi.org/10.1039/c2dt30468f.
[134] A.M. Kluwer, R. Kapre, F. Hartl, M. Lutz, A.L. Spek, A.M. Brouwer, P.W.N.M. van Leeuwen, J.N.H. Reek, Self-assembled biomimetic [2Fe2S]-hydrogenase-based photocatalyst for molecular hydrogen evolution, Proc. Natl. Acad. Sci. (U.S.A.) 106 (2009) 10460–10465, https://doi.org/10.1073/pnas.0809666106.
[135] H.-H. Cui, M.-Q. Hu, H.-M. Wen, G.-L. Chai, C.-B. Ma, H. Chen, C.-N. Chen, Efficient [FeFe] hydrogenase mimic dyads covalently linking to iridium photosensitizer for photocatalytic hydrogen evolution, Dalton Trans. 41 (45) (2012) 13899, https://doi.org/10.1039/c2dt31618h.
[136] E.D. Cline, S.E. Adamson, S. Bernhard, Homogeneous catalytic system for photoinduced hydrogen production utilizing iridium and rhodium complexes, Inorg. Chem. 47 (22) (2008) 10378–10388, https://doi.org/10.1021/ic800988b.
[137] U.-P. Apfel, Y. Halpin, H. Görls, J.G. Vos, W. Weigand, Influence of the introduction of cyanido and phosphane ligands in multifunctionalized (Mercaptomethyl)silane [FeFe] hydrogenase model systems, Eur. J. Inorg. Chem. 2011 (4) (2011) 581–588, https://doi.org/10.1002/ejic.201000918.
[138] U.-P. Apfel, H. Görls, G.A.N. Felton, D.H. Evans, R.S. Glass, D.L. Lichtenberger, W. Weigand, {1,1′-(Dimethylsilylene)bis[methanechalcogenolato]}diiron Complexes [2Fe2E(Si)] (E=S, Se, Te) - [FeFe] Hydrogenase Models, Helv. Chim. Acta 95 (11) (2012) 2168–2175, https://doi.org/10.1002/hlca.201200429.
[139] G. Frapper, M. Kertesz, Geometrical and electronic structures of.pi.-conjugated silicon ring polymers, Organometallics 11 (10) (1992) 3178–3184, https://doi.org/10.1021/om00046a011.
[140] M. Hissler, P.W. Dyer, R. Réau, Linear organic π-conjugated systems featuring the heavy Group 14 and 15 elements, Coord. Chem. Rev. 244 (1-2) (2003) 1–44, https://doi.org/10.1016/S0010-8545(03)00098-5.
[141] G. Yu, S. Yin, Y. Liu, J. Chen, X. Xu, X. Sun, D. Ma, X. Zhan, Q. Peng, Z. Shuai, B. Tang, D. Zhu, W. Fang, Y.i. Luo, Structures, electronic states, photoluminescence, and carrier transport properties of 1,1-disubstituted 2,3,4,5-tetraphenylsiloles, J. Am. Chem. Soc. 127 (17) (2005) 6335–6346, https://doi.org/10.1021/ja044628b.
[142] R. Goy, U.-P. Apfel, C. Elleouet, D. Escudero, M. Elstner, H. Görls, J. Talarmin, P. Schollhammer, L. González, W. Weigand, A Silicon-heteroaromatic system as photosensitizer for light-driven hydrogen production by hydrogenase mimics, Eur. J. Inorg. Chem. 2013 (25) (2013) 4466–4472, https://doi.org/10.1002/ejic.201300537.
[143] R. Goy, L. Bertini, T. Rudolph, S. Lin, M. Schulz, G. Zampella, B. Dietzek, F.H. Schacher, L. De Gioia, K. Sakai, W. Weigand, Photocatalytic hydrogen evolution driven by [FeFe] hydrogenase models tethered to fluorene and silafluorene sensitizers, Chem. Eur. J. 23 (2) (2017) 334–345, https://doi.org/10.1002/chem.201603140.
[144] G. Si, W.-G. Wang, H.-Y. Wang, C.-H. Tung, L.-Z. Wu, Facile synthesis and functionality-dependent electrochemistry of Fe-only hydrogenase mimics, Inorg. Chem. 47 (18) (2008) 8101–8111, https://doi.org/10.1021/ic800676y.
[145] H.-Y. Wang, G. Si, W.-N. Cao, W.-G. Wang, Z.-J. Li, F. Wang, C.-H. Tung, L.-Z. Wu, A triad [FeFe] hydrogenase system for light-driven hydrogen evolution, Chem. Commun. 47 (29) (2011) 8406, https://doi.org/10.1039/c1cc12200b.
[146] K.S. Schanze, D. Brent MacQueen, T.A. Perkins, L.A. Cabana, Studies of intramolecular electron and energy transfer using the fac-(diimine)ReI(CO)3 chromophore, Coord. Chem. Rev. 122 (1-2) (1993) 63–89, https://doi.org/10.1016/0010-8545(93)80042-4.
[147] D. Rehm, A. Weller, Kinetics of Fluorescence Quenching by Electron and H-Atom Transfer, Isr. J. Chem. 8 (2) (1970) 259–271, https://doi.org/10.1002/ijch.v8.210.1002/ijch.197000029.
[148] D. Chong, I.P. Georgakaki, R. Mejia-Rodriguez, J. Sanabria-Chinchilla, M.P. Soriaga, M.Y. Darensbourg, Electrocatalysis of hydrogen production by active site analogues of the iron hydrogenase enzyme: structure/function relationships, Dalton Trans. (21) (2003) 4158–4163, https://doi.org/10.1039/B304283A.
[149] S.J. Borg, T. Behrsing, S.P. Best, M. Razavet, X. Liu, C.J. Pickett, Electron transfer at a dithiolate-bridged diiron assembly: electrocatalytic hydrogen evolution, J. Am. Chem. Soc. 126 (2004) 16988–16999, https://doi.org/10.1021/ja045281f.
[150] G.A.N. Felton, A.K. Vannucci, J. Chen, L.T. Lockett, N. Okumura, B.J. Petro, U.I. Zakai, D.H. Evans, R.S. Glass, D.L. Lichtenberger, Hydrogen Generation from Weak Acids: Electrochemical and Computational Studies of a Diiron Hydrogenase Mimic, J. Am. Chem. Soc. 129 (2007) 12521–12530, https://doi.org/10.1021/ja073886g.
[151] L.-Z. Wu, B. Chen, Z.-J. Li, C.-H. Tung, Enhancement of the efficiency of photocatalytic reduction of protons to hydrogen via molecular assembly, Acc. Chem. Res. 47 (7) (2014) 2177–2185, https://doi.org/10.1021/ar500140r.
[152] P. Poddutoori, D.T. Co, A.P.S. Samuel, C.H. Kim, M.T. Vagnini, M.R. Wasielewski, Photoinitiated multistep charge separation in ferrocene–zinc porphyrin–diiron hydrogenase model complex triads, Energy Environ. Sci. 4 (7) (2011) 2441, https://doi.org/10.1039/c1ee01334c.
[153] M.E. Bodini, M.A. Del Valle, Redox chemistry and spectroscopy of 2-mercaptobenzoic acid and its manganese(II) and (III) complexes in dimethylsulphoxide, Polyhedron 9 (9) (1990) 1181–1186, https://doi.org/10.1016/S0277-5387(00)86893-X.
[154] J.-M. Lehn, Supramolecular chemistry—scope and perspectives molecules, supermolecules, and molecular devices(nobel lecture), Angew. Chem. Int. Ed. Engl. 27 (1) (1988) 89–112, https://doi.org/10.1002/anie.198800891.
[155] J.-M. Lehn, Perspectives in Supramolecular chemistry—from molecular recognition towards molecular information processing and self-organization, Angew. Chem. Int. Ed. Engl. 29 (11) (1990) 1304–1319, https://doi.org/10.1002/anie.199013041.
[156] J.-M. Lehn, Toward self-organization and complex matter, Science 295 (2002) 2400–2403, https://doi.org/10.1126/science.1071063.
[157] J.-M. Lehn, From supramolecular chemistry towards constitutional dynamic chemistry and adaptive chemistry, Chem. Soc. Rev. 36 (2) (2007) 151–160, https://doi.org/10.1039/B616752G.
[158] J.-M. Lehn, Towards complex matter: supramolecular chemistry and self-organization, Eur. Rev. 17 (2) (2009) 263–280, https://doi.org/10.1017/S1062798709000805.
[159] M.L. Singleton, J.H. Reibenspies, M.Y. Darensbourg, A cyclodextrin host/guest approach to a hydrogenase active site biomimetic cavity, J. Am. Chem. Soc. 132 (26) (2010) 8870–8871, https://doi.org/10.1021/ja103774j.
[160] M.L. Singleton, D.J. Crouthers, R.P. Duttweiler, J.H. Reibenspies, M.Y. Darensbourg, Sulfonated Diiron complexes as water-soluble models of the [Fe–Fe]-hydrogenase enzyme active site, Inorg. Chem. 50 (11) (2011) 5015–5026, https://doi.org/10.1021/ic200272x.
[161] X. Li, M. Wang, D. Zheng, K. Han, J. Dong, L. Sun, Photocatalytic H2 production in aqueous solution with host-guest inclusions formed by insertion of an FeFe-hydrogenase mimic and an organic dye into cyclodextrins, Energy Environ. Sci. 5 (8) (2012) 8220, https://doi.org/10.1039/c2ee22109h.
[162] M. Cheng, M. Wang, S. Zhang, F. Liu, Y. Yang, B. Wan, L. Sun, Photocatalytic H 2 production using a hybrid assembly of an [FeFe]-hydrogenase model and CdSe quantum dot linked through a thiolato-functionalized cyclodextrin, Faraday Discuss. 198 (2017) 197–209, https://doi.org/10.1039/C6FD00207B.
[163] J.-X. Jian, Q. Liu, Z.-J. Li, F. Wang, X.-B. Li, C.-B. Li, B. Liu, Q.-Y. Meng, B. Chen, K. Feng, C.-H. Tung, L.-Z. Wu, Chitosan confinement enhances hydrogen photogeneration from a mimic of the diiron subsite of [FeFe]-hydrogenase, Nat. Commun. 4 (2013) 2695, https://doi.org/10.1038/ncomms3695.
[164] F. Quentel, G. Passard, F. Gloaguen, Electrochemical hydrogen production in aqueous micellar solution by a diiron benzenedithiolate complex relevant to [FeFe] hydrogenases, Energy Environ. Sci. 5 (7) (2012) 7757, https://doi.org/10.1039/c2ee21531d.
[165] F. Quentel, G. Passard, F. Gloaguen, A binuclear iron-thiolate catalyst for electrochemical hydrogen production in aqueous micellar solution, Chem. Eur. J. 18 (42) (2012) 13473–13479, https://doi.org/10.1002/chem.v18.4210.1002/chem.201201884.
[166] R. Fritzsch, O. Brady, E. Adair, J.A. Wright, C.J. Pickett, N.T. Hunt, Encapsulating subsite analogues of the [FeFe]-hydrogenases in micelles enables direct water interactions, J. Phys. Chem. Lett. 7 (14) (2016) 2838–2843, https://doi.org/10.1021/acs.jpclett.6b01338.
[167] H.-Y. Wang, W.-G. Wang, G. Si, F. Wang, C.-H. Tung, L.-Z. Wu, Photocatalytic hydrogen evolution from rhenium(I) complexes to [FeFe] hydrogenase mimics in aqueous SDS micellar systems: A biomimetic pathway, Langmuir 26 (12) (2010) 9766–9771, https://doi.org/10.1021/la101322s.
[168] C. Orain, F. Quentel, F. Gloaguen, Photocatalytic hydrogen production using models of the iron-iron hydrogenase active site dispersed in micellar solution, ChemSusChem 7 (2) (2014) 638–643, https://doi.org/10.1002/cssc.201300631.
[169] F. Wang, M. Wen, K.e. Feng, W.-J. Liang, X.-B. Li, B. Chen, C.-H. Tung, L.-Z. Wu, Amphiphilic polymeric micelles as microreactors: improving the photocatalytic hydrogen production of the [FeFe]-hydrogenase mimic in water, Chem. Commun. 52 (3) (2016) 457–460, https://doi.org/10.1039/C5CC07499A.
[170] K. Menzel, U.-P. Apfel, N. Wolter, R. Rüger, T. Alpermann, F. Steiniger, D. Gabel, S. Förster, W. Weigand, A. Fahr, [FeFe]-Hydrogenase models assembled into vesicular structures, J. Liposome Res. 24 (1) (2014) 59–68, https://doi.org/10.3109/08982104.2013.833225.
[171] S. Troppmann, E. Brandes, H. Motschmann, F. Li, M. Wang, L. Sun, B. König, Enhanced photocatalytic hydrogen production by adsorption of an [FeFe]-Hydrogenase subunit mimic on self-assembled membranes, Eur. J. Inorg. Chem. 2016 (4) (2016) 554–560, https://doi.org/10.1002/ejic.201501377.
[172] S. Troppmann, B. König, Functionalized vesicles with Co-embedded CdSe quantum dots and [FeFe]-hydrogenase mimic for light-driven hydrogen production, ChemistrySelect. 1 (7) (2016) 1405–1409, https://doi.org/10.1002/slct.201600032.
[173] T. Vermonden, R. Censi, W.E. Hennink, Hydrogels for protein delivery, Chem. Rev. 112 (5) (2012) 2853–2888, https://doi.org/10.1021/cr200157d.
[174] P.W.J.M. Frederix, R. Kania, J.A. Wright, D.A. Lamprou, R.V. Ulijn, C.J. Pickett, N. T. Hunt, Encapsulating [FeFe]-hydrogenase model compounds in peptide hydrogels dramatically modifies stability and photochemistry, Dalton Trans. 41 (42) (2012) 13112, https://doi.org/10.1039/c2dt30307h.
[175] A. Jablonskytė, J.A. Wright, C.J. Pickett, Mechanistic aspects of the protonation of [FeFe]-hydrogenase subsite analogues, Dalton Trans. 39 (12) (2010) 3026, https://doi.org/10.1039/b923191a.
[176] J.A. Aušra Jablonskytė, C.J.P. Wright, [FeFe]-hydrogenase models: unexpected variation in protonation rate between dithiolate bridge analogues, Eur. J. Inorg. Chem. (2011 (2011)) 1033–1037, https://doi.org/10.1002/ejic.201001072.
[177] T. Yu, Y.i. Zeng, J. Chen, X. Zhang, G. Yang, Y.i. Li, Efficient photochemical production of hydrogen in aqueous solution by simply incorporating a water-

insoluble hydrogenase mimic into a hydrogel, J. Mater. Chem. A 2 (48) (2014) 20500–20505, https://doi.org/10.1039/C4TA04914D.
[178] F. Rosati, G. Roelfes, Artificial metalloenzymes, ChemCatChem 2 (8) (2010) 916–927, https://doi.org/10.1002/cctc.201000011.
[179] P.J. Deuss, R. den Heeten, W. Laan, P.C.J. Kamer, Bioinspired catalyst design and artificial metalloenzymes, Chem. Eur. J. 17 (17) (2011) 4680–4698, https://doi.org/10.1002/chem.201003646.
[180] A. Onoda, T. Hayashi, M. Salmain, Artificial Metalloenzymes Containing an Organometallic Active Site, in: Bioorganometallic Chem. Appl. Drug Discov. Biocatal. Imaging, 2015. doi:10.1002/9783527673438.ch10.
[181] A. Onoda, T. Hayashi, Artificial hydrogenase: biomimetic approaches controlling active molecular catalysts, Curr. Opin. Chem. Biol. 25 (2015) 133–140, https://doi.org/10.1016/j.cbpa.2014.12.041.
[182] A.K. Jones, B.R. Lichtenstein, A. Dutta, G. Gordon, P.L. Dutton, Synthetic hydrogenases: incorporation of an iron carbonyl thiolate into a designed peptide, J. Am. Chem. Soc. 129 (2007) 14844–14845, https://doi.org/10.1021/ja075116a.
[183] Y. Sano, A. Onoda, T. Hayashi, A hydrogenase model system based on the sequence of cytochrome c: photochemical hydrogen evolution in aqueous media, Chem. Commun. 47 (29) (2011) 8229, https://doi.org/10.1039/c1cc11157d.
[184] Y. Sano, A. Onoda, T. Hayashi, Photocatalytic hydrogen evolution by a diiron hydrogenase model based on a peptide fragment of cytochrome c556 with an attached diiron carbonyl cluster and an attached ruthenium photosensitizer, J. Inorg. Biochem. 108 (2012) 159–162, https://doi.org/10.1016/j.jinorgbio.2011.07.010.
[185] S. Roy, S. Shinde, G.A. Hamilton, H.E. Hartnett, A.K. Jones, Artificial [FeFe]-Hydrogenase: On Resin Modification of an Amino Acid to Anchor a Hexacarbonyldiiron Cluster in a Peptide Framework, Eur. J. Inorg. Chem. 2011 (2011) 1050–1055, https://doi.org/10.1002/ejic.201000979.
[186] S. Roy, T.-A. Nguyen, L.u. Gan, A.K. Jones, Biomimetic peptide-based models of [FeFe]-hydrogenases: utilization of phosphine-containing peptides, Dalton Trans. 44 (33) (2015) 14865–14876, https://doi.org/10.1039/C5DT01796C.
[187] A. Roy, C. Madden, G. Ghirlanda, Photo-induced hydrogen production in a helical peptide incorporating a [FeFe] hydrogenase active site mimic, Chem. Commun. 48 (79) (2012) 9816, https://doi.org/10.1039/c2cc34470j.
[188] A. Onoda, Y. Kihara, K. Fukumoto, Y. Sano, T. Hayashi, Photoinduced Hydrogen Evolution Catalyzed by a Synthetic Diiron Dithiolate Complex Embedded within a Protein Matrix, ACS Catal. 4 (8) (2014) 2645–2648, https://doi.org/10.1021/cs500392e.
[189] W. Chen, X. Cai, L. Ji, X. Li, X. Wang, X. Zhang, Y. Gao, F. Feng, A photosynthesis-inspired supramolecular system: caging photosensitizer and photocatalyst in apoferritin, Photosynth. Res. 142 (2) (2019) 169–180, https://doi.org/10.1007/s11120-019-00671-4.
[190] F. Wang, W.-J. Liang, J.-X. Jian, C.-B. Li, B. Chen, C.-H. Tung, L.-Z. Wu, Exceptional Poly(acrylic acid)-Based Artificial [FeFe]-Hydrogenases for Photocatalytic H 2 Production in Water, Angew. Chem. Int. Ed. 52 (31) (2013) 8134–8138, https://doi.org/10.1002/anie.v52.3110.1002/anie.201303110.
[191] W.-J. Liang, F. Wang, M. Wen, J.-X. Jian, X.-Z. Wang, B. Chen, C.-H. Tung, L.-Z. Wu, Branched Polyethylenimine Improves Hydrogen Photoproduction from a CdSe Quantum Dot/[FeFe]-Hydrogenase Mimic System in Neutral Aqueous Solutions, Chem. Eur. J. 21 (8) (2015) 3187–3192, https://doi.org/10.1002/chem.v21.810.1002/chem.201406361.
[192] M. Wen, X.-B. Li, J.-X. Jian, X.-Z. Wang, H.-L. Wu, B. Chen, C.-H. Tung, L.-Z. Wu, Secondary coordination sphere accelerates hole transfer for enhanced hydrogen photogeneration from [FeFe]-hydrogenase mimic and CdSe QDs in water, Sci. Rep. 6 (2016) 29851, https://doi.org/10.1038/srep29851.
[193] S.M. Grayson, J.M.J. Fréchet, Convergent Dendrons and Dendrimers: from Synthesis to Applications, Chem. Rev. 101 (2001) 3819–3868, https://doi.org/10.1021/cr990116h.
[194] L. Röglin, E.H.M. Lempens, E.W. Meijer, A. Synthetic, "Tour de Force": Well-Defined Multivalent and Multimodal Dendritic Structures for Biomedical Applications, Angew. Chem. Int. Ed. 50 (2011) 102–112, https://doi.org/10.1002/anie.201003968.
[195] D. Astruc, Electron-transfer processes in dendrimers and their implication in biology, catalysis, sensing and nanotechnology, Nat. Chem. 4 (4) (2012) 255–267, https://doi.org/10.1038/nchem.1304.
[196] Y.i. Zeng, Y. Li, M. Li, G. Yang, Y.i. Li, Enhancement of Energy Utilization in Light-Harvesting Dendrimers by the Pseudorotaxane Formation at Periphery, J. Am. Chem. Soc. 131 (25) (2009) 9100–9106, https://doi.org/10.1021/ja902998g.
[197] T. Yu, W. Wang, J. Chen, Y.i. Zeng, Y. Li, G. Yang, Y.i. Li, Dendrimer-Encapsulated Pt Nanoparticles: An Artificial Enzyme for Hydrogen Production, J. Phys. Chem. C 116 (19) (2012) 10516–10521, https://doi.org/10.1021/jp3021672.
[198] X. Liu, Y.i. Zeng, X. Zhang, T. Yu, J. Chen, Y.i. Li, Dendrimers-merging biomimics and photoenergy conversion, Sci. China Chem. 58 (3) (2015) 390–399, https://doi.org/10.1007/s11426-014-5293-6.
[199] T. Yu, Y.i. Zeng, J. Chen, Y.-Y. Li, G. Yang, Y.i. Li, Exceptional Dendrimer-Based Mimics of Diiron Hydrogenase for the Photochemical Production of Hydrogen, Angew. Chem. Int. Ed. 52 (21) (2013) 5631–5635, https://doi.org/10.1002/anie.201301289.
[200] K.A. Brown, S. Dayal, X. Ai, G. Rumbles, P.W. King, Controlled Assembly of Hydrogenase-CdTe Nanocrystal Hybrids for Solar Hydrogen Production, J. Am. Chem. Soc. 132 (28) (2010) 9672–9680, https://doi.org/10.1021/ja101031r.
[201] K.A. Brown, M.B. Wilker, M. Boehm, G. Dukovic, P.W. King, Characterization of Photochemical Processes for H 2 Production by CdS Nanorod–[FeFe] Hydrogenase Complexes, J. Am. Chem. Soc. 134 (12) (2012) 5627–5636, https://doi.org/10.1021/ja2116348.
[202] V. Polliotto, S. Morra, S. Livraghi, F. Valetti, G. Gilardi, E. Giamello, Electron transfer and H2 evolution in hybrid systems based on [FeFe]-hydrogenase anchored on modified TiO2, Int. J. Hydrogen Energy 41 (25) (2016) 10547–10556, https://doi.org/10.1016/j.ijhydene.2016.05.002.
[203] E. Reisner, D.J. Powell, C. Cavazza, J.C. Fontecilla-Camps, F.A. Armstrong, Visible Light-Driven H 2 Production by Hydrogenases Attached to Dye-Sensitized TiO 2 Nanoparticles, J. Am. Chem. Soc. 131 (51) (2009) 18457–18466, https://doi.org/10.1021/ja907923r.
[204] C.A. Caputo, L. Wang, R. Beranek, E. Reisner, Carbon nitride–TiO 2 hybrid modified with hydrogenase for visible light driven hydrogen production, Chem. Sci. 6 (10) (2015) 5690–5694, https://doi.org/10.1039/C5SC02017D.
[205] C.-B. Li, Z.-J. Li, S. Yu, G.-X. Wang, F. Wang, Q.-Y. Meng, B. Chen, K.e. Feng, C.-H. Tung, L.-Z. Wu, Interface-directed assembly of a simple precursor of [FeFe]–H2ase mimics on CdSe QDs for photosynthetic hydrogen evolution in water, Energy Environ. Sci. 6 (9) (2013) 2597, https://doi.org/10.1039/c3ee40992a.
[206] A.C.C. Esteves, T. Trindade, Synthetic studies on II/VI semiconductor quantum dots, Curr. Opin. Solid State Mater. Sci. 6 (4) (2002) 347–353, https://doi.org/10.1016/S1359-0286(02)00079-7.
[207] I. Hernández-Calderón, Epitaxial growth of thin films and quantum structures of II–VI visible-bandgap semiconductors, in: Mol. Beam Ep., Elsevier, 2013: pp. 311–346. doi:10.1016/B978-0-12-387839-7.00014-2.
[208] Y. Hong, J. Zhang, X. Wang, Y. Wang, Z. Lin, J. Yu, F. Huang, Influence of lattice integrity and phase composition on the photocatalytic hydrogen production efficiency of ZnS nanomaterials, Nanoscale. 4 (9) (2012) 2859, https://doi.org/10.1039/c2nr30150d.
[209] F. Zhang, X. Wang, H. Liu, C. Liu, Y. Wan, Y. Long, Z. Cai, Recent Advances and Applications of Semiconductor Photocatalytic Technology, Appl. Sci. 9 (2019) 2489, https://doi.org/10.3390/app9122489.
[210] J. Zhang, Y. Wang, J. Zhang, Z. Lin, F. Huang, J. Yu, Enhanced Photocatalytic Hydrogen Production Activities of Au-Loaded ZnS Flowers, ACS Appl. Mater. Interfaces 5 (3) (2013) 1031–1037, https://doi.org/10.1021/am302726y.
[211] F. Wen, X. Wang, L. Huang, G. Ma, J. Yang, C. Li, A Hybrid Photocatalytic System Comprising ZnS as Light Harvester and an [Fe2S2] Hydrogenase Mimic as Hydrogen Evolution Catalyst, ChemSusChem. 5 (2012) 849–853. doi:10.1002/cssc.201200190.
[212] X.-W. Song, H.-M. Wen, C.-B. Ma, M.-Q. Hu, H. Chen, H.-H. Cui, C.-N. Chen, Photocatalytic hydrogen evolution by two comparable [FeFe]-hydrogenase mimics assembled to the surface of ZnS, Appl. Organomet. Chem. 28 (4) (2014) 267–273, https://doi.org/10.1002/aoc.v28.410.1002/aoc.3119.
[213] M.V. Pavliuk, A.M. Cieślak, M. Abdellah, A. Budinská, S. Pullen, K. Sokołowski, D.L.A. Fernandes, J. Szlachetko, E.L. Bastos, S. Ott, L. Hammarström, T. Edvinsson, J. Lewiński, J. Sá, Hydrogen evolution with nanoengineered ZnO interfaces decorated using a beetroot extract and a hydrogenase mimic, Sustain. Energy Fuels. 1 (1) (2017) 69–73, https://doi.org/10.1039/C6SE00066E.
[214] A.M. Cieślak, M.V. Pavliuk, L. D'Amario, M. Abdellah, K. Sokołowski, U. Rybinska, D.L.A. Fernandes, M.K. Leszczyński, F. Mamedov, A.M. El-Zhory, J. Föhlinger, A. Budinská, M. Wolska-Pietkiewicz, L. Hammarström, J. Lewiński, J. Sá, Ultra long-lived electron-hole separation within water-soluble colloidal ZnO nanocrystals: Prospective applications for solar energy production, Nano Energy 30 (2016) 187–192, https://doi.org/10.1016/j.nanoen.2016.09.045.
[215] J. Lee, O.K. Farha, J. Roberts, K.A. Scheidt, S.T. Nguyen, J.T. Hupp, Metal–organic framework materials as catalysts, Chem. Soc. Rev. 38 (5) (2009) 1450, https://doi.org/10.1039/b807080f.
[216] J.-R. Li, R.J. Kuppler, H.-C. Zhou, Selective gas adsorption and separation in metal–organic frameworks, Chem. Soc. Rev. 38 (5) (2009) 1477, https://doi.org/10.1039/b802426j.
[217] A. Corma, H. García, F.X, Llabrés i Xamena, Engineering Metal Organic Frameworks for Heterogeneous Catalysis, Chem. Rev. 110 (2010) 4606–4655, https://doi.org/10.1021/cr9003924.
[218] L.E. Kreno, K. Leong, O.K. Farha, M. Allendorf, R.P. Van Duyne, J.T. Hupp, Metal-Organic Framework Materials as Chemical Sensors, Chem. Rev. 112 (2) (2012) 1105–1125, https://doi.org/10.1021/cr200324t.
[219] H. Li, M. Eddaoudi, M. O'Keeffe, O.M. Yaghi, Design and synthesis of an exceptionally stable and highly porous metal-organic framework, Nature 402 (6759) (1999) 276–279, https://doi.org/10.1038/46248.
[220] J.L.C. Rowsell, O.M. Yaghi, Metal–organic frameworks: a new class of porous materials, Microporous Mesoporous Mater. 73 (1-2) (2004) 3–14, https://doi.org/10.1016/j.micromeso.2004.03.034.
[221] H.-C. Zhou, J.R. Long, O.M. Yaghi, Introduction to Metal-Organic Frameworks, Chem. Rev. 112 (2) (2012) 673–674, https://doi.org/10.1021/cr300014x.
[222] M. Zhang, Z.-Y. Gu, M. Bosch, Z. Perry, H.-C. Zhou, Biomimicry in metal–organic materials, Coord. Chem. Rev. 293–294 (2015) 327–356, https://doi.org/10.1016/j.ccr.2014.05.031.
[223] I. Nath, J. Chakraborty, F. Verpoort, Metal organic frameworks mimicking natural enzymes: a structural and functional analogy, Chem. Soc. Rev. 45 (15) (2016) 4127–4170, https://doi.org/10.1039/C6CS00047A.

[224] B.D. McCarthy, A.M. Beiler, B.A. Johnson, T. Liseev, A.T. Castner, S. Ott, Analysis of electrocatalytic metal-organic frameworks, Coord. Chem. Rev. 406 (2020) 213137, https://doi.org/10.1016/j.ccr.2019.213137.
[225] B.A. Johnson, A.M. Beiler, B.D. McCarthy, S. Ott, Transport Phenomena: Challenges and Opportunities for Molecular Catalysis in Metal-Organic Frameworks, J. Am. Chem. Soc. 142 (28) (2020) 11941–11956, https://doi.org/10.1021/jacs.0c0289910.1021/jacs.0c02899.s001.
[226] S. Pullen, S. Ott, Photochemical Hydrogen Production with Metal-Organic Frameworks, Top. Catal. 59 (19-20) (2016) 1712–1721, https://doi.org/10.1007/s11244-016-0690-z.
[227] S.M. Cohen, Z. Zhang, J.A. Boissonnault, Toward "metalloMOFzymes": Metal-Organic Frameworks with Single-Site Metal Catalysts for Small-Molecule Transformations, Inorg. Chem. 55 (15) (2016) 7281–7290, https://doi.org/10.1021/acs.inorgchem.6b0082810.1021/acs.inorgchem.6b00828.s001.
[228] S. Roy, V. Pascanu, S. Pullen, G. González Miera, B. Martín-Matute, S. Ott, Catalyst accessibility to chemical reductants in metal–organic frameworks, Chem. Commun. 53 (22) (2017) 3257–3260, https://doi.org/10.1039/C7CC00022G.
[229] C. Bozal-Ginesta, S. Pullen, S. Ott, L. Hammarström, Self-Recovery of Photochemical H 2 Evolution with a Molecular Diiron Catalyst Incorporated in a UiO-66 Metal-Organic Framework, ChemPhotoChem. 4 (4) (2020) 287–290, https://doi.org/10.1002/cptc.v4.410.1002/cptc.201900273.
[230] K. Sasan, Q. Lin, C. Mao, P. Feng, Incorporation of iron hydrogenase active sites into a highly stable metal–organic framework for photocatalytic hydrogen generation, Chem. Commun. 50 (72) (2014) 10390, https://doi.org/10.1039/C4CC03946G.
[231] W. Wang, X.-W. Song, Z. Hong, B. Li, Y. Si, C. Ji, K. Su, Y. Tan, Z. Ju, Y. Huang, C.-N. Chen, D. Yuan, Incorporation of iron hydrogenase active sites into a stable photosensitizing metal-organic framework for enhanced hydrogen production, Appl. Catal. B 258 (2019) 117979, https://doi.org/10.1016/j.apcatb.2019.117979.
[232] C.T. Kresge, M.E. Leonowicz, W.J. Roth, J.C. Vartuli, J.S. Beck, Ordered mesoporous molecular sieves synthesized by a liquid-crystal template mechanism, Nature 359 (6397) (1992) 710–712, https://doi.org/10.1038/359710a0.
[233] S. Fukuzumi, Y. Yamada, Shape- and Size-Controlled Nanomaterials for Artificial Photosynthesis, ChemSusChem 6 (10) (2013) 1834–1847, https://doi.org/10.1002/cssc.v6.1010.1002/cssc.201300361.
[234] W. Wang, T. Yu, Y. Zeng, J. Chen, Y. Li, An [Fe-Fe]-Hydrogenase Mimic Immobilized on MCM-41 for the Photochemical Production of Hydrogen in Pure Water, Chinese J. Chem. 32 (6) (2014) 479–484, https://doi.org/10.1002/cjoc.v32.610.1002/cjoc.201400083.
[235] W. Wang, T. Yu, Y. Zeng, J. Chen, G. Yang, Y. Li, Enhanced photocatalytic hydrogen production from an MCM-41-immobilized photosensitizer–[Fe–Fe] hydrogenase mimic dyad, Photochem. Photobiol. Sci. 13 (11) (2014) 1590–1597, https://doi.org/10.1039/C3PP50446H.
[236] P. Van Der Voort, D. Esquivel, E. De Canck, F. Goethals, I. Van Driessche, F.J. Romero-Salguero, Periodic Mesoporous Organosilicas: from simple to complex bridges; a comprehensive overview of functions, morphologies and applications, Chem. Soc. Rev. 42 (9) (2013) 3913–3955, https://doi.org/10.1039/C2CS35222B.
[237] D. Esquivel, O. van den Berg, F.J. Romero-Salguero, F. Du Prez, P. Van Der Voort, 100% thiol-functionalized ethylene PMOs prepared by "thiol acid–ene" chemistry, Chem. Commun. 49 (23) (2013) 2344, https://doi.org/10.1039/c3cc39074h.
[238] M. Cao, Z. Wang, J. Zhang, S. Xu, S. Zhang, X. Dai, X. Jiang, Preparation, characterization and photocatalytic properties of diiron mimic modified Nano Silica, Inorganica Chim. Acta. 469 (2018) 402–407, https://doi.org/10.1016/j.ica.2017.09.007.
[239] R.-X. Li, X.-T. Ren, M.-Y. Tang, M.-X. Chen, G.-B. Huang, C.-H. Fang, T. Liu, Z.-H. Feng, Y.-B. Yin, Y.-M. Guo, S.-K. Mei, J. Yan, Fabrication of covalently linked graphene-mediated [FeFe]-hydrogenases biomimetic photocatalytic hydrogen evolution system in aqueous solution, Appl. Catal. B 224 (2018) 772–782, https://doi.org/10.1016/j.apcatb.2017.09.062.
[240] V. Georgakilas, J.N. Tiwari, K.C. Kemp, J.A. Perman, A.B. Bourlinos, K.S. Kim, R. Zboril, Noncovalent Functionalization of Graphene and Graphene Oxide for Energy Materials, Biosensing, Catalytic, and Biomedical Applications, Chem. Rev. 116 (9) (2016) 5464–5519, https://doi.org/10.1021/acs.chemrev.5b00620.
[241] J.M. Camara, T.B. Rauchfuss, Combining acid–base, redox and substrate binding functionalities to give a complete model for the [FeFe]-hydrogenase, Nat. Chem. 4 (1) (2012) 26–30, https://doi.org/10.1038/nchem.1180.
[242] H. Tian, Molecular Catalyst Immobilized Photocathodes for Water/Proton and Carbon Dioxide Reduction, ChemSusChem 8 (22) (2015) 3746–3759, https://doi.org/10.1002/cssc.201500983.
[243] B. Kumar, M. Llorente, J. Froehlich, T. Dang, A. Sathrum, C.P. Kubiak, Photochemical and Photoelectrochemical Reduction of CO 2, Annu. Rev. Phys. Chem. 63 (1) (2012) 541–569, https://doi.org/10.1146/annurev-physchem-032511-143759.
[244] A. Sartorel, M. Bonchio, S. Campagna, F. Scandola, Tetrametallic molecular catalysts for photochemical water oxidation, Chem. Soc. Rev. 42 (6) (2013) 2262–2280, https://doi.org/10.1039/C2CS35287G.
[245] X. Zou, Y. Zhang, Noble metal-free hydrogen evolution catalysts for water splitting, Chem. Soc. Rev. 44 (15) (2015) 5148–5180, https://doi.org/10.1039/C4CS00448E.
[246] C.D. Windle, R.N. Perutz, Advances in molecular photocatalytic and electrocatalytic CO2 reduction, Coord. Chem. Rev. 256 (21-22) (2012) 2562–2570, https://doi.org/10.1016/j.ccr.2012.03.010.
[247] K.J. Young, L.A. Martini, R.L. Milot, R.C. Snoeberger, V.S. Batista, C.A. Schmuttenmaer, R.H. Crabtree, G.W. Brudvig, Light-driven water oxidation for solar fuels, Coord. Chem. Rev. 256 (21-22) (2012) 2503–2520, https://doi.org/10.1016/j.ccr.2012.03.031.
[248] S.N. Habisreutinger, L. Schmidt-Mende, J.K. Stolarczyk, Photocatalytic Reduction of CO 2 on TiO 2 and Other Semiconductors, Angew. Chem. Int. Ed. 52 (29) (2013) 7372–7408, https://doi.org/10.1002/anie.201207199.
[249] J. Li, N. Wu, Semiconductor-based photocatalysts and photoelectrochemical cells for solar fuel generation: a review, Catal. Sci. Technol. 5 (3) (2015) 1360–1384, https://doi.org/10.1039/C4CY00974F.
[250] F. Niu, D. Wang, F. Li, Y. Liu, S. Shen, T.J. Meyer, Hybrid Photoelectrochemical Water Splitting Systems: From Interface Design to System Assembly, Adv. Energy Mater. 10 (11) (2020) 1900399, https://doi.org/10.1002/aenm.v10.1110.1002/aenm.201900399.
[251] P.D. Tran, V. Artero, M. Fontecave, Water electrolysis and photoelectrolysis on electrodes engineered using biological and bio-inspired molecular systems, Energy Environ. Sci. 3 (6) (2010) 727, https://doi.org/10.1039/b926749b.
[252] N. Queyriaux, N. Kaeffer, A. Morozan, M. Chavarot-Kerlidou, V. Artero, Molecular cathode and photocathode materials for hydrogen evolution in photoelectrochemical devices, J. Photochem. Photobiol. C Photochem. Rev. 25 (2015) 90–105, https://doi.org/10.1016/j.jphotochemrev.2015.08.001.
[253] T. Nann, S. Ibrahim, P.-M. Woi, S. Xu, J. Ziegler, C. Pickett, Water Splitting by Visible Light: A Nanophotocathode for Hydrogen Production, Angew. Chem. Int. Ed. 49 (9) (2010) 1574–1577, https://doi.org/10.1002/anie.200906262.
[254] B. Kumar, M. Beyler, C.P. Kubiak, S. Ott, Photoelectrochemical Hydrogen Generation by an [FeFe] Hydrogenase Active Site Mimic at a p-Type Silicon/Molecular Electrocatalyst Junction, Chem. Eur. J. 18 (5) (2012) 1295–1298, https://doi.org/10.1002/chem.v18.510.1002/chem.201102860.
[255] S. Chandrasekaran, T.J. Macdonald, Y.J. Mange, N.H. Voelcker, T. Nann, A quantum dot sensitized catalytic porous silicon photocathode, J. Mater. Chem. A 2 (25) (2014) 9478–9481, https://doi.org/10.1039/C4TA01677G.
[256] N.B. Williams, A. Nash, N. Yamamoto, M. Patrick, I.C. Tran, J. Gu, Unraveling Activity and Decomposition Pathways of [FeFe] Hydrogenase Mimics Covalently Bonded to Silicon Photoelectrodes, Adv. Mater. Interfaces 8 (10) (2021) 2001961, https://doi.org/10.1002/admi.v8.1010.1002/admi.202001961.
[257] H. Tian, Solid-state p-type dye-sensitized solar cells: progress, potential applications and challenges, Sustain. Energy Fuels. 3 (4) (2019) 888–898, https://doi.org/10.1039/C8SE00581H.
[258] J.M. Gardner, M. Beyler, M. Karnahl, S. Tschierlei, S. Ott, L. Hammarström, Light-Driven Electron Transfer between a Photosensitizer and a Proton-Reducing Catalyst Co-adsorbed to NiO, J. Am. Chem. Soc. 134 (47) (2012) 19322–19325, https://doi.org/10.1021/ja3082268.
[259] A.M. Brown, L.J. Antila, M. Mirmohades, S. Pullen, S. Ott, L. Hammarström, Ultrafast Electron Transfer Between Dye and Catalyst on a Mesoporous NiO Surface, J. Am. Chem. Soc. 138 (26) (2016) 8060–8063, https://doi.org/10.1021/jacs.6b0388910.1021/jacs.6b03889.s001.
[260] L.J. Antila, P. Ghamgosar, S. Maji, H. Tian, S. Ott, L. Hammarström, Dynamics and Photochemical H 2 Evolution of Dye–NiO Photocathodes with a Biomimetic FeFe-Catalyst, ACS Energy Lett. 1 (6) (2016) 1106–1111, https://doi.org/10.1021/acsenergylett.6b0050610.1021/acsenergylett.6b00506.s001.
[261] M.G. Gatty, S. Pullen, E. Sheibani, H. Tian, S. Ott, L. Hammarström, Direct evidence of catalyst reduction on dye and catalyst co-sensitized NiO photocathodes by mid-infrared transient absorption spectroscopy, Chem. Sci. 9 (22) (2018) 4983–4991, https://doi.org/10.1039/C8SC00990B.
[262] M. Wen, H.-L. Wu, J.-X. Jian, X.-Z. Wang, X.-B. Li, B. Chen, C.-H. Tung, L.-Z. Wu, Integrating CdSe Quantum Dots with a [FeFe]-Hydrogenase Mimic into a Photocathode for Hydrogen Evolution at a Low Bias Voltage, ChemPhotoChem. 1 (6) (2017) 260–264, https://doi.org/10.1002/cptc.201700041.
[263] D. Mersch, C.-Y. Lee, J.Z. Zhang, K. Brinkert, J.C. Fontecilla-Camps, A.W. Rutherford, E. Reisner, Wiring of Photosystem II to Hydrogenase for Photoelectrochemical Water Splitting, J. Am. Chem. Soc. 137 (26) (2015) 8541–8549, https://doi.org/10.1021/jacs.5b03737.
[264] W. Wang, H. Wang, Q. Zhu, W. Qin, G. Han, J. Shen, X. Zong, C. Li, Spatially Separated Photosystem II and a Silicon Photoelectrochemical Cell for Overall Water Splitting: A Natural-Artificial Photosynthetic Hybrid, Angew. Chem. Int. Ed. 55 (32) (2016) 9229–9233, https://doi.org/10.1002/anie.v55.3210.1002/anie.201604091.
[265] D.H. Nam, J.Z. Zhang, V. Andrei, N. Kornienko, N. Heidary, A. Wagner, K. Nakanishi, K.P. Sokol, B. Slater, I. Zebger, S. Hofmann, J.C. Fontecilla-Camps, C. B. Park, E. Reisner, Solar Water Splitting with a Hydrogenase Integrated in Photoelectrochemical Tandem Cells, Angew. Chem. Int. Ed. 57 (33) (2018) 10595–10599, https://doi.org/10.1002/anie.v57.3310.1002/anie.201805027.
[266] Lívia.S. Mészáros, P. Ceccaldi, M. Lorenzi, H.J. Redman, E. Pfitzner, J. Heberle, M. Senger, S.T. Stripp, G. Berggren, Spectroscopic investigations under whole-cell conditions provide new insight into the metal hydride chemistry of [FeFe]-hydrogenase, Chem. Sci. 11 (18) (2020) 4608–4617, https://doi.org/10.1039/D0SC00512F.